Dissertation

submitted to the

Combined Faculties for the Natural Sciences and for Mathematics

of the Ruperto-Carola University of Heidelberg, Germany

for the degree of

Doctor of Natural Sciences

presented by

M.Sc. Berthe Youness

born in: Gebrayel, Lebanon

Oral-examination: 10 January 2018

Molecular genetic analysis of functional *FMR1*/FMRP expression on human folliculogenesis and ovarian reserve

Referees: Prof. Dr. rer. nat. Hans-Peter Vogt

Prof. Dr. rer. nat. Gudrun Rappold

Summary

Aim of this thesis was to investigate various possible mechanisms involved in *FMR1* gene epigenetic expression control in human granulosa cells.

Systematic CpG site methylation analysis within the extended *FMR1* promoter domain in COV434 and in primary human granulosa cells by subsequent sequence analysis revealed four distinct regions with a unique CpG site methylation pattern: "*FMR1*-UMR, *FMR1*-DMR1;-DMR2 and –DMR3", of which two (*FMR1*-DMR1 and –DMR2) with distinct patterns were found earlier in leukocytes. Most interesting, *FMR1*-DMR3 contained a conserved double binding site for E2F1, binding only to unmethylated CpG sites. I experimentally confirmed that E2F1 binds to its predicted consensus sequence within *FMR1*-DMR3 but only when containing an unmethylated CpG 94 site. In human primary granulosa cells, the CpG 94 site methylation rate within *FMR1*-DMR3 was found to be dependent on patient ovarian reserve; being lower when the amount of matured follicles seems low (i.e., in POR patients). Increased binding of E2F1 to CpG 94 is the consequence activating *FMR1* transcript expression. This, however, results in reduction of the cellular FMRP protein level due to the well-known gene´s negative feedback loop mechanism. My experimental data therefore indicate that there is an epigenetic control mechanism of *FMR1*/FMRP expression in human granulosa cells that is functionally associated with the rate of E2F1 binding to CpG94 located in *FMR1*-DMR3 and that its impairment probably interferes with women ovarian reserve.

FMR1-UMR a completely CpG unmethylated region, covered the *FMR1* minimal promoter and the CGG repeat block in exon1. CpG sites located within *FMR1*-UMR were demethylated on both gene alleles but only in granulosa cells indicating that *FMR1* transcription is activated on both alleles in these cells. Escape from X inactivation seemed to be focused on *FMR1*-UMR, since outside of this region, the CpG sites methylation pattern reflected the presence of one CpG methylated and one unmethylated allele, respectively three differentially methylated regions coined DMR1, DMR2 and DMR3, respectively.

Analysis of the complex splicing pattern of the *Anstisense FMR1 gene* (*ASFMR1*), a long non coding RNA expressed in antisense direction, revealed three novel and probably granulosa cell specific initiation sites characterized by at least 8 different *ASFMR1* transcript splice forms in human granulosa cells, not previously described in the literature. Similar to *FMR1*, *ASFMR1* expression varied between patients with different ovarian reserve. Taken together, these observations suggest that in addition to the CpG methylation control of *FMR1* expression, *ASFMR1* expression may also contribute to the variable ovarian reserve observed in patients entering the *in vitro* fertilization (IVF) clinic.

Analysis of putative signal pathways involved in the regulation of *FMR1*-gene expression in human granulosa cells, by microarray assays after *FMR1* gene knock down revealed 748 genes with significant differential expression. They could be grouped into 7 main signal pathways covering a wide range of regulatory networks, including cell cycle regulation, apoptosis, mRNA decay and vesicle transport. Among the most important signal pathways is the PI3K/AKT/mTOR pathway already known to be involved in primordial follicle activation and follicular pool maintenance. Inhibition of *FMR1* gene expression induced an increase of *mTOR*, *AKT*, *S6K* at both transcripts and protein levels. Most interesting *S6K* expression reached a statistical significant difference at both mRNA (p=0.05) and protein level (p=0.03). Another identified signal pathway was the methionine salvage pathway (MTA). This pathway is highly conserved from yeast to human and was reported to be involved in *Drosophila* fecundity. These results provide new starting points to study functional *FMR1*/FMRP expression in human folliculogenesis and ovarian reserve.

Zusammenfassung

Ziel dieser Doktorarbeit war es, epigenetische Kontrollmechanismen der *FMR1*-Genexpression an humanen Granulosazellen zu untersuchen.

Durch eine systematische Analyse des CpG-Methylierungsmusters entlang des *FMR1* Promotors in der COV434-Zellinie (Modelsystem) und in primären humanen Granulosazellen durch Sequenz-Analyse wurden vier unterschiedliche Regionen mit einem einzigartigen CpG-Methylierungsmuster detektiert: "*FMR1*-UMR, *FMR1*-DMR1, -DMR2 und – DMR3, von denen zwei (*FMR1*-DMR1 und -DMR2) bereits früher in Leukozyten gefunden wurden. Interessanterweise enthielt *FMR1*-DMR3 eine doppelte Bindungstelle für den Transkriptionsfaktor E2F1, an der dieser lediglich bei unmethylierten CpG-Dinukleotiden binden kann. Ich habe experimentell bestätigt, dass E2F1 an dieser Sequenz von *FMR1*-DMR3 nur dann gebunden wird, wenn ein unmethyliertes CpG in Position 94 enthalten ist. In humanen primären Granulosazellen von Frauen mit unterschiedlicher Eizell-Reserve (NOR; POR) erschien die Methylierungsrate in *FMR1*-DMR3 abhängig von dieser ovariellen Reserve. Diese Daten deuten daher darauf hin, dass die epigenetische Kontrolle der *FMR1* Expression in Granulosazellen funktionell mit der Bindung von E2F1 an *FMR1*-DMR3 verbunden ist und, dass dies einen Einfluss auf die ovarielle Reserve der Frau haben könnte.

FMR1-UMR bezeichnet eine neu entdeckte unmethylierte CpG Region im *FMR1*-Gen, die den minimalen Promotorbereich und den CGG-Repeat in Exon1 umfasst. Alle CpGs der *FMR1*-UMR waren auf beiden Allelen des Gens, aber nur in Granulosazellen, demethyliert, was impliziert, dass *FMR1* in diesen Zellen auf beiden Allelen transkribiert wird. Die Abwesenheit der sonst auf dem X Chromosom üblichen Inaktivierung eines Gen-Allels war auf die *FMR1*-UMR beschränkt. Außerhalb dieser Region wird das typische CpG-Methylierungsmuster eines methylierten und eines unmethylierten Gen-Allels gefunden, beziehungsweise drei differentiell CpG methylierte Regionen genannt DMR1, DMR2 und DMR3.

Die Analyse des *Antisense FMR1 Gens* (*ASFMR1*), einer langen nicht kodierenden RNA in Antisense Richtung zu *FMR1*, ergab drei neue und wahrscheinlich granulosazellspezifische Initiationsstellen, die durch mindestens 8 verschieden gesplicte *ASFMR1* Transkripte in menschlichen Granulosazellen charakterisiert werden, welche nicht vorher in der Literatur beschrieben wurden. Ähnlich wie bei *FMR1* variiert die *ASFMR1* Expression zwischen Patienten mit unterschiedlicher ovarieller Reserve. Zusammenfassend deuten die Ergebnisse darauf hin, dass neben der Kontrolle durch *FMR1* auch *ASFMR1* einen Einfluss auf die variable ovarielle Reserve von Patientinnen in der Kinderwunschbehandlung hat.

Die Analyse vermeintlicher Signalwege, die bei der Regulation der *FMR1*-Gen-Expression in menschlichen Granulosazellen involviert sind, durch Microarray Analyse nach *FMR1* Gene Knock-Down ergab 748 Gene mit signifikant unterschiedlicher Expression. Davon konnten 7 Haupt-Signalwege, die eine breite Palette von regulatorischen Netzwerken umfassen, involviert bei der Zell-Zyklus-Regulierung, der Apoptose, des mRNA decay und des Vesikeltransports. Zu den wichtigsten Signalwegen gehört der PI3K/Akt/mTOR-Signalweg, der bereits bekannt ist, bei der Aktivierung primordialer Follikel und ihrer Reifung eine wichtige Rolle zu spielen. Die Inhibierung der *FMR1* Gen-Expression führte zu einer Zunahme der Expression von mTOR, Akt und S6K sowohl auf Transkript- als auch auf Protein-Ebene. S6K Expression erreichte hierbei einen statistisch signifikanten Unterschied sowohl bei der mRNA ($p = 0.05$) als auch bei der Protein-Expression ($p = 0.03$). Als ein weiterer potentiell wichtiger Signalweg für die Eizell-Reifung wurde der Methionine Salvage Pathway (MTA) erkannt. MTA ist von der Hefe bis zum Menschen konserviert; bei *Drosophila* wurde nach seiner Beeinträchtigung von einer Verringerung der Fruchtbarkeit berichtet. Die in dieser Studie gefundenen experimentellen Resultate liefern neue Ansatzpunkte, für die funktionelle Analyse der *FMR1*/FMRP Expressionsregulation in der menschlichen Follikulogenese und zur ovariellen Reserve.

“If you are working on something that you really care about, you don’t have to be pushed. The vision pulls you.”- Steve Jobs

Contents

List of figures

List of tables

Abbreviations

°C	Dgree Celsius
µ	Micro-
A	Adenosine
AFC	Antral Follicles Count
AM	Amplicon Methylated primer
AMH	Anti Müllerian hormone
AR	*Androgen Receptor*
ASFMR1	*Antisense of the FMR1 gene*
AU	Amplicon unmethylated primer
bp	base pair
BSP	Bisulifite -conversion Specific PCR
C	Cytosin
cDNA	Complementary DANN
COS	Controlled Ovarian Stimulation
CpG	5'-C-phosphate-G-3'
Ct	Cycle treshhold
Ctrl	Control
DNA	Desoxyribonucleic acid
dATP	Desoxyadenosin-5'-triphosphate
dCTP	Desoxycytidin-5'-triphosphate
dGTP	Desoxyguanosin-5'-triphospate
dNTPs	Deoxynucleoside-5'-triphospahate
DORs	Diminished Ovarian Reserves
DTT	Dithiothreitol
dTTP	Desoxythymidin-5'-triphosphate
EMSA	electrophoretic mobility shift assay
FISH	Fluorescence In Situ Hybridization
FITC	Fluorescein isothiocyanate
FMR1	*Fragile X Mental Retardation 1-gene*
FMR1-DMR	*FMR1* differentially methylated region
FMR1-UMR	*FMR1* unmethylated region
FMRP	FMR protein
FREE	Fragile-X-Epigenetic Element
FSH	Follicle Stimulating Hormone
FXPOI	Fragile X POI
FXS	Fragile X Syndrome
FXTAS	Fragile X-associated Tremor/Ataxia Syndrome
G	Guanine
g	Gramm
gDNA	geomicDNA
GSP	Gene Specific Primer
h	hour(s)
H. sapiens	Human
H2O	Water
HPRT	Hypoxanthine-guanine phosphoribosyltransferase
IVF	*In vitro* Fertilization
kb	kilobase
KH	K-homology RNA-binding domains
l	liter
lncRNA	long non-coding RNA
M	Molar
m	Milli-

MB	methylation boundary
min	minute(s)
miRNA	micro RNA
mRNA	messanger RNA
MSP	Methyl Specific PCR
MTA	Methionine salvage pathway
n	Nano-
n.a.	not applicable
NAT	Natural Antisense Transcript
NOR	normal responders
O.N	Overnight
ORF	Open Reading Frame
PAS	Polyadenylation site
PCR	Polymerase Chain Reaction
PCOS	Polycystic Ovarian Syndrome
PGCs	Primordial Germ Cells
pH	pH-value
PM	Pre-Mutation
POI/POF	Premature Ovarian Insufficiency/Failure
POR	Poor Responders
p-value	probability value (significance)
RLM-RACE	RNA Ligase Mediated Rapid Amplification of cDNA Ends
RNA	Ribonucleic Acid
rpm	rounds per minute
RT	Room Temperature
RT-PCR	Revervse Transcription-PCR
s	second(s)
siRNA	Short interfering RNA
T	Thymin
TF	Transcription Factor
TSS	Transcriptional Start Site
U	Uracil
U	Units
UTR	Untranslated Region
v/v	volume/volume
X	times
XIST	*X-inactive specific transcript*

1. Introduction

1.1. Human female fertility

Human female fertility can be defined by the functional quality and quantity of oocytes in the follicles during female's reproductive life cycle[1]. According to the world health organization, female infertility or subfertility is defined by the inability of a woman to become pregnant, the inability to maintain a pregnancy or the inability to carry a pregnancy to live birth (http://www.who.int/topics/infertility/en/ 2017). Female infertility is multifactorial and can be due to social factors, genetic factors, endocrinological factors and autoimmune diseases and other reasons[2-8]. It is estimated that for 40% to 50% of couples, subfertility may result from factors affecting women[8].

1.1.1. Folliculogenesis

Folliculogenesis is the process of activation and growth of primordial resting follicles in order to release a mature oocyte, which can be fertilized[9]. In human during embryogenesis the primordial germ cells (PGCs) migrate into the genital ridge. Once arrived in the ridge, these cells become surrounded by a layer of supporting somatic cells. In women with 46, XX karyotype, the PGCs will differentiate into oocytes. The oocyte will be blocked at prophase I of the first meiosis while the supportive cells will differentiate into granulosa cells (4-4.5 gestational months). The ovaries become discernible at this stage. This will constitute the primordial follicles pool of a female for her lifetime[7; 10; 11].

Shortly after ovaries colonization a first wave of primordial follicles will leave the resting pool. This recruitment is unidirectional and irreversible. It is marked by a modification in germ cells morphology (from squamous to cuboidal). Immediately a first wave of primordial follicles is recruited for activation. The transition from primordial to primary follicles is not yet fully understood. Based on the mouse model, a number of activating and inhibiting factors play a role to fine- tune this process[7; 12] (Figure 1). This transition is independent from follicle stimulating hormone (FSH) expression[7; 13].

After birth, follicles continue their maturation. Granulosa cells actively proliferate which will increase FSH receptor expression; follicles increase in size and layers of theca cells (stromal cells) will surround granulosa cells. The subsequent follicle transition phases are called: secondary, preantral and antral follicle phases. Follicle development up to and including early antral development are independent of the pituitary gonadotrpins, FSH and LH[14; 15]. Only the antral/late antral follicle development is gonadotropin dependent. FSH expression then

stimulates granulosa cell proliferation, prevents granulosa cell apoptosis, promotes estradiol production and LH-receptor expression[14]. Granulosa cells then differentiate into two cell types: cumulus cells, that are in direct contact with the oocyte and mural cells (cell type used in this thesis) that are lining the follicular wall. The most developed follicle (which has the highest number of FSH receptors) will become dominant (i.e. will be selected for ovulation). Mural granulosa cells of the dominant follicle will secrete inhibins which block FSH secretion by a negative feedback loop mechanism. As a result the other antral follicles that are still FSH dependent developing will degenerate by apoptosis[15].

After oocyte ovulation, the post ovulatory follicle will develop to the corpus luteum. If pregnancy occurs the corpus luteum will be maintained and produces progesterone (corpus luteum cells are former granulosa cells) for the first pregnancy trimester. In the absence of pregnancy it will regress to a corpus albicans and disappear completely over time[15].

The process of primordial follicle recruitment is continuous during women reproductive life cycles until menopause. Once a follicle leaves the resting pool it is also subjected to atresia at all developmental stages or, respectively, to ovulation. At each stage many factors play a role in controlling which follicle will continue development or degenerate[7; 13]. Genetic factors playing an important role in different stages of follicular development, fertilization and implantation (mainly by functional studies in mice) are illustrated in Figure. 1[7].

The most important somatic cell type are granulosa cells (cell type used in this thesis) that are crucial for oocyte growth, meiosis maturation and thereby regulating oocytes' transcriptional activities. However, development of the follicles requires a bidirectional communication between oocytes and surrounding granulosa cells[13; 16]. This dialogue takes place via their cytoplasmic extensions and gap junctions[16; 17].

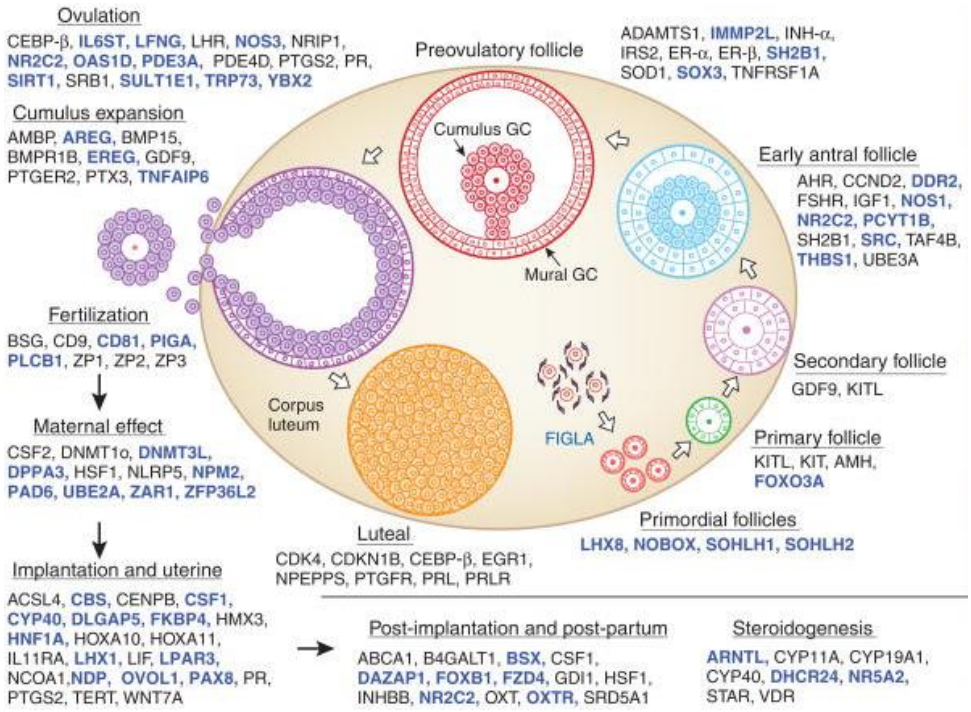

Figure 1: Genetic dissection of female fertility pathways (based on mouse model).
The different stages of the follicles development are presented (see section 1.1). From primordial follicle recruitment till ovulation and even in fertilization and implantation, a number of key genes are involved to ensure proper development and oocyte maturation. *The following picture is a direct copy from Matzuk et al.,*[7].

1.1.2. Ovarian reserve/response

Ovarian reserve refers to the quantity and quality of the ovarian primordial follicle pool[18]. This pool serves as a source of developing follicles and oocytes. From a peak of 6–7 million at 20 weeks of gestation, the number of oocytes falls radically down that there approximately 300,000 to 400,000 remaining oocytes per ovary at birth[19; 20]. During reproductive years in humans, the decline in the number of primordial follicles remains steady at about 1,000 follicles per month and accelerates after the age of 37, causing ovarian aging (resulting in menopause)[21]. Over the last years, some ovarian reserve tests have been used to diagnose the woman's remaining follicular pool, including measurement of gonadotropins (FSH), Anti Müllerian hormone (AMH) and the antral follicles count (AFC) by ultrasound[22; 23]. One major cause of female infertility in many couples is accounted to Diminished Ovarian Reserves (DOR). This is manifested by a limited reproductive lifespan in women due to reduction in the quantity of ovarian follicular pool and affects women from different age groups and risk increases physiologically with age[24-26]. Major factor determining the success of infertility treatment in DOR patients' is their response to controlled ovarian stimulation (COS) applied in the *in vitro* fertilization (IVF) clinic. Patients with DOR show generally a poor response to COS and are therefore called poor responders (POR)[24; 25]. POR patients are at risk of lower

pregnancy rate compared to patients with normal ovarian reserve/response called normal responders (NOR) from the same age group[26]. The most severe form of DOR is the premature ovarian insufficiency/failure (POI/POF; POF; MIM: 615723) syndrome[27]. Clinically, POI/POF patients develop oligoamenorrhoea or amenorrhea with an increased level of FSH (>25 IU/ ml for POI[28]) before the age of 40[29].

1.2. Genetic factors impacting folliculogenesis and ovarian reserve

Many genes have been reported to be crucial for optimal ovarian maintenance. Interestingly, these genes seem to be concentrated on the X chromosome[30; 31]. In women up to 15% of X-linked genes are bi-allelically expressed[32]. Women carrying one X chromosome (Turner Syndrome) suffer from accelerated depletion of their follicular poo already before birth[33]. This led to the assumption that important ovarian development genes are located on the X chromosome[32]. In addition, the requirement of biallellic gene expression from both X-chromosomes was further supported from reports of women with POI/POF carrying different X-chromosome deletions and translocations (reviewed in Fassnacht et al.,[27]). Three major regions X chromosomal regions with genes functional in expression of POF-syndrome were identified: *POF1* (Xq26-q28) and *POF2* (Xq13.3-q22) and *POF4* also called Turner syndrome locus[34] (Xp11.2-p22.1) (Figure 2). The most prominent X-gene associated with the POI/POF syndrome is the *Fragile X Mental Retardation 1*-gene[35] (*FMR1*, MIM 309550) located in *POF1* (Xq27.3).

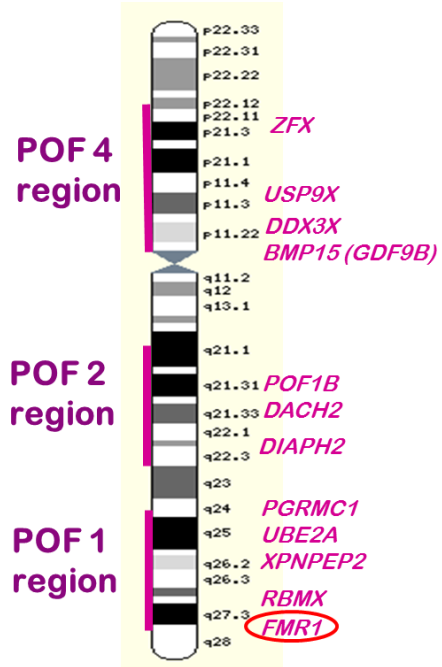

Figure 2: Multiple genetic loci for maintenance and progression of human folliculogenesis are located on the X chromosome.
According to the OMIM database they are summarized under *POF1* (OMIM: #311360) with *FMR1* (highlighted with a red circle) as the most prominent POF candidate gene (because most frequently mutated), *POF2* (OMIM: #300511 and #300604) and *POF4* (OMIM: #300247) Associated POF candidate genes, i.e., genes known to be expressed during human folliculogenesis of which some were already found with mutations in women with POI/POF syndrome are listed at the right (*Figure and legend are copied from Vogt et al.*,[34]).

1.2.1. The *FMR1* gene

The *FMR1* gene, located within *POF1* region, was first identified in 1991 through positional cloning[35]. It contains 17 exons spanning 38 kb[36]. The *FMR1* gene produces a 4.4 kb mRNA with an open reading frame (ORF) of 1.9 kb, plus up to 16 isoforms resulting from alternative splicing[37]. The most common splicing events involve the inclusion or exclusion of exon 12 and 14 and the use of different splice acceptors located in exons 15 and 17[38]. The gene is characterized by presence of variable CGG-triplet numbers (26<n<32 in general population[39]) in the 5′-untranslated region of exon1[35]. The expansion of the CGG triplet block to the range of 55 to 200 repeats has been called Pre-Mutation (PM), because CGG triplet numbers above 54 repeats become unstable and much longer CGG triplet blocks (500-2000 repeats) can occur in the next generation[39] causing the fragile X syndrome (FXS; OMIM 30955). In women, the presence of a *FMR1*-PM allele has been associated with the onset of fragile X-associated tremor/ataxia syndrome (FXTAS; OMIM 300623)[40; 41] and Fragile X POI (FXPOI; MIM 311360)[29; 42] or POI/POF[42] respectively. Expansion of the CGG triplet block to more than 200 repeats is usually associated with DNA hypermethylation at CpG sites of the promoter region which leads to an epigenetic silencing of the gene, resulting in the lack of its protein translation, the FMR protein (FMRP)[35; 43] (Figure 3).

1.2.2. FMR-protein (FMRP)

FMRP, a 632amino acids protein is the main product of *FMR1* expression[44]. In mouse brain up to 12 different isoforms of FMRP exist due to *FMR1* transcripts alternative splicing[45]. FMRP was first described in brain as a RNA binding protein that regulates translation of target mRNAs associated with neuronal development[46]. Recent reports suggested that FMRP may also bind to noncoding RNA (*BC1* rodent specific) as well[47]. FMRP function can be modulated by phosphorylation. The phosphorylated FMRP mostly inhibits translation of associated mRNA targets including its own mRNA[48; 49]. FMRP involvement in the miRNA pathway require the association of the non-phosphorylated form with the Dicer complex[48; 49] . FMRP harbors two K-homology RNA-binding domains (KH1 and KH2 encoded by exons 8-10 and exon 13), an arginine glycine glycine (RGG) high affinity RNA-binding domain encoded by exon15, a nuclear export signal (encoded by exon 14), Tudor domains (encoded by exon 3) and a nuclear localization signal (encoded by exons 5 and 6)[50-54]. Therefore, splicing and removal of exons encoding one or more of these functional motifs may have a major impact on protein function and localization[55-57].

FMRP expression is affected by the dynamic expansion of the CGG triplet block into the PM range, where elevated *FMR1*-PM mRNA levels are accompanied by reduced FMRP levels suggesting a negative feedback loop[58; 59].

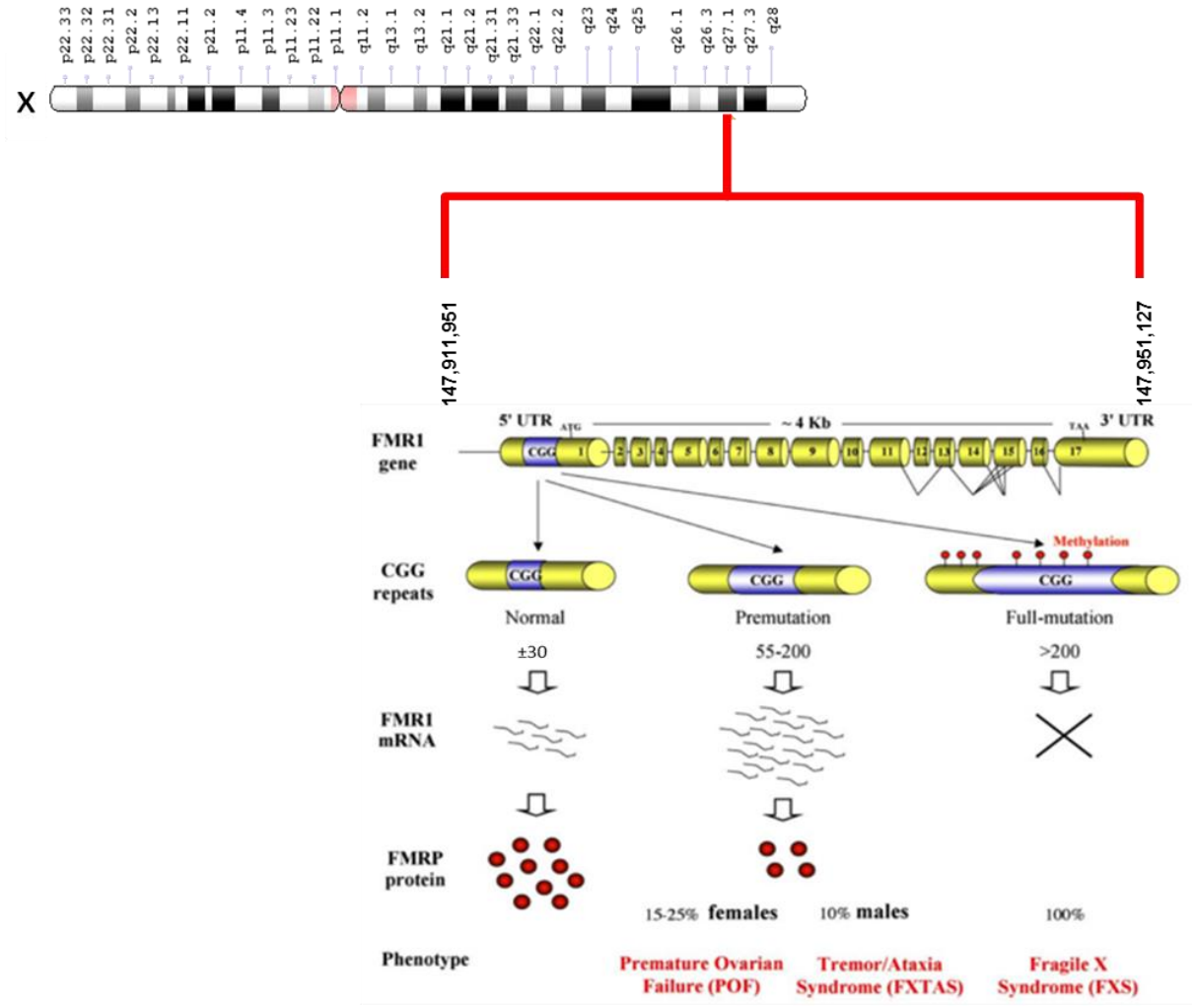

Figure 3: Molecular structure of the *FMR1* gene.
The *FMR1* gene (NC_000023.11:147,911,951-147,951,127 *H. sapiens*) consists of 17 exons represented by yellow cylinders. Major splicing sites involving exons 12, 14, 15 and 17 are indicated. The CGG triplet block repeat located in the 5' UTR of exon1 is indicated by a violet cylinder. Three classes of *FMR1* alleles and their associated phenotypes are presented. CGG triplet repeats ranging around 30 repeats lead to normal *FMR1* mRNA transcription and translation, and normal function of FMRP. The PM range (55-200 repeats) is associated with elevated *FMR1* mRNA transcription and reduced FMRP expression. Presence of the PM increases the risk of developing FXTAS in males or FXPOI or POF in females. When the CGG triplet repeats exceeds 200 repeats, the *FMR1* gene is silenced due to hypermethylation. Absence of FMRP leads to the FXS (*Figure is adapted from Zalfa et al.[47]).*

1.2.3. *FMR1* gene implication in folliculogenesis

a- Influence of the size of the CGG triplet block

FMR1 gene expression, is supposed to be functional also during folliculogenesis. Women carrying an *FMR1*-PM allele (55 <CGG< 200 repeats) display increased *FMR1* expression in

their leukocytes and granulosa cells have a risk of around ~20% to develop POI/POF also called FXPOI[42; 60]. Yet, it is not known why the development of FXPOI ovarian dysfunction is limited to *FMR1*-PM allele carriers and the underlying pathogenesis of FXPOI is still under investigation.

Several studies[61-65] proposed a toxic gain of function of the elevated *FMR1*-PM mRNA as was observed in brain of women diagnosed with FXTAS and carrying an *FMR1*-PM allele[40; 41]. In the brain tissue of female carrying an *FMR1*-PM allele, the excess of *FMR1*-PM mRNA was proposed to induce the formation of intranuclear neuronal and astrocytic inclusions probably resulting from aberrant protein binding to specific hairpin structures (resulting from the extended CGG triplet block) within the 5′ UTR of *FMR1*-PM message within the nucleus[66; 67]. The sequestration of the *FMR1*-PM message in nucleus was proposed as causative agent of the elevated rate of transcription. Accordingly, by investigating the expression of up to 16 *FMR1* isoforms in leukocytes from normal and PM allele carriers, Pretto et al.,[37] reported an up to eight fold increase in expression of nuclear isoforms (lacking both exons 12 and 14) in leukocytes of *FMR1*-PM carriers which further supports the nuclear sequestration theory of *FMR1*-PM messages. However, Tassone et al.,[58] showed in male lymphoblastoid cell lines that *FMR1* mRNA was mainly located in the cytoplasm for both normal and *FMR1*-PM alleles, ruling out the observed nuclear sequestration phenotype as a contributing factor for the elevated mRNA levels[58].

In women leukocytes the presence of a *FMR1*-PM allele is also associated with increased levels of *FMR1*-PM mRNA and decreased levels of FMRP[58] suggesting the presence of a negative feedback *FMR1*/FMRP control loop. Beilina et al.,[68] identified multiple *FMR1* transcriptional initiation sites (TSS) in most *FMR1*-PM-transcripts located upstream of the main TSS used for transcription of gene alleles carrying a normal range of CGG triplet numbers. It suggests some influence of the CGG repeat number on the transcriptional start site in the *FMR1* promoter.

The negative feedback loop control of *FMR1*/FMRP expression was found to be present also with *FMR1* transcripts including CGG triplet number below the PM range[69]. Investigations performed with human neuronal and fetal kidney cell lines showed that with a CGG triplet block size higher than 30 repeats FMRP expression decreased, while *FMR1* expression is slightly increased[69]. However, *FMR1* transcripts with CGG triplet number below the normal range showed a lower expression rate in these cell lines associated with an increase of their transcription rate[69]. These data suggest that the CGG repeats may act as a translational modulator of the *FMR1* transcripts[69]. It has been assumed that causative agent for reduced

FMRP levels may be a decrease in translation efficiency due to ribosome stalling of *FMR1* transcripts with extended CGG repeat block. Folding of the *FMR1* 5'UTR including the CGG repeat block transcripts into quadruplex structures was recently shown for human embryonic kidney cells[70]. Such structures also decrease their translation efficiency.

Variations in *FMR1* expression levels were also observed in leukocytes from POI/POF patients not carrying a CGG-PM allele[71]. Accordingly, it has been postulated that even a small deviation in the normal CGG triplet repeats number from the normal range ($26<n<32$)[39] has some impact on human ovarian reserve and fertility[72-75]. Patients carrying shorter CGG triplet block ($n < 26$) were suggested to be more prone to have lower follicular reserve[72-74]. Based on expression observations in female leukocytes, Gleicher et al.,[72] suggested a possible implication of *FMR1* expression in follicular recruitment, although expression of *FMR1* in the female germline has not been yet studied up to now.

These findings remain controversial since there were not observed in other studies[76; 77].

b- POI/ POF animal models

More insight about the involvement of *FMR1* CGG-PM allele in the development of POI/POF was provided from studies performed *in vivo* with several mouse models carrying an *FMR1*-PM allele[78-80].

Hoffman et al.,[78] reported that increased *fmr1*-PM (CGG n=130) transcripts were associated with a faster loss of follicles and the presence of ovarian abnormalities involving both the oocytes and GCs. Similar observations were reported in ovaries of mice carrying *fmr1*-PM (CGG n=98) on both alleles[79]. Both studies revealed that *FMR1*-PM transcripts expression impaired folliculogenesis after birth probably interfering with the follicular development phase. Another mouse POF model created with a human transgene carrying an *FMR1*-PM allele. In the ovaries of these animals, increase of human *FMR1-PM* transcript level was again associated with reduction in the number of growing follicles and impaired fertility[80]. The impairment in phosphorylation of key protein elements involved in the Akt/mTOR (Activated protein kinase B/ mammalian target of rapamycin) pathway in the ovaries of these mice led the authors to hypothesize the presence of a functional link between the presence of human *FMR1*-PM transcript expression and the mTOR pathway[80].

In vitro experiments mainly performed using mouse mouse models showed that two cellular pathways are essential for activation of primordial follicles and their further development: the PI3K /Akt (intacellular Phosphoiosid 3 kinase/ activated protein kinase B) pathway[81 82; 83] and mTORC1 pathway[7; 81-83]. Endpoint of both signaling pathways is phosphorylation of S6K1 (ribosomal protein S6 kinase polypeptide) that controls the translation of mRNA via

stimulation of ribosomes leading to follicle activation[84]. The *PI3K/Akt* pathway is activated by growth factors such as kit ligand and a cascade of enzymatic reactions that results in AKT phosphorylation for activation. Phosphorylated AKT will in turn phosphorylate its downstream effector FOXO3 (Forkhead box O3). This leads to its translocation to the cytoplasm. Unphosphorylated FOXO3 acts as a transcription repressor[85]; *foxo3* knockout mice have an excessive recruitment of primordial follicles and suffer from follicles depletion at an early age[85]. The importance of FOXO3 on primordial follicle depletion was also observed in pig and bovine ovaries[86; 87].

Although all these studies reveal potential implication of the *FMR1* gene and the mTORC/ PI3K /Akt in murine folliculogenesis, little is yet known about their implication in human folliculogenesis. In human ovaries, FMRP is mainly expressed in GCs after birth[71]. So far only one study reported a potential functional link between *FMR1*/FMRP expression and the AKT/mTOR signalling pathway in a human proliferating granulosa cell model system not carrying an *FMR1*-PM allele[88].

1.3. Epigenetic regulation of *FMR1* gene expression

Epigenetic defines all heritable changes in gene expression not coded within the DNA sequence itself but by methylation of distinct nucleotides; mainly CpGs and the post-translational modification of histones sites[89; 90]. Epigenetic mechanisms contribute to stabilize cell type-specific gene expression[89]. Four major levels of epigenetic controls have been identified: DNA methylation, histone modification, chromatin remodeling and non-coding RNAs[90; 91]. In this thesis, I will put the focus on the epigenetic control of *FMR1* gene expression by CpG methylation and by long non-coding RNA (lncRNA) expression.

1.3.1. CpG methylation and CpG islands

CpG methylation is defined by addition of a methyl group at the 5' position of cytosine residues located within the dinucleotide CpG in the DNA sequence, established by DNA methyltransferases[92-95]. In the human genome, differentially CpG methylation mainly occurs in the genes promoter regions but also in the gene body (exons and introns) and in intergenic regions[96]. The majority of CpG dinucleotides concentrated in CpG islands[97]. It has been shown that the pattern of CpG site methylation has an impact on the control of gene expression. For example, CpG methylation located in close proximity of the TSS blocks transcription initiation, whereas methylation of CpG sites located in the gene body seem to help in transcription elongation and might be also involved in their splicing processes[93; 98].

In the literature there is no standard definition for CpG islands. Bird et al.,[97] defined CpG islands as stretches of DNA roughly 1000 base pairs long that have a higher CpG density than the rest of the genome and are often not methylated. Gardiner-Garden and Frommer.,[99] defined CpG islands as 200-500 base pair DNA stretches with a CG content greater than 50%. CpG islands usually encompass the promoter, the first exon, and sometimes also the first intron of a gene[100]. Promoters having CpG islands are usually, when transcriptionally active, non-methylated and characterized by nucleosome-depleted regions at their TSS[92] and their gene expression level is usually controlled by specific transcription factors that bind to their CG rich regions[94]. It can be assumed that CpG islands possess a functional importance since their location among the genome seems to be conserved throughout evolution[101]. Methylation of CpG islands is a mechanism used to repress gene transcription such as for genes located on the inactive X chromosome[93; 102]. Possible mechanisms leading to gene silencing associated with CpG sites hypermethylation include the loss of transcription factors binding within the promoter region[103; 104] and the formation of an inactive chromatin structure which facilitates transcriptional silencing[105].

1.3.2. CpG island in the *FMR1* promoter

The functional *FMR1* promoter includes a CpG island[106]. The CpG rich promoter lacks a canonical TATA box, but includes three initiator-like sequences located within the minimal core promoter. The minimal core promoter has been estimated with an extension of 131 bases upstream of the main TSS[107]. The conserved downstream regions may represent regulatory elements in the first intron, but they have not been studied in detail so far[107]. This core promoter sequence seems to be evolutionary conserved across human, chimpanzee, macaque, dog and mouse[107]. It contains several restriction enzyme methylation sensitive cutting sites and five conserved evolutionary DNA footprint patterns which include consensus binding sites for various positive regulator proteins of *FMR1* transcription: α-Pal/Nrf-1, Sp1, Sp1-like, USF1/USF2 and E-box[106-108]. Interestingly, the binding of α-Pal/Nrf-1 and USF1/USF2 transcription factors was shown to be functionally influenced by CpG methylation[107]. The putative functional sequence promoter domains include upstream a long CpG island bordered at the 5' side by a methylation boundary zone (MB) that acts as a transition zone to the hypermethylated upstream genomic region of both alleles[109; 110]. Downstream, the proposed functional *FMR1* promoter domain extends probably to intron1[111].

Methylation of the *FMR1* promoter CpG island associated with the expansion of the CGG triplet block interferes with *FMR1* transcription by directly preventing the binding of

transcription factors within the core promoter[107]. Since CpG hypermethylation is accompanied by a number of modifications in histone N-tails, also the chromatin structure is modified[112]. In addition, it has been postulated that inactivation of the *FMR1* gene by CpG methylation could be initiated by down-regulation of transcription and chromatin modifications prior to CpG methylation in human embryonic stem cells[113] and through the binding of methyl-CpG structures[92]. However, silencing of *FMR1* by CpG methylation of the promoter region was also reported to occur independently of the presence of the CGG triplet block repeat[114]. This suggests that size of the CGG triplet block is not the only epigenetic factor controlling *FMR1* gene expression.

It is important to note that most epigenetic studies described the association of CpG methylation within the *FMR1* promoter and gene its expression with male patient DNA probes or male cell lines that have only one X chromosome. Only few studies[109-111; 115; 116] investigated the influence of CpG methylation status within the *FMR1* promoter region on gene expression in leukocytes and brain tissue of women carrying normal or expanded CGG triplet block alleles.

Using direct bisulfite sequencing analysis, Naumann et al.,[109; 110] showed the presence of a mosaic CpG methylation pattern in the region located between the MB and the CGG triplet block in leukocytes of women carrying normal and *FMR1*-PM allele,. This mosaic pattern probably reflected the disparity of CpG methylation levels on the two female X chromosomes, one being highly CpG methylated and the other CpG unmethylated or hypomethylated[109; 110]. However, variation of *FMR1* expression in leukocytes of these women in relation to CpG methylation patterns in the *FMR1* promoter was not explored.

In brain tissues of two sisters carrying one *FMR1*-PM allele, development of FXTAS was correlated with the activation ratio of the *FMR1* gene, which reflects the degree of CpG methylation of the promoter region[115]. Similar findings were reported in a larger cohort of women (82 patients), in which the activation ratio of the *FMR1* gene was dependent on the size of the CGG triplet block and probably contributed to the onset of FXTAS[116]. A correlation between the activation status of the PM *FMR1* allele and FXPOI manifestations was also reported from an assessment performed in leukocytes of three sibling pairs with similar *FMR1* expansions, but different FXPOI phenotype[117]. This discordance in the FXPOI phenotype was suggested to be associated with a variable X-inactivation rate of the *FMR1*-PM allele. However the X-inactivation ratio in leukocytes does not necessarily resemble that of the ovarian tissue.

Recently, two epigenetic control elements located outside the minimal core promoter region were mapped to the extended *FMR1* promoter domain because also contribute to the transcription efficiency of *FMR1* in women leukocytes[111]. They were designated Fragile-X-Epigenetic Element-1and-2 (FREE1 and FREE2) respectively[111; 118]. FREE1 contains 10 CpG sites whereas FREE2 contains 12. Godler et al[111; 119] found that the methylation pattern of specific CpG sites located in these elements influence FMRP expression levels in women's leukocytes. In addition, single CpG methylation patterns within FREE1 and FREE2 were also found to be dependent on the size of the CGG triplet block in exon 1[119; 120]. Although these FREE elements were found to be present also in other female somatic cells[111], they were not yet studied in female germline cells.

1.3.3. Long non-coding RNA (lncRNAs) expression in folliculogenesis

Another mechanism to regulate gene expression involves long non protein coding transcripts located on the same (sense) or the antisense DNA strand in the form of antisense transcripts. It is believed that these RNAs might affect gene expression by triggering histone modifications and DNA methylation including heterochromatin formation[91].

Expression of lncRNAs is involved in the regulation of protein encoding gene transcription stability, in splicing, in subcellular localization and in translational efficiency[121]. LncRNAs, are characterized as ncRNAs with more than 200 nucleotides[122]. The transcription of lncRNA can be initiated from introns, promoters, exons and 3'end regions from both sense and antisense strands of protein-coding genes[122]. In the past few years, several lncRNAs were proposed to be important for human folliculogenesis as they were associated with proper oocyte growth and maturation e.g *NEAT1*, *MALAT-1*, *GAS5*, *XIST* and *OIP5-AS1*[123; 124]. In addition, differential expression patterns of several lncRNAs were reported to play a role in the differentiation of ovarian somatic cells, granulosa and cumulus cells[124; 125]. In human ovarian cumulus cells, the aberrant expression of several lncRNAs (*XLOC_011402*, *ENST00000454271*, *ENST00000433673*, *ENST00000450294*, and *ENST00000432431*) was found to be associated with a folliculogenesis disorder, the polycystic ovarian syndrome (PCOS)[126]. Furthermore, the expression level of the lncRNA *AK124742* in these somatic cells showed a correlation with the embryo quality in women undergoing infertility treatments and was, therefore, proposed to be used as potential biomarker for embryo selection[127]. In mouse ovarian granulosa cells, an increased expression of the lncRNA-*Meg3* promoted the inhibition of granulosa cells proliferation and led to premature ovarian failure[128].

Four lncRNAs seem to be associated with the *FMR1* gene locus: the *Antisense of the FMR1 gene* (*ASFMR1*), *FMR4*, *FMR5* and *FMR6* [129-132] (Figure 4). Only *FMR5* is located sense-

oriented upstream of the TSS of *FMR1* (Figure 4). *ASFMR1*, *FMR4* and *FMR6* levels seem to be influenced by the length of the CGG triplet repeats in *FMR1* exon 1[129; 130; 132]. Only *FMR5* expression was found to be independent of the size of the CGG triplet block[131]. *ASFMR1* and *FMR4* use the same promoter domain of the *FMR1* gene. In contrast to *FMR4*, *ASFMR1* displays complex alternative splicing process and its transcription could also be initiated also downstream of the CGG triplet repeats in intron 2 of the *FMR1* gene[130]. *FMR6* overlaps with exons 15–17 including the 3'UTR of the *FMR1* gene. Thereby, its transcript uses the same acceptor/donor splicing sites as *FMR1* exons 15, 16 and 17 and starts in its 3'UTR[131].

All of these lncRNAs associated with *FMR1* seem to be expressed in a wide range of tissues. In human ovarian tissues, *FMR4* and *FMR6* expression was analyzed in primary granulosa cells[133]. Both transcripts were found to be highly expressed in these somatic cells, although *FMR4* was not identified in ovarian tissue earlier[129]. Expression of *ASFMR1* and *FMR5* transcripts in human granulosa cells have not yet been investigated so far.

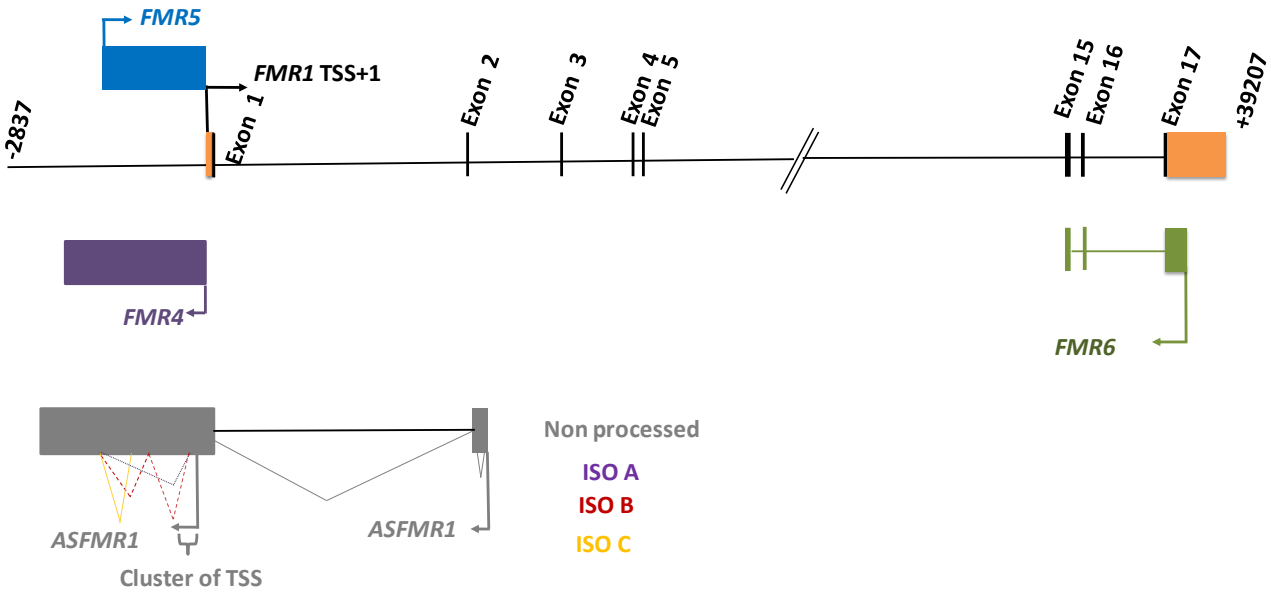

Figure 4: Schematic view of lncRNAs transcripts associated with *FMR1* gene.
The horizontal axes are formed by the intronic sequence, and the numbered vertical filled boxes represent the exons. 5' and 3' UTRs of the *FMR1* gene are shown in orange. The arrows represent the TSS of *FMR5* (blue), *ASFMR1* (grey), *FMR4* (purple), *FMR1* (black), and *FMR6* (green) genes. All genomic positions are indicated according to the TSS +1 of the *FMR1* gene. The four isoforms (Non- processed, ISO A, B and C) and the PM specific transcript of the *ASFMR1* gene identified in leukocytes[130] are indicated.

2. Aims of the thesis

Major aim of my thesis was to investigate the complexity of epigenetic control elements involved in the expression of *FMR1* in human granulosa cells in order to reveal the potential contribution of *FMR1* gene expression during follicular oocyte maturation. In addition, I wanted to explore whether expression of this gene may affect differences in women ovarian response after controlled ovarian stimulation during the in vitro fertilization protocols used in any IVF clinic.

For this purpose,

- the CpG methylation pattern of the extended *FMR1* promoter in a human granulosa cell line, COV434, was analyzed in order to confirm its usefulness as a model system for human primary granulosa cells, usually only available in small amounts from the IVF laboratory.
- Expression pattern of *ASFMR1* lncRNA expressed in antisense from the *FMR1* locus in human leukocytes was analyzed in COV434, to judge its putative contribution to the epigenetic control of *FMR1* besides the CpG methylation pattern.

After confirmation of COV434 as model system for *FMR1* gene expression in primary granulosa cells, it was used:

(a) for the analyses of putative variabilities of the observed CpG site methylation pattern in primary granulosa cells of women with a variable ovarian response.

(b) for EMSA studies using COV434 nuclear protein extracts to identify first putative transcription factors binding to differentially methylated CpG sites.

(c) for functional knockdown of *FMR1* in these cells by an optimal siRNA expression protocol to reveal putative signal pathways expressed in human granulosa cells interacting with *FMR1*/FMRP during ovarian maturation.

3. Material

3.1 Equipment

Table 1: Equipment used in this study

name	supplier
ABI PRISM 3100 Genetic Analyzer	Applied Biosystems, USA
Accu-Jet Pro	Brand, Germany
Agilent 2100 bioanalyzer	Agilent, USA
Autoclave 3870 ELV	Tuttnauer, Netherlands
Bacterial incubator shaker IH 50 K/15/500	Noctua, Germany
Bench centrifuge TMC 1601012	NeoLab, Germany
Biophotometer No. 613101974	Eppendorf, Germany
Blotting and transfer system Serva	Serva, Germany
Blotting System, CTI	CTI, Germany
Cell culture bench HERASAFEKSP Typ KSP 12	Herasafe KSP, Germany
Centrifuge cooling Heraeus FRESCO 21	Thermo fisher scientific, USA
Cryotank GT55	Air Liquide Cryotechnik, Germany
Digestorium Weiler 0179	Weiler, Germany
Electrophoresis Chamber CTI	CTI, Germany
Fluorescence microscope Spectra Cube Model CCD-1300DS	Leica, Germany
Freezer -20°C	Liebherr, Germany
Freezer -80°C NapCOIL UF600	Napco, USA
Freezer -80°C NapCOIL UF650	Napco, USA
GS GENE linker™	BioRad, Germany
Homogenisator Ultra Turrax T8	IKA Labortechnik, Germany
Icemachine Scotsman AF 80	Scotsman, USA
Incubator for bacteria Typ 1511530000202 No 950373	WTB Binder Germany
Incubator for cell culture CB 150 #05-8892	WTB Binder Germany
Magnetic stirrer MR2000	Heidolph, Germany
Magnetic stirrer RCT	IKA Labortechnik, Germany
Microcentrifuge Typ 1-14 #10014	Sigma, Germany
Microscope DIAVERT 114191	Leitz, Germany
Microwave Sharp Express R-239	Sharp, Germany
Milli-Q biocel Water system A10	Millipore, Germany
Nanodrop Spectrophotometer ND-1000	peqLab, Germany
pH-Meter Calimatic 761	Knick, Germany
Plate centrifuge 2019R	Napco, USA
Plate shaker LS10	Gerhardt, Germany
Power Supplies 500V 0,5A	Fischer, Germany
Scale EW 150-3M	Kern, Germany
Spectral photometer LS 500	Dr. Lange, Germany
sonifier cell disruptor Branson B15	Branson sonic power co Germany
SRX-101A Film developper	Konica, Japan
T1 Thermocycler PCR machine	Biometra, Germany
TaqMan machine 7500 Fast Real Time PCR-System	Applied Biosystems, USA
T-Gradient PCR machine	Biometra, Germany

Thermoblock QBT2	Grant instruments, England
Thermoblock TDB-120	Biosan, Lettland
Thermomixer comfort	Eppendorf, Germany
UV plate reader Photometer	Anthos labtec instruments, Germany
UV-Imager GelDoc2000	BioRad Germany
UV-Transilluminator IL-200-M	Bachhofer, Germany
Vortex-Mixer Reax 2000	Heidolph, Germany
Water bath GFL 1083	GFL GmbH, Germany

3.2 . Chemicals

Table 2: Chemicals and reagents used in this study

name	supplier, catalog number
Acetic acid (100%)	Roth, Germany #3738
Acrylamide 30%	Roth, Germany #3029.1
Agar	Roth, Germany #5210.3
Agarose	Biozym, Germany #840004
Ampicillin Sodium	AGS GmbH, Germany #101195
Ammoniumperoxodisulfat (APS)	Roth, Germany # 9592.1
Anti Anti (Antibiotic/Antimycotic) 100x	Thermo fisher scientific, USA #15240-062
Bacto Yeast Extract	Becton Dickinson, USA #212750
Bacto Trypton	Becton Dickinson, USA #211705
β-ME (2-Mercaptoethanol), 99%	ICN Biomedicals, USA #806443
Biorad Protein Assay	BIORAD, Germany #500-0006
Boric acid	Sigma-Aldrich, Germany#31146
Bromphenol blue	Sigma-Aldrich (Merck), Germany #69010
BSA (Bovine Serum albumin, Albumin Fraktion V)	Roth, Germany#8076.4
Calcium chloride ($CaCl_2$-$2H_2O$)	Merck, Germany #611TA143982
Chloroform	Fluka, Germany #25690
D-(+)-Glucose	Merck, Germany #620K1261442
DAPI	Thermo fisher scientific, USA #62247
DABCO	Sigma-Aldrich (Merck), Germany #D2522
Desoxyribonucleotides (dNTPs)	Bioron, Germany #110012
DMEM (Dulbecco Modifiziertes Eagle Medium) + L-Glutamine, low Glucose	Biochrom, Germany #FG0415
DMSO (Dimethylsulfoxide)	Serva, Germany #20385
DTT (1,4-Dithiothreitol)	Sigma-Aldrich, Germany #D-8255
EDTA (Ethylendiamintetraacetat)	Roth, Germany #8043
Ethanol absolute	Roth, Germany #9065.2
Ethanol denaturated	Roth, Germany #K928.4
Ethidiumbromid	Serva, Germany #21238
FCS, heat activated	Thermo fisher scientific, USA #10500064
Formaldehyde, 37%	Sigma-Aldrich GmbH, Germany #252549
Gene Ruler™ 100bp DNA ladder plus	Fermentas, USA #SM0322
Gene Ruler™ 1000bp DNA ladder plus	Fermentas, USA #SM0311
GeneRuler Ultra Low Range DNA Ladder	Thermo fisher scientific, USA #SM1211

Glycerin, 100%	J.T. Baker (Avantor), Germany #7044
Glycine 1M Solution	Sigma-Aldrich GmbH, Germany #67419
H_2O Ampuwa	Fresenius Kabi, Germany, #6605508
H_2O Aqua ad injectabilia	B. Braun Melsungen AG, Germany #2351744
H_2O destilled RNAse free	Thermo fisher scientific, USA #10977035
HCl (37%)	Merck, Germany #1.00317.2500
HiPerFect Transfection Reagent	Qiagen GmbH, Germany #301705
HPLC-water	J.T. Baker (Avantor), Germany #4218
Isopropanol (2-Propanol)	Roth, Germany #9866.2
L-Asparagine	Sigma-Aldrich (Merck), Germany #A4159
Lipofectamine® RNAiMAX Transfection Reagent	Thermo fisher scientific, USA #13778075
Lipofectamine-2000 Reagent	Thermo fisher scientific, USA #11668027
Magnesium chloride ($MgCl_2$)	Roth Germany #2189.1
Magnesium sulfate ($MgSO_4$)	JT. Baker USA #0168
Methanol 99,9%	Roth, Germany #4627
MOPS (3-[N-Morpholino]-propanesulfonic acid)	AppliChem, Germany#A1076
Orange G	Merck, Germany #A1404
PBS w/o $CaCl_2$ and $MgCl_2$	Thermo fisher scientific, USA #14190-094
PGEM-T Easy Vector	Promega, USA #A1360
PMSF (Phenylmethylsulfonylfluoride)	Roth, Germany #6367.3
PageRuler Plus Prestained Protein Ladder	Fermentas, USA #SM1811
Potassium Chloride (KCl)	Baker USA #0509
SDS (Natriumdodecylsulfate, ultrarein)	Serva Germany #20763
TEMED	Roth, Germany #2367.3
Sodium acetate	Roth, Germany #6773
Sodium chloride (NaCl)	Roth, Germany #3957.1
Sodium hydroxide	Roth, Germany #6771
TaqMan Uiversal PCR Master Mix, no AmpErase UNG	Thermo fisher scientific, USA #4364343
Tris-Borate-EDTA buffer (5x)	Sigma-Aldrich, Germany #T7527-4L
Tris EDTA Buffer Solution pH = 8	Sigma-Aldrich, Germany #93283
TRIS (Tris-[hydroxymethyl]-aminomethane)	Roth, Germany #4855
Trypan blue	Serva, Germany #47285
Trypsine/EDTA-Solution (10x)	Biochrom AG, Germany #L2153
Tween 20	Gerbu, Germany #2001.0500
X-Gal (5-Bromo-4-Chloro-3-Indoyl-ß-D-Galactoside)	Promega, USA #V394

3.3 Consumables

Table 3: Consumables used in this study

name	supplier
Adhesive sealing cover for sequencing plates	Neolab, Germany
Cryotubes	Nunc, Germany
Microplates Luminomator 96-Well Format	Berthold, Germany
Gloves TouchNTuff	Ansell, Germany
Parafilm	Pechiney, USA
Pasteur serological pipettes	WU-Mainz, Germany

PCR-plates for sequencing, 96-Wells, 0.2ml	Nerbe Plus, Germany
PCR reaction tubes	Biozym, Germany
Petri dishes	Greiner, Germany
Pipette Tips 10, 20, 200, 1000µl	Steinbrener, Germany
Pipette Tips with filter	Stein Labortechnik, Germany
Reaction tubes	Starstedt, USA
RN ase free tubes	AppliChem, Germany
UV-cuvettes	Neolab, Germany
Cell culture flasks	Sarstedt, USA
Drigalski glas column	Neolab, Germany
Neubauer Cell counter	LO Laboroptik, Germany
Combitips 0,1 - 0,2 - 0,5 - 10ml	Eppendorf, Germany
Dispenser for combitips	Eppendorf, Germany
Rainin Encode tips 0,1ml sterile	Steinbrenner, Germany
Rainin Encode tips 0,5ml sterile	Steinbrenner, Germany
Filterpapier MN 827 B	Macherey-Nagel, Germany
Nylon Membran, positiv charged	Roche Diagnostics, Germany
PVDF Membrane	Immobilon Membran; Millipore, USA
Adhesive cover for PCR plates	Applied Biosystems, USA
Tubes 15, 50 ml	Sarstedt, Germany
X-ray films **Syringe filter 0.2µm**	Konica Medical Films, Germany Sarstedt, Germany

3.4 . Kits

Table 4: Kits used in this study

name	**supplier, catalog number**
ABI Big Dye™ Terminator v1.1 Cycle Sequencing RR100	Applied Biosystems #4336768
ABI High-Di™ Formamide	Applied Biosystems #4311302
CST-PathScan Phospho mTOR Sandwich ELISA Kit	New Englan Biolabs #7976C
CST-PathScan Phospho-Akt Sandwich ELISA Kit	New Englan Biolabs #7252
CST-PathScan total AKT1 Sandwich ELISA Kit	New Englan Biolabs #7170C
CST-PathScan total mTOR Sandwich ELISA Kit	New Englan Biolabs #7974C
CST-PathScan total p70 S6K Sandwich ELISA Kit	New Englan Biolabs #7038
EpiTect Bisulfite Kit	Qiagen, Hilden #59104
FirstChoice™ RLM-RACE Kit	Thermo fisher scientific #AM1700
Human FMR1/FMRP ELISA-Kit	Biozol Diagnostica #LS-F9020-1
NE-PER Nuclear and Cytoplasmic Extraction Reagents	Thermo fisher scientific #78833
Nuclear Extraction Kit 200 rxns	Biocat GmbH #SK-0001-SO
NucleoSpin® Triprep	Macherey-Nagel #740966:50
One Step PCR Kit	Quiagen GmbH #210212
PGEM®-T Easy Vector	Promega #A1360
Protein Quantification Assay	Macherey-Nagel #74096250
QIAprep® Spin Miniprep Kit	Qiagen, Hilden #27106
Rneasy Minikit	Qiagen, Hilden #74106

Signosis E2F-1 Emsa-Kit-Gel shift Kit 30 rxns	Biocat GmbH #GS-0011-SO
Signosis Emsa-Kit-Gel shift Kit 30 rxns	Biocat GmbH #GS-0000-SO
Wizard DNA Clean-Up System	Promega #A7280
Western Lightning® Plus-ECL	PerkinElmer #NEL10400EA

3.5 . Enzymes

Table 5: Enzymes used in this study

name	supplier, catalog number
Taq PCRx DNA Polymerase	Invitrogen #11508-017
GO Taq DNA Polymerase	Promega #M300B
M-MLV Reverse Transcriptase	Promega #M368C
Pfu DNA Polymerase	Promega #M7774
Proteinase K	Merck, Darmstadt #1245680500
RNase free DNase Set	Qiagen, Hilden #79254
RNase A	Invitrogen #12091021
Rnase H	Promega #M428C
SuperScript™ III Rnase H- Reverse Transcriptase	Invitrogen #18080-093
SupersScript® VILO™	Invitrogen #100002279
Taq DNA Polymerase	Invitrogen #10342-020
***T4* DNA Ligase**	Promega #M180A
***T4* DNA Polymerase**	Fermentas # EP0061

3.6 . Antibodies

Table 6: Antibodies used in this study

name	supplier, catalog number
FMRP	Euromedex (mAb1C3)
Anti-Histone H3	Abcam (ab 9053)
Anti-GAPDH	Santa Cruz (sc-25778)
Peroxidase-AffiniPure Goat Anti-Rabbit IgG,	Jackson (111-035-046)
Peroxidase AffiniPure Goat Anti-Mouse IgG	Jackson (115-035-062)

3.7 . siRNAs

Table 7: siRNAs used in this study

name	supplier, catalog number
siRNA *FMR1* homo 10919	Thermo fisher scientific AM16708
siRNA *FMR1* homo 11010	Thermo fisher scientific AM16708
Silencer Select Pre-Designed si RNA *FMR1*	Thermo fisher scientific 4392420 ID: s5316
Silencer Select Negative Control 1	Thermo fisher scientific 4390843

3.8 . Buffers and Solutions

Ampicillin, 50mg/ml: 5g of ampicillin sodium salt were dissolved in 100ml of H_2O (Ampuwa) and passed through a 0.2µm syringe filter. The solution was aliquoted and stored at -20°C.

dNTP, 10mM: For 100 µl, 10µl of 100mM dATP, dCTP, dGTP and dTTP were mixed with 60µl of H_2O (Ampuwa) and stored at -20°C.

LB-Medium (Luria-Bertani): 10g of Bacto Tryptone, 5g of yeast extract and 5g of NaCl were dissolved in 950ml of Milli-Q H_2O. The solution was autoclaved and stored at room temperature. For minipreps, the medium was supplemented with 50µg / ml of ampicillin.

LB-Agar plates: 10g of Bacto Trypton, 5g yeast extract, 5g NaCl and 16g agar were dissolved in 1liter (l) of Milli-Q-H_2O, autoclavated and cooled to 56°C. Subsequently ampicillin (100µg / ml) and 2% X-Gal were added. 10cm petri dishes were filled with 20ml of LB agar and stored at 4°C.

SOC-Medium: 20g Bacto Trypton, 5g Yeast extract, 0.6g NaCl and 0.2g KCl were dissolved in 1l Milli-Q H_2O. The solution was then autoclaved. For each 100ml medium, 1M $MgSO_4$ (sterile), 1ml 1M $MgCl_2$ (sterile) and 2ml 1M D-(+)-Glucose were added.

Lysis-buffer for gDNA extraction from granulosa cells: 40mM Tris buffer pH 7.8, 20 mM sodium acetate, 1mM EDTA, 1%SDS and H_2O (Ampuwa) were mixed in a final volume of 100ml.

Lysis-buffer for gDNA extraction from leukocytes: 1l solution contained a final concentration of: 155 mM NH_4Cl (8.29g), 10mM $KHCO_3$ (1 g) and 0.1mM Na_2EDTA (200µl 0.5M solution). pH was adjusted using glacial acetic acid solution to 7.4.

10X TAE buffer: 1l solution contained a final concentration of: 40mM Tris-Acetat pH 7,8, 1mM EDTA and 18.6g of Na_2EDTA. pH was adjusted to 7.2.

SE buffer : 1l solution contained a final concentration of: 75mM NaCl (4.39 g) and 25mM Na_2EDTA (8.41g). pH was adjusted to 8.0.

Saturated NaCl: NaCl was dissolved in water until a sediment is formed, and subsequently autoclaved

RLT + β-Mercaptoethanol: 10µl β-Mercaptoethanol in 1ml RLT-Puffer (RNeasy Mini Kit)

3M Sodium acetate: 61.5g of sodium acetate were dissolved in 250ml of distilled water. pH was adjusted to 4.3.

Anode buffer I: 1l solution contained a final concentration of: 0.3M Tris and 10% methanol. pH was adjusted to 10.4.

Anode buffer II: 1l solution contained a final concentration of: 0.025M Tris and 10% methanol. pH was adjusted to 10.4

Cathode buffer: 1l solution contained a final concentration of: 0.025M Tris, 0.040M ammonium caproic acid and 10% methanol. pH was adjusted to 9.4.

TNT buffer 1X: 1l solution contained a final concentration of: 50mM Tris, 150mM NaCl, 5mM EDTA, and 0.05% Tween 20. pH was adjusted to 7.6.

3.9 . Cell lines and human tissues

The COV434 cell line: was derived from a 27-year-old woman suffering from a solid granulosa cell tumour. It shares characteristics with proliferating granulosa cells such as FSH-dependency, 17β-oestradiol production, the formation of intercellular connections[134]. This cell line was grown in DMEM medium supplemented with 10%FBS and 3mM L-asparagine.

gDNA for CpG methylation studies was also extracted from PBS pellets of **female fibroblasts (06FO31)**, from primary female tissues (**primary granulosa cells and leukocytes**) and from tissues (**female kidney and ovary**).

The DH5α bacterial strain: was used for all cloning experiments. Genotype: F-Φ80*lac*ZΔM15 Δ(*lac*ZYA-*arg*F) U169 *rec*A1 *end*A1 *hsd*R17 (rK-, mK+) *pho*A *sup*E44 λ-*thi*-1 *gyr*A96 *rel*A1.

3.10 . Oligonucleotides and primers

Table 8: Oligonucleotides and primers used in this study

***H. sapiens FMR1* gene region (147,911,046-147,912,539) (Figure 12)**					
name	sequence 5‘ to3‘	genomic position		type	CpG site covered
A9	TATAGTGGAATGTAAAGGGTTGT	147,911,046	F	BSP	-5 to 5
A9	CCAAAATAACCCAAACTTTTAT	147,911,526	R	BSP	-5 to 5
A1M	AGAGGTCGAATTGGGATAATC	147,911,609	F	MSP	11 to 18
A1M	ACGATAACAAATCGCACTACCT	147,911,683	R	MSP	11 to 18
A1U	TAGAGAGGTTGAATTGGGATAATT	147,911,607	F	MSP	11 to 18
A1U	AAAACAATAACAAATCACACTACCT	147,911,685	R	MSP	11 to 18
A2M	CGAGGTAGTGCGATTTGTTATC	147,911,672	F	MSP	16 to 32
A2M	GCATACGCGCTACTAAAAACC	147,911,794	R	MSP	16 to 32
A2U	GTGAGGTAGTGTGATTTGTTATT	147,911,671	F	MSP	16 to 32
A2U	C ACATACACACTACTAAAAACC	147,911,799	R	MSP	16 to 32
A3M	TTCGGTCGGTTTTTAGTAGC	147,911,766	F	MSP	29 to 36
A3M	ACGTCACGTAATCAACGCTA	147,911,860	R	MSP	29 to 36
A3U	TATTTTGGTTGGTTTTTAGTAGT	147,911,762	F	MSP	29 to 36
A3U	ACCACATCACATAATCAACACTA	147,911,865	R	MSP	29 to 36

A4M	GGGTTCGGTTTTAGTTAGGC	147,911,910	F	MSP	46 to 65
A4M	CTAACAACGACGCCTCC	147,912,036	R	MSP	46 to 65
A4U	GGGGGTTTGGTTTTAGTTAGGT	147,911,908	F	MSP	46 to 65
A4U	CCCTAACAACAACACCTCCA	147,912,038	R	MSP	46 to 65
A10	TAGTTTYGTTTYGGTTTTATT	147,911,934	F	BSP	36 to 72
A10	CATCTTCTCTTCAACCCTACTAAC	147,912,161	R	BSP	36 to 72
A5M	GTAGTTTATTTTTCGGGGGC	147,912,128	F	MSP	72 to 77
A5M	AAACCAAATACCTTATAAAAAACGC	147,912,243	R	MSP	72 to 77
A5U	AGTTTATTTTTTGGGGGTGG	147,912,126	F	MSP	72 to 77
A5U	AACCAAATACCTTATAAAAAACACC	147,912,244	R	MSP	72 to 77
A6M	TTTTTTTTTTGGTGTCGGC	147,912,278	F	MSP	79 to 92
A6M	CTATCGAAATGAGAGACCAGCGA	147,912,457	R	MSP	79 to 92
A6U	TTTTTTTTTTTTTGGTGTTGGT	147,912,276	F	MSP	79 to 92
A6U	CCTCACTAATCTCTCATTTCAATAAAC	147,912,459	R	MSP	79 to 92
A7M	GGGGTTTTTTTTTCGAGTATC	147,912,310	F	MSP	82 to 92
A7M	TCGCTAATCTCTCATTTCGA	147,912,457	R	MSP	82 to 92
A7U	GGGGTTTTTTTTTTGAGTATT	147,912,310	F	MSP	82 to 92
A7U	TCACTAATCTCTCATTTCAA	147,912,457	R	MSP	82 to 92
A8M	CGATTTCGAGAGGTTTTAGC	147,912,412	F	MSP	88 to 101
A8M	CCCGACTCTATACCTACCGC	147,912,539	R	MSP	88 to 101
A8U	TTTGATTTTGAGAGGTTTTAGT	147,912,409	F	MSP	88 to 101
A8U	CCCAACTCTAATACCTACCACC	147,912,539	R	MSP	88 to 101

X78592.1 *H.sapiens* DNA for *AR* promoter: 5570-5750 (Figure15)

name	sequence 5‘ to3‘	genomic position		type
AR1	TTTAGGGTTAGAGTTAGTTTTTTT TGTTTT	5570–5599	F	BSP
AR2	CCTCCTCTACCTATAAACTTACTC	5833–5856	R	BSP

5’RLM RACE primers NC_000023.11:147,911,951-147,951,127 *H. sapiens FMR1* gene region (Figure 9)

name	sequence 5‘ to3‘	genomic position	
5‘ outer adaptor primer	CGCGGATCCGAACACTGCGTTTGCTGGCTTTGATG AAA		F
5‘ inner adaptor primer	TTTCAGTGTTTACACCCGCAG		F
3’outer GSP	CTCGCCGTCGGCCCGCCGCC	147,9120,097	R
3’inner GSP	CCTCCACCGGAAGTGAAACCGAAA	147,9120,018	R

Oligonucleotides used for EMSA (Figure20)

Name	Sequence 5‘ to3‘
E2F CG84 non-methylated	TTCTCTTTCGGCGCCGAGCCC
E2F CG84 non-methyatedl complementary	GGGCTTGGCGCCGAAAGAGAA
E2F CG84 mutated	TTCTCTTTCTTTTCCGAGCCC

E2F CG84 mutated complementary	GGGCTTGGAAAAGAAAGAGAA
E2F biotin CG84 non-methylated	5' Biotin-TTCTCTTTCGGCGCCGAGCCC
E2F biotin CG84 non-methylated complementary	5' Biotin-GGGCTTGGCGCCGAAAGAGAA

NC_000023.11:147,909,431-147,911,817, complement *H. sapiens AFMR1* gene region (Figure22, 24)			
name	sequence 5‘ to3‘	genomic position Relative to *FMR1* TSS+1	
-1805F	CTGAAAACAAGGACCCTGTAGGGACTGA	-1805	F
-1000F	CAGTGTCTGGCACACGATAGATGCTC	-1000	F
-274R	GGTGCACTCAGTGGCGTGGGAAATC	-274	R
-196R	GGTGGAGGGCGGGAAGGCTGAAGGG	-196	R
+15F	GCTCAGCTCCGTTTCGGTTTCACTTCCGGT	+15	F
+59R	CAGAGGCGGCCCTCCACCGGAAGTG	+59	R
+210F	CCCGCAGCCCACCTCTCGGGGGCG	+210	F
+295R	AGCCCCGCACTTCCACCACCAGCTCCTCCA	+295	R
+10028F	AGGATGTTCATGAAGATTCAATAAG	+10028	F
+10243R	AGCAGAAACAGTCATTCCATTAG	+10243	R
+13848R	ATCTGCCTATCAGGCTGCCA	+13848	R

5’RACE primers *ASFMR1* (Figure 23)			
+210F	CCCGCAGCCCACCTCTCGGGGGCG	+210	
-258F	CTGGCCCTCGCGAGGCAGTGCGAC	-258	
Sequencing primers			
pUC/M13	CAGGAAACAGCTATGAC	176-192 from T7	F
pUC/M13	GTAAAACGACGGCCAGT	2956-2972 from T7	R

***FMR1* isoforms (Figure10, 11)**			
name	sequence 5‘ to3‘	position	
A For	TGGCTTCATCAGTTGTAGCAGG	exon 12	F
A Rev	TCT CTC CAAACG CAA CTG GTC	exon 14	R
B For	GAGGAGCTGGTGGTGGAAG	exon 1	F
B Rev	CAGAATTAGTTCCTTTAAATAGTTCAGG	exons 13-15	R
C For	TCCAGAGGGGTATGGTACCATT	exons 11-13	F
C Rev	GCTTCAGAATTAGTTCCTGAAGTATATCC	exon 14	R
D For	TCCAGAGGGGTATGGTACCATT	exons 11-13	F
D Rev	CAGAATTAGTTCCTTTAAATAGTTCAGG	exonx 13-15	R
E For	GTGAGGGTGAGGATTGAGGC	exon 11	F
E1 Rev	ACTAATTCTGAAGCATCAAATGCT	exon 15	R
E2 Rev	CACTGAGTTCGTCTCTGTGGT	exon 15	R
E3 Rev	TCCCTCTCTTCCTCTGTTGGA	exon 15	R

TaqMan Probe	Company	Catalog number
TaqMan Gene Expression Assay ***HPRT1***	Thermo fisher scientific	#4331182 Assay Hs99999909_m1
TaqMan Gene Expression Assay ***AR***	Thermo fisher scientific	#4331182 Assay Hs00171172_m1
TaqMan Gene Expression Assay ***FMR1***	Thermo fisher scientific	#4331182 Assay Hs00924544_m1
TaqMan Gene Expression Assay ***AKT1***	Thermo fisher scientific	#4331182 Assay Hs00178289_m1
TaqMan Gene Expression Assay ***mTOR***	Thermo fisher scientific	#4331182 Assay Hs00234508_m1
TaqMan Gene Expression Assay ***S6K***	Thermo fisher scientific	#4331182 Assay Hs00177357_m1
TaqMan Gene Expression Assay ***XIST***	Thermo fisher scientific	#4331182 Assay Hs01079824_m1

3.11 . Vectors

pGEM® -T easy Vector

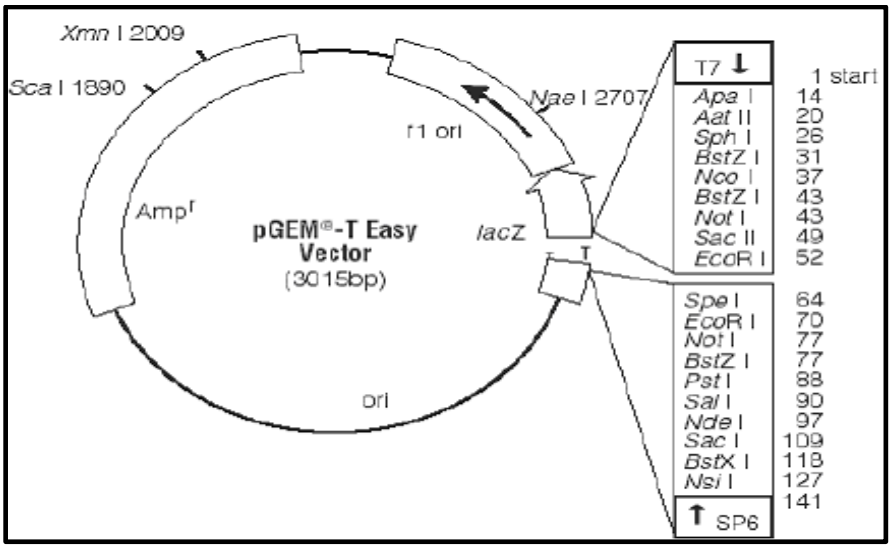

Figure 5: PGEM®-T easy map and sequence reference points. This figure is a direct copy from: https://www.promega.de//media/files/resources/protocols/technical-manuals/0/pgem-t-and-pgem-t-easy-vector-systems-protocol.pdf- 2017

3.12 . Databases and software

ECR browser: https://ecrbrowser.dcode.org/xB.php?db=hg19.

USCS genome browser: http://genome.ucsc.edu/cgi-bin/hgTracks?db=hg38.

Methyl Primer Express software v1:

https://www.google.de/search?source=hp&q=methyl+primer+express+software+v1+0&oq=methylprimer+software.

National Center for Biotechnology Information (NCBI): http://www.ncbi.nlm.nih.gov.

Primer Blast:

https://www.ncbi.nlm.nih.gov/tools/primerblast/index.cgi?LINK_LOC=BlastHome.

Ensembl Genome Browser: http://www.ensembl.org.

Chromas 2.2.: for sequences analysis after Big-Dye-Sequencing (license provided by the laboratory).

geneXplain platform (TRANSFAC):

http://www.cisreg.ca/cgibin/tfe/articles.pl?tfid=131&tab=tfbs.

MicrosoftOffice: MS Excel, Word and PowerPoint 2010 (license provided by the clinic)

SPSS 20: for statistical analysis (license provided by the clinic)

Sequence alignment using Clustal W2: https://www.ebi.ac.uk/Tools/msa/clustalw2/.

JASPAR: transcription factors database, http://jaspar.genereg.net/.

4. Methods

Part of Methods are copied from Youness et al., (manuscript submitted)

4.1. Gene expression analysis

Primer design for Reverse transcription-Polymerase Chain Reaction (RT-PCR) assays

Primers used in RT-PCR, nested PCR and gene specific PCR (GSP-PCR) were designed using NCBI primer Blast website. Whenever possible, RT-PCR primers were designed encompassing at least two exonic regions to avoid any possible PCR products by contamination with gDNA that can occur during RNA extraction.

RNA extraction

Total RNA was extracted from cells PBS pellets using the RNAeasy mini kit as described in the kit protocol manual. Extracted RNA was digested on Shredder column using DNAse I to ensure the removal of gDNA. Quality and concentration of extracted RNA were measured using a Nanodrop®.

cDNA synthesis

For cDNA synthesis, total mRNA was reverse transcribed (RT) using oligo$(dT)_{15}$-primer and the Moloney Murine Leukemia Virus (M-MLV)-enzyme. This method was used to select for mature and polyadenylated fraction of mRNA. Briefly, 1µg of mRNA was mixed with 2µl oligo$(dT)_{15}$-primer and brought up to a final volume of 14µl with RNAse free H_2O. Samples were incubated 5 min at 70°C. Subsequently, samples were transferred to ice for 5 min prior to the addition of 5µl RT-buffer, 1.25µl dNTP-mix, 1µl M-MLV enzyme and 3.75µl of RNase free H_2O. Samples were incubated for 10 min at 40°C, 50 min at 42°C, 15 min at 70°C. Residual RNA was then degraded by adding 1µl of RNase H and incubated for additional 20 min at 37°C. cDNA was stored at -20°C.

For gene specific RT, the oligo$(dT)_{15}$-primer was replaced with the a gene specific primer and the Superscript™ III enzyme was used. This method selected preferentially synthesis of the gene of interest and was used for the lncRNAs study (Chapter 3). Briefly, 1µg total RNA and 1µl of 2µM GSP and 1µl 10mM dNTP mix, made up to 13µl with RNase free H_2O. Samples were incubated at 65˚C for 5 min and then transferred to ice for 1 minute. Subsequently, 4µl 5X Superscript™ III-First-Strand Buffer, 1µl 0.1M Dithiothreitol (DTT), 1µl RNaseOUT™ and 1µl Superscript™ III RT were added. Samples were then incubated for 60 minutes at 55˚C. Enzyme was then inactivated by incubation at 70˚C for 15 min. cDNA was stored at -

20˚C. The quality of the cDNA synthesis was checked by performing a PCR for the *Beta-Actin* gene.

PCR

All PCR reactions for transcript analysis (RT-PCR) were set up using 1µl of the prepared cDNA (40ng), 3.75µl 10X *Taq*- Polymerase buffer (without Mg^{++}), 1.25µl $MgCl_2$, 0.25 µl dNTP mix, 0.25µl forward primer, 0.25µl reverse primer, 0.3µl *Taq*-Polymerase (5U/µl) and made up to a final volume of 25µl with sterile H_2O. PCR reactions were carried out using the following thermal cycling conditions: 1 cycle at 95°C for 4 min; 35 cycles (4 min at 95°C, 30 s at 95°C, 45 s at annealing temperature (59-63°C) for 45s, 50 s at 72°C, and a final elongation for 4 min at 72°C).

For nested PCR, 1µl of the first PCR product was used as template. The reaction mix was set up as previously described using 0.5µl of each forward and reverses nested primers.

For GSP-PCR, primer used for cDNA synthesis was used as forward primer and another GSP primer was used as a reverse primer.

Real time PCR

10ng of cDNA was used as template for TaqMan®- real time PCR. Briefly 2.75µl master mix containing TaqMan®- probes and the corresponding universal master mix were added to 2.25µl cDNA. The mix was pipetted into a 96 well plate sealed by a plastic cover. Gene expression measurements were performed in 7500 Fast Real Time PCR-System using the following cycling conditions: 15 min at 95°C and 45 cycles at 60°C. All reactions were performed in triplicates. Data analysis was performed using the comparative ΔΔCt method[135].

Rapid Amplification of cDNA Ends (5'RLM-RACE and 3'RACE)

RACE is a PCR based technique which allows the cloning of full length cDNA sequences[136] starting at the cap site (5') and ending after the Polyadenylation Start Site (PAS) in the 3'UTR. RACE results in the production of a cDNA copy of the RNA sequence of interest, produced through reverse transcription, followed by PCR amplification of the cDNA copies at the 5' and 3' ends respectively. The amplified cDNA copies are sequenced and should map to unique genomic regions. RNA Ligase Mediated Rapid Amplification of cDNA Ends (RLM-RACE) represents a major improvement to the classic RACE technique. RLM-RACE is designed to improve amplification of cDNA only from full-length, capped mRNA, usually producing only a single band after PCR. 5' and 3' end of *FMR1* and *ASFMR1* genes were analyzed using the FirstChoice RLM-RACE Kit using published methods[68; 130; 137]. PCR products were ligated into the pGEM®-T Easy Vector and sequenced afterwards.

4.2. CpG site methylation analysis

The human cell lines, primary tissues and DNA samples used in this work for the analysis of CpG methylation patterns are listed in Materials section 3.9.

Extraction of genomic DNA (gDNA) from primary cells and PBS pellets

The gDNA was extracted using an optimized protocol for small cell numbers. Briefly, cells were suspended in 200µl lysis buffer (40mM Tris buffer pH 7.8, 20 mM sodium acetate, 1mM EDTA and 1%sodium dodecyl sulfate). After addition of 66µl of sodium chloride (5M), samples were centrifuged at 16000 g for 10 min. The supernatant was transferred into a new tube and one volume of phenol:chloroform:isoamyl alcohol (25:24:1) was added. After centrifugation at 14000g for 3 min the aqueous layer was transferred to new tubes and DNA was precipitated with 90% ethanol and 0,3M sodium acetate overnight at -20°C. The next day samples were centrifuged 10 min at 14000g. Precipitated DNA was washed with 70% ethanol and again re-centrifuged. Finally, DNA was air-dried and re-suspended in 20µl nuclease free water.

Extraction of gDNA from leukocytes

Blood was collected from patients using EDTA tubes. 5ml from the blood was transferred to 50 ml falcon, 15ml of cold SE Lysis buffer were added, and cells were lysed for 30 min on ice. The lysate was centrifuged at 1200 rpm for 10 min at 4°C. Supernatant was then discarded and cell pellet was washed with SE Lysis buffer and re-centrifuged until a white pellet was obtained. The pellet was resuspended using 5ml of warm SE buffer, 40µl Proteinase K and 250µl of 20% SDS. The mix was incubated overnight (O.N) at 37°C. The next day, an ethanol precipitation was performed. Briefly, 10ml of SE buffer and 3.3ml of saturated NaCl and were added to the cell lysate and then centrifuged 5 times at 3000 rpm for 15 min at RT. After each centrifugation the supernatant was transferred to a new falcon. gDNA was then precipitated by adding 1.7ml Na-Acetate (3M) and 17ml Isopropanol. gDNA threads were transferred to a 1.5ml microcentrifuge tube and washed with 80% ethanol. The gDNA was allowed to air dry and then resuspended with 500µl TE 10/1 O.N at 4°C under gentle rotation. gDNA concentration was measured using the NanoDrop™ and stored at 4°C.

Bisulfite conversion

The most common used method for analyzing the cytosine residues methylation within a CpG pair is bisulfite conversion of DNA followed by sequencing. gDNA that has been treated with bisulfite retains only cytosines if methylated since bisulfite treatment induces a spontaneous deamination of non-methylated cytosines that will be subsequently converted to uracil in the

sequencing reaction. An overview is provided in Figure 6. Bisulfite treatment of the genomic DNA was carried out with aid of the EpiTect Bisulfite Kit. Briefly, in a PCR tube, 200-400ng of gDNA samples were mixed with reagents and filled up with RNase-free water to a total volume of 20µl as described in the kit manual. The conversion reaction was performed in a thermocycler according to the program listed in the kit manual. After 5 h of conversion, single stranded converted gDNA was cleaned up using a spin column, washed, desulfonated, washed again and eluted in 20µl of elution buffer according to manufacturer's instructions. The eluate was then stored at -80°C.

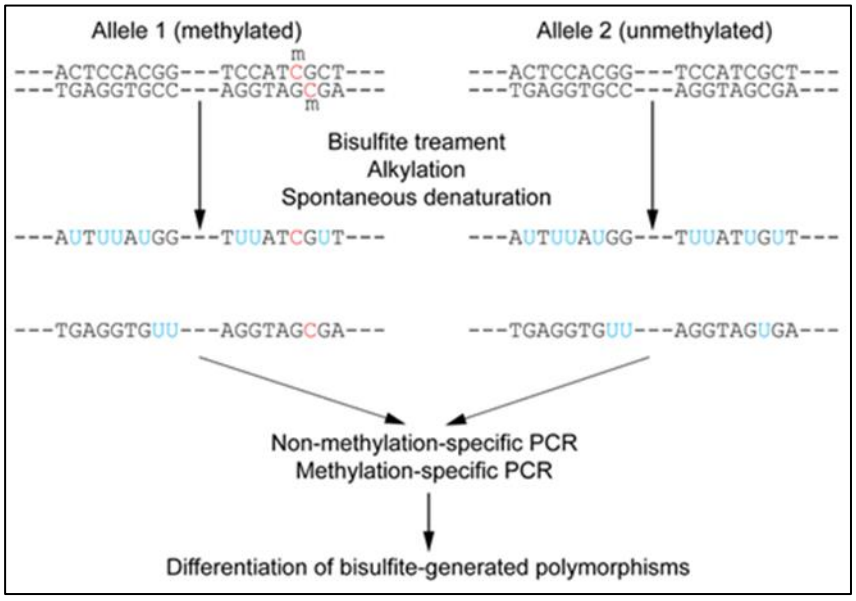

Figure 6: Outline of bisulfite conversion of sample sequence of genomic DNA Nucleotides indicated in blue are unmethylated cytosines converted to uracils by bisulfite, while red nucleotides are 5-methylcytosines resistant to conversion. This figure is a direct copy from Wikipedia (https://en.wikipedia.org/wiki/Bisulfite_sequencing 2017).

Methyl Specific PCR (MSP) and Bisulfite-conversion Specific PCR (BSP) assays

MSP is a sensitive method to measure CpG methylation of candidate genes. MSP allows to discriminate between methylated and unmethylated alleles after gDNA bisulfite conversion[138] by cloning the reaction products and subsequent sequence analyse of at least 10 clones samples for comparison of CpG methylation pattern. MSP is highly sensitive and able to detect one methylated allele in a population of more than 1000 unmethylated[139] alleles and requires only small quantities of gDNA. In addition, it allows the elimination of false positive results that may generate from using PCR-based approaches which relied on differential restriction enzyme cleavage to distinguish methylated from unmethylated gDNA[139]. Primers were designed using the Methyl_Primer_Express software v_1 and defaults parameter. The primers covered amplicons with a size of 89 to 500 base pairs. For MSP analysis of each amplicon a methylated set (forward and reverse named AM) and an unmethylated primer set (forward and reverse named AU) were designed. Unlike MSP primers, the BSP[140] assay use

primers which bind to both the methylated and the unmethylated amplicon since the software excludes regions with CpG dinucleotides for potential primer binding sites. CpG methylation patterns of the extended *FMR1* promoter including the first intron region were analyzed mainly using MSP. When MSP analysis was not possible due to low sequence complexity, PCR and sequence analysis was applied directly after bisulfite treatment using the BSP assay. Briefly, 4µl of bisulfite converted gDNA served as a template for each 25µl PCR reactions. A master mix using reagents from the GoTaq DNA Polymerase with the appropriate primer sets (AM, AU or BSP, listed in Material section 3.10) was then prepared before addition of gDNA. Thermal cycling conditions were as follows: 1 cycle at 95°C for 10 min; 39 cycles (10 min at 95°C, 30 s at 95°C, 45 s at annealing temperature (59-63°C) for 45 s, 50 s at 72°C, and a final elongation for 4 min at 72°C). Non-converted gDNA and water were included as negative control in each PCR reaction.

Agarose gel electrophoresis

Agarose gel electrophoresis was used to determine the length of MSP, BSP and any other linearized gDNA fragments to separate them for further applications. For preparation of 2% concentrated gels, agarose powder was added to TAE (1X) and the mixture was heated in a microwave oven until the agarose was completely dissolved. Gels were then casted and mounted in the electrophoresis tank prefilled with TAE (1X). PCR products were mixed with (5X) loading buffer and loaded into the slots of the gel. A 100bp or 1Kb size standards were used. Gels were run at 100V until the loading dye reached the bottom of the gel. Afterwards, gels were stained with ethidium bromide for 10 min and then visualized using a UV-plate.

Extraction of PCR products from agarose gels

After visualization, PCR products selected for cloning were extracted from gel. Gels were placed on a UV-lamp and desired bands were extracted using a scalpel and transferred to a 1.5ml microcentrifuge tube. Gel slices were then weighed and extracted using the Wizard® SV Gel and PCR Clean-Up System as described in the manual of the kit. The concentration of purified PCR products was measured using a NanoDrop™ and either used immediately for cloning or stored at -20°C.

Cloning

Preparation of chemical competent bacteria

With the aid of a sterile tooth pick a portion from the top of the frozen *E.Coli DH5α* was scraped off and then streaked into a culture LB agar plate. The plate was incubated O.N at 37°C. The second day, a colony was picked from the culture plate and served to inoculate 5 ml of LB medium O.N at 37°C under shaking at 250 rpm . On the third day, 1ml of the

resulting bacterial culture was transferred to a container filled with 100 ml of sterile LB medium. The bacterial culture was allowed to grow at 37°C under shaking at 250 rpm until an optical density of 0.4 to 0.6 was reached. Cells were then collected into a 50ml falcon, incubated for 5 min on ice and then centrifuged at 4000g for 10 min at 4°C. Supernatant was then removed and cell pellet was resuspended with 1.6ml ice cold 100mM $CaCl_2$. After an incubation of 30 min on ice, cells were centrifuged, supernatant was discarded and cell pellet was re-suspended as previously described. Finally 300µl of sterile glycerol was added to cell suspension. Bacterial glycerol stocks were then stored at -80°C.

Ligation

PCR products were ligated into a pGEM®-T easy vector. Ligation was carried out over night at 16°C in a volume of 10µl. the following components were added to the ligation reaction: 1µl T4 DNA ligase, 0.5µl pGEM®-T vector, 1µl T4 DNA ligase and 5µl 2X ligation buffer and up to 3.5 µl of purified PCR product.

Transformation

Chemical competent bacterial cells were allowed to thaw on ice. Subsequently, 4µl of the ligation reaction product was added to cells and incubated 20 min on ice. Heat shock was performed for 45 s at 42°C followed by incubation for 2 min on ice. 200µl of SOC medium were then added and cells were incubated for 90 min at 37°C under shaking of 300 rpm. Bacterial cells were then plated out on LB-agar culture plate containing ampicillin 1mg/ml and 50 mg/ml X-gal and incubated O.N at 37°C.

Single colony PCR

Only white colonies were picked to ensure the greatest chance of picking colonies containing the insert. The white color indicates a successful insertion of the insert due to the disruption of the *β-galactosidase* gene sequence which is a feature of the pGEM-T easy vector. Undisrupted plasmids are capable of producing the *β-galatosidase* enzyme that can utilize the X-gal producing a blue by-product; thus blue colonies probably have empty plasmids while white colonies have inserts. Selected colonies were picked with the aid of 200µl pipette tip and stroke into a LB agar culture plate. The remaining bacteria on the tip were then used as material for PCR colony. PCR products were then loaded into a 2% agarose gel, stained with ethidium bromide and visualized as previously described.

Plasmid DNA Minipreps

Clones that showed the presences of inserts were further amplified O.N in 5ml LB culture medium containing 1 µg/ml ampicillin. Plasmid-DNA was extracted using the Qiagen

Minipreps system according to the manufacturer's instructions. The concentration of the extracted plasmid was measured using NanoDrop™ and then stored at -20°C.

Sequencing

Sequencing PCR products according to Sanger chain termination method[141].

For sequencing PCR, Big Dye Terminator v3.1 Cycle Sequencing Kit was used according to manufacturer's recommendations using 200ng DNA. Cycling program was as follow 1 cycle at 94°C for 10 min; 25 cycles (4 min at 94°C, 30 s at 95°C, 25 s at 50°C, 30 s at 72°C and a final elongation for 7 min at 72°C).

Purification of DNA fragments

Following sequencing reaction, samples were precipitated O.N at -20°C using a precipitation buffer (250 µl of 100% ethanol and 3M sodium acetate). The next day, samples were centrifuged at 16.000g for 15 min, washed once with 70% ethanol (v/v) and centrifuged as previously described. Supernatant was removed and samples were allowed to air dry. Pellets were resuspended in 20 µl Hi-Di Formamide and transferred into a 96-well sequencing plate. DNA sequencing was performed at the department of Human genetics (Heidelberg University, Germany).

Analysis of the sequencing results

Sequence analysis was proofread using Chromas version 2 and compared with NCBI reference sequence.

4.3. Electromobility shift assay (EMSA)

EMSA is a rapid and sensitive mean for detecting sequence-specific DNA-binding proteins. The assay is based upon the ability of a transcription factor to bind in a sequence specific manner to a biotin labeled oligonucleotide probe[142] and retard its migration through a non-denaturing polyacrylamide gel.

For the extraction of sufficient cell nuclei, COV434 cells were grown in triplicates at a density of 1 million cells in 100 mm petri dishes. Nuclear extracts were prepared using NE-PER™ Nuclear and Cytoplasmic Extraction kit and protein concentrations were measured using Bradford reagent according to manufacturer's instructions. Purity of nuclear protein was checked by western blot for cytoplasmic GAPDH expression.

Biotin labeled and non-labeled oligonucleotides spanning the region of interest (positions +552 to + 567 relative to the *FMR1* TSS +1 (listed in section Materials section 3.10) were designed to contain the desired transcription factor binding site and then orderd with their respective complementary strands. Complementary oligonucleotides were annealed with a thermocycler initially at 95°C for 1 min, then for 70 cycles by decreasing temperature of the

heating block 1°C per cycle. Nuclear protein extract preparations (2 µg) were mixed with 1× binding buffer, poly-dI-dC and preincubated, when appropriate, with unlabeled oligonucleotide or with E2F1 antibody (2 µg) as described in the protocol manual of the EMSA assay kit. The binding reaction products were mixed with 1µl of loading dye and separated on a 6,3% polyacrylamide gel. After electrophoresis, DNA-protein complexes were transferred to a nylon membrane, blocked and exposed using a Konica SRX- 101A chemiluminescence imaging system.

4.4. Patients selection

This study was approved by the local ethical committee of the University of Heidelberg, Germany (S-145/2012). All patients included in this study gave written informed consent. The study population consisted of women entering the clinic for *in vitro* fertilization (IVF) treatments. Of these patients, 20 women were selected randomly, excluding patients suffering from gynecological problems that can affect female fertility and ovarian response (e.g. endometriosis and myomas). Patients from the same age group were then divided into two groups according to their ovarian response after COS, the Anti-Müllerian hormone (AMH) level and reproductive parameters (antral follicle count [AFC]), total number of oocytes recovered and MII oocytes retrieved). The poor responder group (POR n=5) was selected according to "Bologna Criteria"[24; 25]. The rest of the patients who did not fulfill criteria of POR were referred as normal responder (NOR n=5). For *XIST* expression evaluation in human granulosa cells 35 NOR and 16 POR were randomly selected.

Table 9:Patients selected for the methylation study

Patient number	Age	Gynecological disease	AMH (ng/ml)	Number of retrieved oocytes	CGG-triplet repeats number
NOR 1	31	None	1.91	20	20/30
NOR 2	34	None	2.46	7	21/26
NOR 3	36	None	2.66	6	23/33
NOR 4	39	None	n.a.	8	29/29
NOR 5	38	None	3.70	6	30/33
NOR 6	27	None	4.74	12	30/40
NOR 7	25	None	2.48	8	29/33
NOR 8	37	None	2.27	11	23/23
NOR 9	39	None	3.43	15	30/30
NOR 10	45	None	2.03	6	31/31
POR 1	31	None	0.64	3	23/31
POR 2	34	None	0.3	4	22/30
POR 3	39	None	1.67	2	23/30
POR 4	40	None	0.55	5	29/32
POR 5	40	None	0.36	2	33/33
POR 6	39	Endometriosis	0.27	4	30/30
POR 7	33	Endometriosis	0.83	3	23/25
POR 9	42	None	0.59	6	30/30
POR 10	44	None	0.25	1	29/29

NOR=Normal Responders, POR= Poor Responders, AMH=Anti Müllerian Hormone (normal range), AFC= Antral Follicular Count. n.a. = not applicable.

Primary granulosa cells retrieval (performed by the IVF lab)

Granulosa cells were collected from follicular fluid after transvaginal ultrasound-guided follicle puncture with an ovum aspiration needle (Cook Medical, Bloomington, IN, USA) connected to a vacuum pump (Cook Medical Inc.). Follicular fluid was moved to 14ml round-bottom tubes and kept at 37°C in a test tube heater (Cook Medical Inc.) or in a Thermo-Cell-Transporter (Labotect, Rosdorf, Germany). After transferring the follicular fluid to a 100mm cell culture dish on a heated table at 37°C (K-Systems, Birkerød, Denmark) mural GCs were identified morphologically as epithelial cell aggregates using a zoom-stereomicroscope (Nikon SMZ1500). In case of bloody follicle fluid, the mural GCs were briefly washed in MHM (with 10% v/v SSS) or Sydney IVF Fertilization medium (Cook Medical Inc.). Mural GCs were taken up in a volume of 2.5µl with a sterile tip, transferred to 1.5ml tubes (Sarstedt, Nümbrecht, Germany) pre-filled with 12-13µl RNAlater® (Ambion, Life technologies, USA).

4.5. Microarray gene expression analysis

Cell culture

Culture of COV434 cells

COV434 cell line was cultured in DMEM medium with stable L-glutamine. The cells were cultured in 75 cm^2 flasks under conditions of 5% CO_2 and 37°C. Cell culture medium was supplemented with 10% FCS, 50µg/ml Antibiotic/antimycotic mix, and 1mM L-Asparagine. For subculture, culture medium was removed and cells were washed with PBS 1X. Subsequently, PBS was removed and cells were incubated with trypsin 1X for 7 min at 37°C. Trypsin reaction was then stopped by adding 10ml of culture medium. Cells were then subcultured at a dilution of 1:3. The doubling rate of the cells was 32 hours. All cell culture work was performed under sterile conditions.

DMSO stocks and Thawing frozen cells

Cells were grown at 80% confluence as previously described, collected in a 15ml falcon tube and centrifuged at 1200rpm for 5min. Cell pellet was then washed twice using PBS 1X and re-suspended using pre-cooled freezing solution (92% FCS, 8% DMSO). DMSO stocks were then incubated for 2h at -20C followed by an incubation O.N at -80°C. The next day stocks were transferred in the liquid nitrogen cell storage (-196°C).When a new cell culture was initiated, frozen cells were directly thaw in a water bath at 37°C and immediately transferred to a T25 flask already filled with 8ml fresh complete medium. Cells were allowed to attach for one day and medium was replaced with fresh complete medium.

PBS pellet generation

Cell pellet was re-suspended after washing steps and cells were counted. Cells were then transferred to 2ml tubes and centrifuged at 1200 rpm for 5 min at 4°C. Supernatant was removed, PBS pellets were snap frozen and stored in liquid nitrogen.

siRNA transient Transfection (Fast forward protocol)

COV434 cells usually grow in tight clusters and are therefore more difficult to transfect than many other cell lines. In order to establish a working transfection protocol, transfections were attempted at varying cell densities ($1x10^6$, $8x10^4$, $4x10^4$ and $2x10^4$ cells) plated on slides, using three liposomal based reagents (Lipofectamine 2000 and Lipofectamine RNAiMax) and 25, 50, 85 and 100nM FITC-labeled siRNA (sc-36869) according to protocol 1 (liposomal reagent manufacturer's protocol) or protocol 2^{143} (a well-established protocol for hard to transfect cells). In parallel experiments, cells treated only with transfection reagent and the non-transfected cells served as negative controls to assess whether the liposomal reaction and

the addition of nucleic acid have an impact on cell viability. Six hours post-transfection, slides were washed twice using PBS 1X. Cells were then fixed using 4% formaldehyde for 10 min at RT under gentle shaking. After fixation, slides were washed 3 times using PBS 1X for 3 min each. Nuclei were stained for 5 min at RT using 500µl DAPI (at a concentration). Slides were then washed with water 3 times for 3 min and mounted using DABCO. Slides were allowed to dry and then stored O.N at 4°C. The next day, the efficiency of transfection was determined under microscope by counting the number of cells with a green signal.

For *FMR1* siRNA, at the day of transfection, transfection mix was prepared in DMEM medium without FBS and antibiotics. A ratio of 7.5µl of RNAi max was used for every 50nM of *FMR1* siRNA (silencer select cat# 4392420) or control siRNA (silencer select cat# 4390843) according to instruction manual. In the meantime, cells were detached and counted at a concentration of 40000 cells /ml. Cells were then transferred to 1.5 ml eppendorfs and centrifuged at 1500 rpm for 5 min. Cell pellet was re-suspended using the transfection reagent followed by an incubation for 20 min at RT. Cells were subsequently seeded in a 6 well plate containing 1ml of fresh complete medium. 24 h post transfection, medium was changed and cells were incubated until lysis.

Total RNA and proteins extraction

At 24, 48, 72 and 96h post- transfection, culture medium was removed and cells were washed twice with PBS 1X. Cells were then lysed with a mix of RP1 buffer and ß-Mercaptoethanol (1:1000), harvested by scraping, collected in 1.5 ml eppendorfs and vortexed. Extraction of total RNA and protein (for western blot) was performed immediately using the NucleoSpin TriPrep kit according to instruction manual. RNA and protein were then stored at -80°C. RNA concentration was measured using a Nanodrop. Protein concentration was measured using Protein Quantification assay kit according to the instruction manual. For ELISA application, transfected cells were lysed at the different time points using lysis buffers provided by the desired ELISA kit.

Analysis of protein expression after *FMR1* knockdown by western blot

Western Blotting

Protein can be easily separated under denaturing conditions in a SDS-polyacrylamide gel based on their mass. The SDS-polyacrylamide gels were composed of two layers: a 12.5% acrylamide/bisacrylamide separating gel that separates the proteins according to size and a lower percentage (4%) stacking gel that insures simultaneous entry of the proteins into the separating gel at the same height. After preparation, the gels were poured into a Mini-PROTEAN® 3 multi-casting chamber.

separating Gel	final concentration	stacking gel	final concentration
1,5 M Tris pH 8,8	0.375M	1.5 M Tris pH 8,8	0.375 M
30%Acrylamide	12.5%	30%Acrylamide	4%
20%SDS	0.1%	20%SDS	0.1%
TEMED	0.15%	TEMED	0.1%
10%APS	0.03%	APS	0.05%
H_2O	Up to 10ml	H_2O	Up to 10ml

Proteins were transferred from the SDS gel onto a PVDF membrane for 60 min at 65 mA using SD Semi-dry Transblot Apparatus. The pre-stained molecular weight protein ladder served as an indication of successful transfer. Afterwards the membrane was quickly rinsed with distilled H_2O. To reduce unspecific binding, the membrane was then blocked using a blocking solution for 90 min at RT under gentle agitation throughout all steps. The blocking solution was then replaced with the primary antibody solution and incubated O.N at 4C. The next day, the membrane was washed 3 times with TBST 1X for 10 min at RT. Then the membrane was incubated with the appropriate secondary antibody solution for 90 min and then washed as described before. The membrane was then washed one time with Millipore water to remove any residual traces of the washing buffer. Finally, the membrane was placed between the two parts of a plastic covering sheet and then covered with an enhanced chemiluminescence solution containing the peroxidase substrates and incubated for approximately 1 min before measuring the luminescence signal. For low intensity signals a more sensitive detection system was used. The luminescence was detected using a chemiluminescence imaging system.

Enzyme-Linked Immunosorbent Assay ELISA

At 48 and 72h post transfection, culture medium was removed and cells were washed with PBS 1X. Cells were then lysed and harvested according to the manufacturer's protocol of the used ELISA kit (see Table 4).

Measuring of total protein for ELISA

Several dilutions of BSA standards ranging from 2mg/ml to 0.2mg/ml were prepared. 20µl of protein lysate was pipetted into spectrophotometer cuvette and then filled up with 4 ml Bradford solution. After incubation of 15 min at RT, protein concentrations were measured using a spectrophotometer and a regression line was calculated.

Illumina HumanHT-12 v4 array

The quality of the extracted RNA was checked for integrity and concentration using a Bioanalyser. Only high quality RNA that showed a RIN value above 9 was used for the microarray analysis. All further handling processes for the Microarray profiling were performed by the DKFZ 'Genomics and Proteomics Core Facility' according to the manufacturer's recommendations using the HumanHT-12 v4 Expression BeadChip Kit. This array offers a comprehensive analysis of the expression of 31,000 annotated genes with more than 47000 probes derived from the NCBI RefSeq and other sources.

Pathway analysis

Microarray data were analyzed using Resolver™ software and exported into Excel tables for further analysis. Pathway analysis was performed at the department of Bioinformatics using the ConsensusPathDB-human (http://cpdb.molgen.mpg.de/) software package. This software integrates interaction networks in *Homo sapiens* including binary and complex protein-protein, genetic, metabolic, signaling, gene regulatory and drug-target interactions, as well as biochemical pathways. The interaction data are integrated in a complementary manner (avoiding redundancies), resulting in a seamless interaction network containing different types of interactions. ConsensusPathDB-human calculates the percentage of the genes measured that meet the following defined criterion for this analysis (log fold change ≥ 0.5 and p-value ≤ 0.05, or p-value ≤ 0.01).

5. Results

Chapter 1: expression of *FMR1* gene in human granulosa cells

1.1.*FMR1* expression in COV434 cell line

The COV434 cell line was derived from a 27-year-old woman suffering from a solid granulosa cell tumour. It shares characteristics with proliferating granulosa cells such as FSH-dependency, 17β-oestradiol production, the formation of intercellular connections[134]. In order to proof the suitability of the COV434 cell line as a model system to study *FMR1* gene expression in human granulosa cells, I first started by analysis of the karyotype of this cancer cell line used in our laboratory. In the literature some sub clones of the cell line were reported to have minor chromosomal aberrations (46XX + 5, 22q+)[144]. Multicolor FISH showed that cells used in our lab have a normal karyotype (46, XX) (Figure 7).

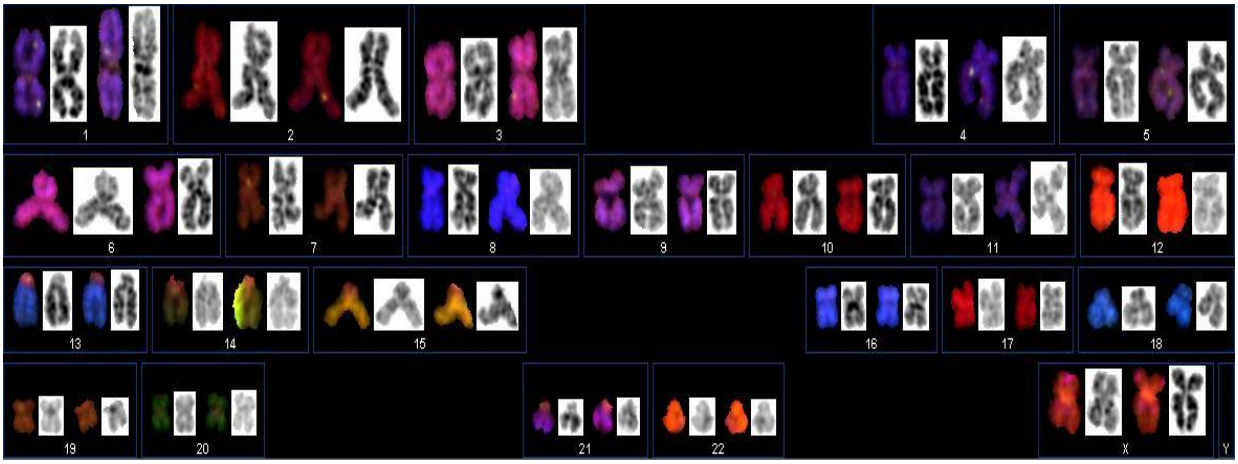

Figure 7: Spectral karyotype from COV434 cells.
The 24 chromosome pairs are depicted in so-called pseudo-colors as shown here. Each chromosome pair is marked with a specific mixture of fluorochromes. In addition a classical banding analysis was performed (black and white), with courtesy of Ulrike Bender.

Further analysis for *FMR1* and FMRP expression in COV434 revealed expression of several alternative spliced transcripts (Figure 10) and phosphorylated/unphosphorylated protein forms (Figure 8A). Immunohistochemical localization of FMRP revealed its expression mainly in the cytoplasm of COV434 cells (Figure 8B)

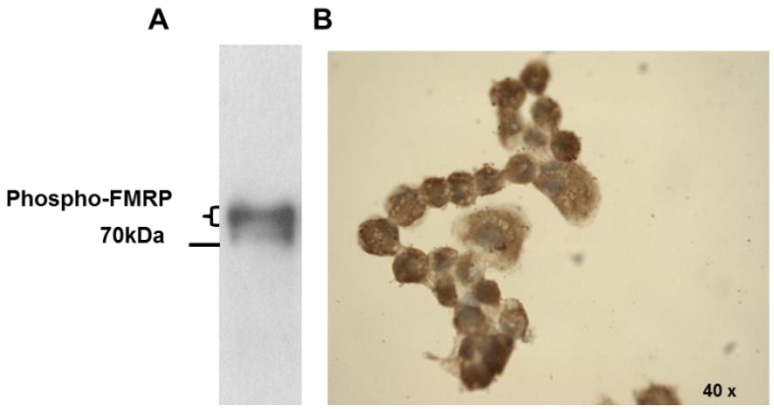

Figure 8: **Expression and localization of FMRP in the COV434 cell line.** **(A)** Representative Western blot of protein extracts from COV434 cells using the anti-FMRP (mAb1C3, Euromedex). 5µg of proteins were loaded. **(B)** Representative IHC for FMRP expression (brownish color) in COV434 cells showed a strong cytoplasmic staining.

1.2.Identification of 5' and 3'ends of the *FMR1* gene transcripts in COV434

To investigate putative variable 5' and 3'ends of *FMR1* gene transcripts in COV434 cell line, 5′-RLM RACE and 3'-RACE were performed. A dominant 5′ transcript end was detected on agarose gels (Figure 9A). Its sequence analysis showed that in COV434 cells the transcription of *FMR1* transcripts is mainly initiated at genomic position 147.911.920 i.e. 135bp upstream of the CGG triplet repeats (Figure 9A). Sequencing of 10 individual clones showed that this initiation site corresponds to the previously reported *FMR1* major TSS[68]. In contrast, several 3' transcripts ends were detected on the agarose gel pointing to the presence of multiple polyadenylation sites (PASs) (Figure 9B). Although, the different detected amplification products were not sequenced, their molecular length were found according published results[145].

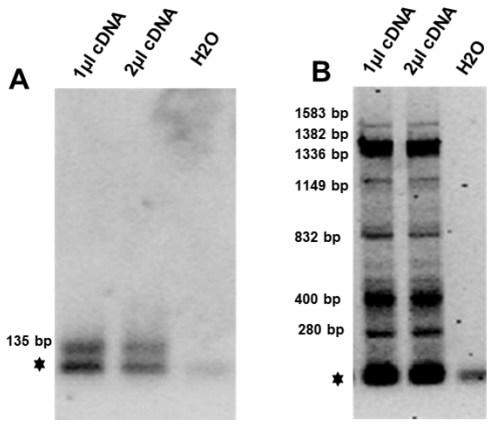

Figure 9: Identification of *FMR1* gene 5' and 3' ends in COV434 granulosa cell line. **(A)** 5'RLM RACE and **(B)** 3'RACE were performed according to published protocols (see Material and Methods). 1 or 2µl of cDNA served as template for the second PCR step of the RACE procedure. Water control was used as a negative control to exclude possible contamination. Primer dimers are indicated by✸.

1.3.*FMR1* gene is alternatively spliced in human granulosa cells

Nothing is known about the set of *FMR1* transcript isoforms expressed in human granulosa cells, and whether expression of some isoforms may vary in patients with different ovarian response. I aimed, therefore, to characterize the four major *FMR1* transcript isoform groups[37] (Figure 10) (see Introduction section 1.2.1.) in COV434 cells and then in human primary granulosa cells of NORs and PORs for comparison. I added a fifth transcript isoforms group, named here group E, which

differs in alternative splicing at exon 15[146]. Expression of *FMR1* transcript isoforms containing both exons 12 and 14 (group A), those missing exon 14 (group B), those missing exon 12 (group C), those simultaneously missing exons 12 and 14 (group D), and those with alternative splice site in exon 15 (group E) were analyzed by RT-PCR with polyadenylated in RNA isolated from COV434 cells and compared to female leukocytes (Figure 10B). All five isoforms groups were detected in COV434 cells (Figure 10B). In addition, groups B and E also displayed some isoforms with probably cell specific expression being detected only in COV434 cells or only in leukocytes. Due to the very low amount of expression of these new isoforms I did not get enough material to proceed with cloning and sequencing procedures.

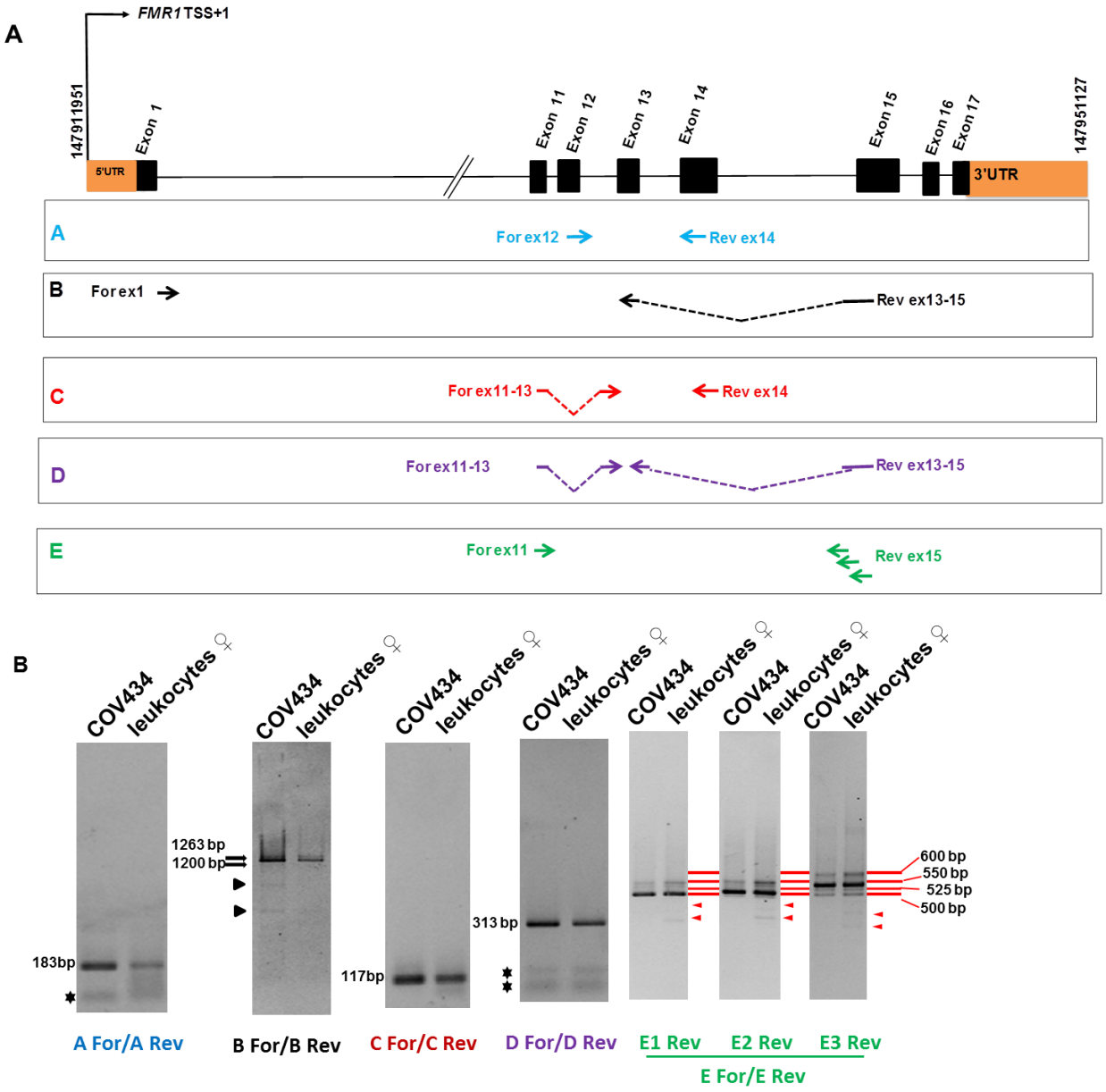

Figure 10: Characterization of *FMR1* isoform groups in COV434 cell line.
(A) Diagram of *FMR1* gene. Nucleotide numbering was adapted from the NCBI nucleotide nomenclature: *FMR1* gene region NC_000023.11: 147,911,951-147,951,127 *H.* sapiens. UTRs are represented by orange boxes with

the CGG repeat block indicated in the 5'UTR region. The identified *FMR1* TSS+1 is indicated with black arrow to the left. Exons are represented by vertical black bars and horizontal axes correspond to introns. Positions of primers used to identify the different isoforms groups are indicated with arrows: Group A (blue), group B (black), group C (red), group D (purple) and group E (green). **(B)** Amplification products detected on agarose gels. Female leukocytes served as a positive control. Unexpected new detected isoforms are indicated by black and red arrow heads. Primer dimers are indicated by✸.

1.4. Expression of *FMR1* in human primary granulosa cells from NORs and PORs

For comparison to COV434, the expression patterns of *FMR1* transcript isoforms within groups A, B, C and D were also analyzed in primary granulosa cells from some NOR and POR patient samples (see Methods section 4.4). Transcripts from leukocytes from the same patients served as control, with exception for group A, due to limited patient material. The four groups of transcript isoforms identified in COV434 cells were also present in primary granulosa cells of both NOR and POR. Also in leukocytes from both NOR and POR, these four transcript groups were identified. The intensities of all detected amplification products suggest no major difference in their expression pattern in leukocytes of the two patients' groups. In granulosa cells, POR samples seemed to express lower levels of isoforms within groups A and B. compared to NOR. As already found in COV434 cells (Figure 10B), some cell specific transcripts present within group B were also detected in the primary granulosa cells of one POR and one NOR (Figure 11B).

In summary, these data confirm the usefulness of COV434 as model system for the molecular analysis of *FMR1* gene expression in human granulosa cells.

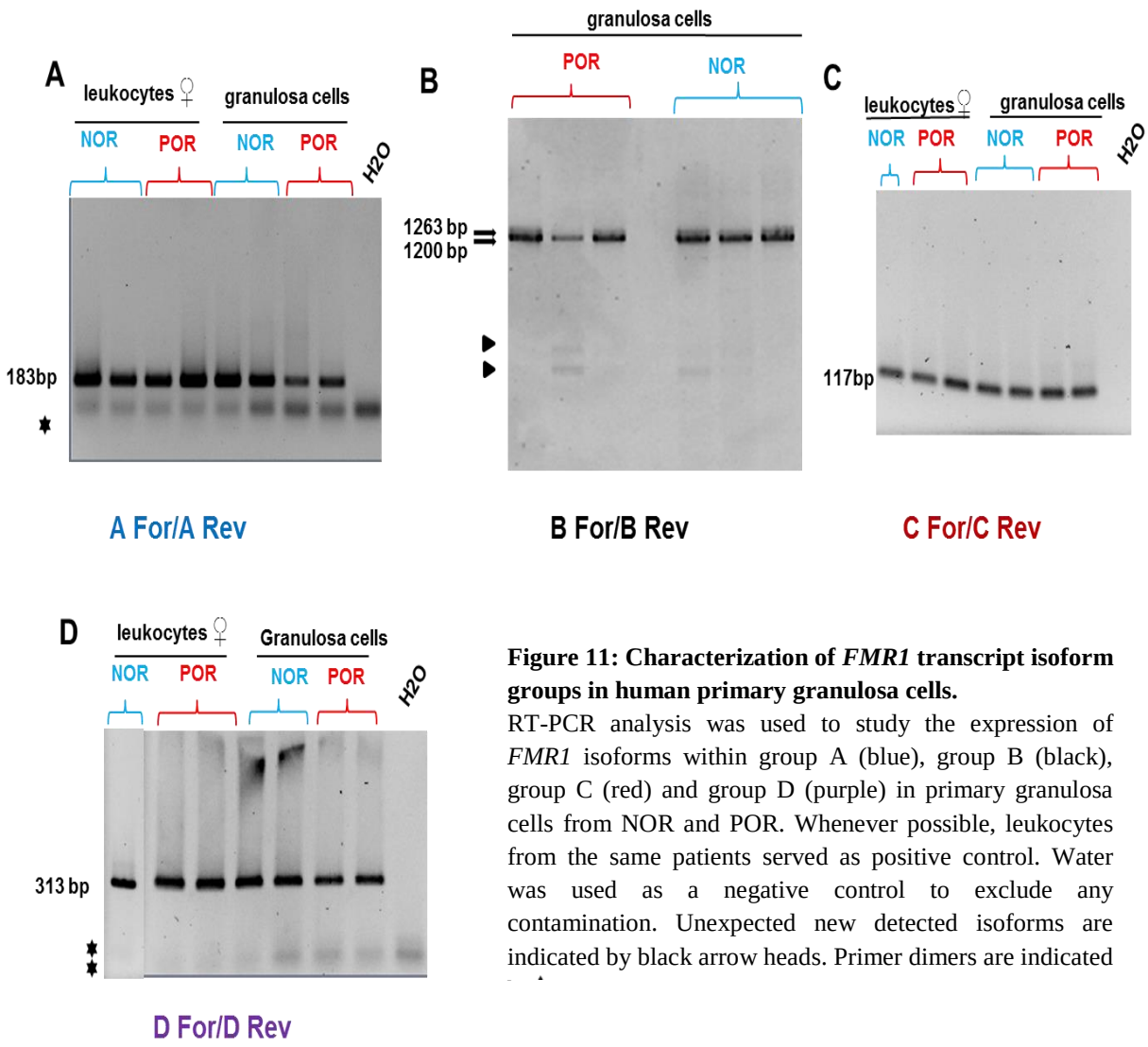

Figure 11: Characterization of *FMR1* transcript isoform groups in human primary granulosa cells.
RT-PCR analysis was used to study the expression of *FMR1* isoforms within group A (blue), group B (black), group C (red) and group D (purple) in primary granulosa cells from NOR and POR. Whenever possible, leukocytes from the same patients served as positive control. Water was used as a negative control to exclude any contamination. Unexpected new detected isoforms are indicated by black arrow heads. Primer dimers are indicated

Chapter 2: Single CpG site methylation mapping along extended *FMR1* promoter

2.1.Identification of *FMR1*-DMR1;-2;-3 and *FMR1*-UMR

Single CpG site methylation analysis was performed along the putative extended promoter region of the *FMR1* gene (Figure 12:147,911,046-147,912,539 *H. sapiens*). In total, the CpG methylation pattern of 10 amplicons was analyzed (Figure 12; see also Youness et al., submitted) including 106 CpG sites along the overlapping amplicons as shown in Figure 13.

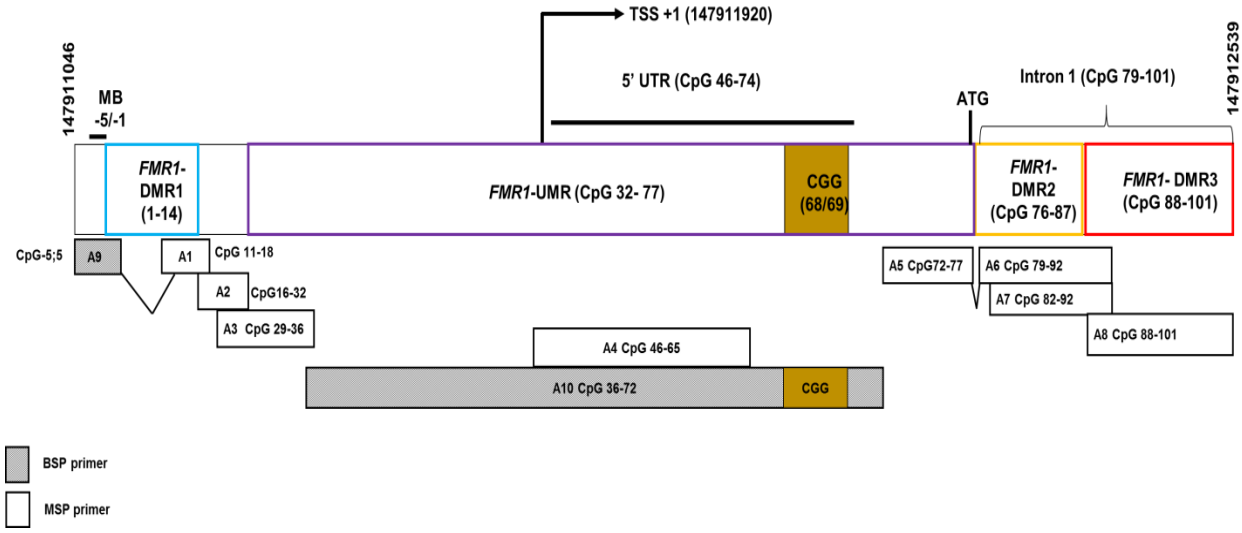

Figure 12: Distribution of MSP and BSP primers among the *FMR1* gene locus (Xq 27.3) in COV434 cells. Nucleotide numbering in this and the following graphs was adapted from the NCBI nucleotide nomenclature: NC_000023.11:147,911,046-147,912,539 *H. sapiens FMR1* gene region. The transcription start site (TSS+1 at genomic position 147,911,920) is indicated by an arrow. The first exon includes CpG sites 46 to 78 and the proximal intron1 includes CpGs 79 to 101. A total of 106 CpGs were covered by the amplicons A1 to A10 (represented as boxes). The exact CpG numbers covered by each of the amplicons are indicated. CpG 1 refers to the first CpG located downstream of the methylation boundary (MB). The MB is designated by a black bar and CpGs located in the upstream amplicons are negatively numerated (CpGs-5 to -1), whereas, CpGs located downstream are positively numerated (CpGs 2 to 101). Methylation patterns of CpGs 6 to 10 and 78 were not analyzed and are indicated by a gap symbol (\/) at their location. CGG triplet repeat position is indicated by a yellow box. The position of the four differentially methylated CpG regions is indicated by a color code: *FMR1*-DMR1 (blue box), 2 (orange box), 3 (red box) = *FMR1* differentially methylated regions, *FMR1*-UMR= *FMR1*-unmethylated region (purple box).

The MB zone was apparent in this cell line at CpG sites -5/-1 and the first CpG site located downstream of it was numbered as CpG +1. Due to difference in CGG triplet repeat numbers on both *FMR1* alleles in this cell line (19/41), I was able to discriminate between the two

alleles by analysis of amplicon A10 (Figure 13). The *FMR1* main transcription start site[68] (TSS +1) was located between CpG sites 46 and 47.

CpG sites covered by A10 (CpGs 46-72) including the CGG triplet block (represented as a unit between CpG sites 68/69) were completely demethylated on both gene alleles (Figure 13). This region was therefore named "*FMR1* unmethylated region" (*FMR1*-UMR). Upstream, *FMR1*-UMR could be extended to all CpG sites located in the *FMR1* minimal promoter (CpG sites: 32-36 covered by A3). Downstream, *FMR1*-UMR includes CpG sites 73-75 (covered by A5) located in exon1; thus, ending at the common ATG translation located between CpG sites75 and 76 (Figure 13).

Next, I explored the presence of the epigenetic FREE1 and FREE2 elements found by Godler et al.,[111] in leukocytes in the COV434 cell line. CpG sites 5-14 in our analysis correspond to CpG sites 1-10 of FREE1[111]. CpG sites 5 and 11-13 were methylated in half of the analyzed clones, whereas CpG 14 was demethylated. Due to technical limitations, CpG sites 6-10 could not be analyzed. CpG sites 1-4 located upstream of FREE1 and downstream of the MB were completely demethylated at CpG sites 1 and 2. Presence of FREE1 was thus confirmed in COV434 and extended upstream. It was therefore named "*FMR1* differentially methylated region 1" (*FMR1*-DMR1).

I also confirmed presence of FREE2 in COV434 cells and named it here, "*FMR1*-DMR2". *FMR1*-DMR2 was located downstream of *FMR1*-UMR at the boundary exon1/ intron1. CpG sites 76-87 located in *FMR1*-DMR2 refer to CpG sites 1-12 of the FREE2 element. *FMR1*-DMR2 reflected a similar methylation pattern as the one reported for FREE2 in female leukocytes carrying a normal CGG triplet block allele[111; 119]. CpG sites 76, 77, 81, 82, 83 and 85 were largely demethylated, whereas the other CpG sites were methylated in half of the analyzed clones.

Bisulfite sequence analysis of amplicons located downstream of *FMR1*-DMR2, showed the presence of a third and novel DMR, covering CpG sites 88-101. This region was accordingly named "*FMR1*-DMR3". I observed a partial methylation for CpG sites 92, 93 and 98 and a full demethylation of CpG sites 94, 95, 96 and 99. CpG sites 88 to 91 and 97 were methylated in half of the analyzed clones (Figure 13).

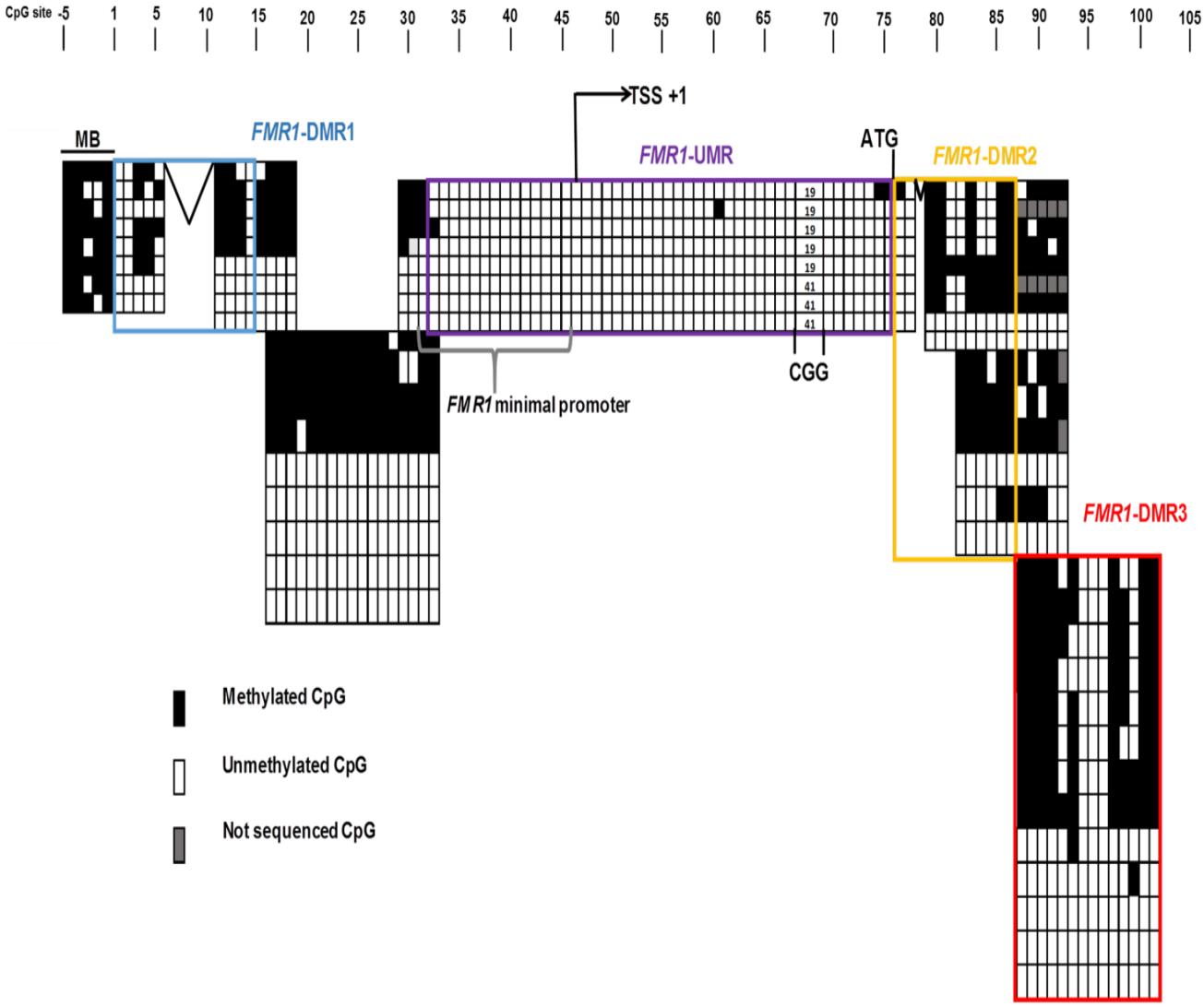

Figure 13: Methylation pattern of CpG sites in the extended *FMR1* promoter region in the COV434 cell line.

The methylation pattern of 106 CpG sites covered by 10 amplicons was combined in this graph. Black, white and grey squares mark methylated, unmethylathed and not sequenced CpG sites respectively. Each square line within a box corresponds to a single DNA clone that was sequenced. The transcription start site (TSS+1) is indicated by an arrow. ATG refers to FMRP translation start site. The location of the *FMR1* minimal promoter is indicated. Two alleles were detected with CGG triplet blocks ranging between ±19/41. The MB zone was apparent in this cell line at CpG sites -5/-1 and is designated by a black bar. The first CpG site located downstream of the MB zone was numbered as CpG +1 and all CpG sites were numbered accordingly. Colored boxes indicate the four most differentially methylated CpG regions identified in COV434 DNA. *FMR1*-DMR1 (blue box), -DMR2 (orange box), -DMR3 (red box) and *FMR1*-UMR (purple box). Methylation patterns of CpGs 6 to 10 and 78 were not analyzed in this study and are indicated by a gap symbol (\/) at their location.

In summary, single CpG site methylation analysis detected for differentially methylated CpG site domains including a full demethylated region in the core promoter domain not yet found in leukocytes.

2.2.Biallelic expression of *FMR1* core promoter in human granulosa cells

2.2.1. *FMR1*-UMR escapes X inactivation specifically in COV434 cells

Presence of *FMR1*-UMR (CpG sites 32 to 77) led me to investigate whether it is specific for COV434 cells, being a tumor cell line or also present in other human cell lines. For this purpose, I screened the A4 amplicon CpG methylation patterns (CpG 46 to 65) also in bisulfite converted gDNA samples extracted from female and male leukocytes and female fibroblasts. A4 was selected since it is located 5' upstream adjacent to the CGG repeat and it is possible to discriminate between methylated and unmethylated allele using MSP assay. gDNA from male fibroblasts served as a control. In both female cell types, one methylated amplicon and one unmethylated amplicon were detected on gel (Figure 14). This result indicated the presence of only one active X chromosome in these somatic female cells. In contrast, only one unmethylated amplicon was detected using COV434 cells gDNA and in male fibroblasts confirming that only demethylated CpG sites are found in *FMR1*-UMR of COV434 as also expected for male fibroblasts containing only one active X chromosome (Figure 14).

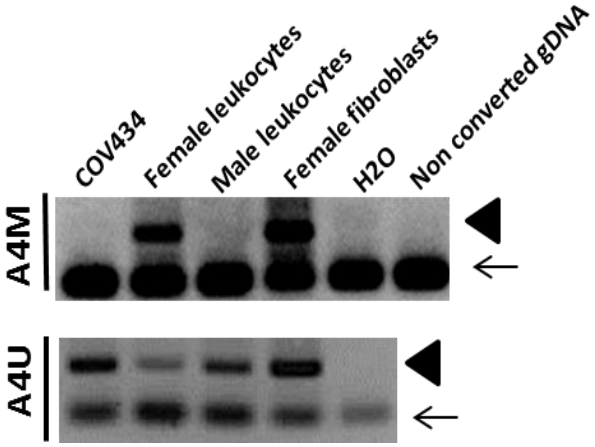

Figure 14: *FMR1*-UMR screening in human female and male cells.
MSP A4U and A4M primer sets covering CpG sites 46-55 were used for amplification of gDNA from three female somatic cells, COV434 cells, leukocytes and fibroblasts and from male leukocytes as control. The A4M primer set was designed to target CpGs within the methylated allele, whereas the A4U primer set targeted the CpG within the unmethylated allele. The 125 bp A4M and A4U amplicons detected on gel are indicated by black arrow heads. Primer dimers are indicated by black arrows. The water and a non-coverted gDNA from COV434 cells served as negative controls.

I wanted to clarify whether also other genes located on the X chromosome may escape X-inactivation in COV434 cells because being a tumor cell line. Therefore, I analyzed the methylation pattern of 11 CpG sites located within an 180bp promoter segment of the *Androgen Receptor* (*AR*) gene in COV434 and in female leukocytes using a well-established BSP protocol[147]. *AR* promoter is one of the most popular genomic regions used to study the rate of X- inactivation in female cells[148; 149]. Both female cell types showed a similar mosaic CpG methylation pattern as expected, which probably reflects the CpG methylation levels on the two X chromosomes (Figure 15).

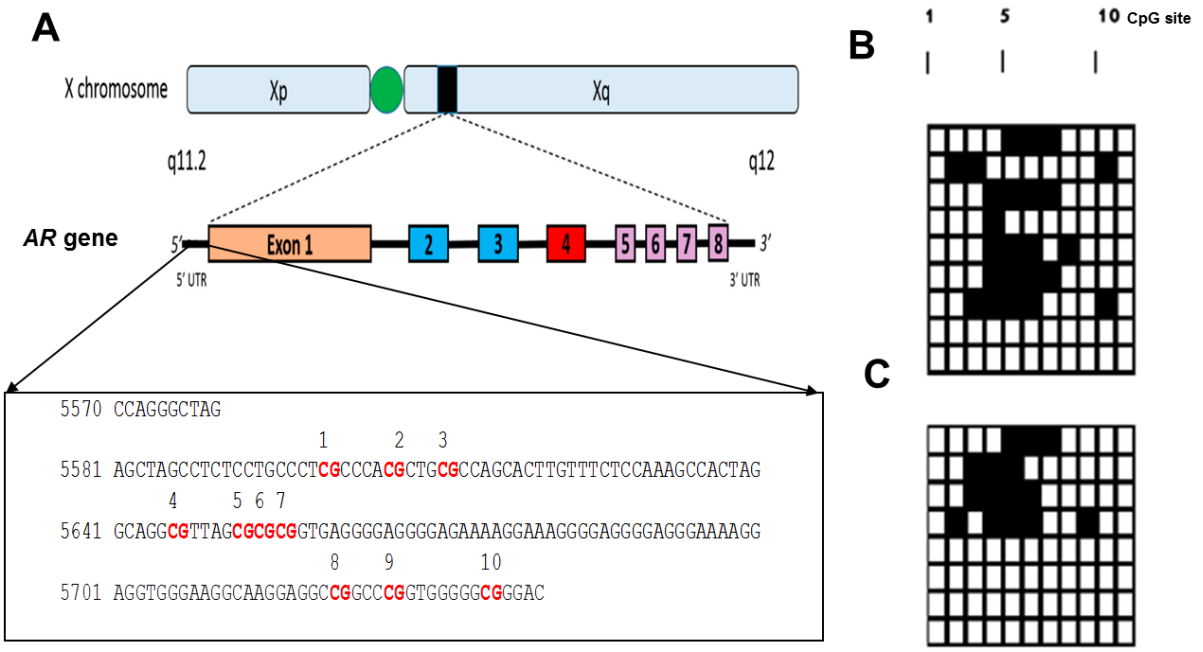

Figure 15: Comparison of CpG site methylation pattern within *AR* promoter in COV434 and female leukocytes.
(A) Genomic map of the *AR* gene (adapted from Crona et al.,[150]). Nucleotide numbering was adapted from NCBI accession number X78592.1 and numbering 5570-5750. CpG sites located within this segment are numbered. BSP assay was used to check for the CpG methylation pattern in gDNA from COV434 **(B)** and in female leukocytes **(C)**. Each line represents one clone. ■ methylated CpG site, □unmethylated CpG site.

2.2.2. *FMR1*-UMR is present in primary human granulosa cells

Presence of *FMR1*-UMR was then analyzed in primary granulosa cells from patients with variable ovarian reserve (1 NOR and 1 POR samples). Leukocytes from the same patients served as control. Similar to the findings observed in COV434 cells (Figure 16A), CpGs 46 to 65 were also largely unmethylated in both NOR and POR primary granulosa cells. However, this was not the case in patients' leukocytes, which showed the presence of one CpG methylated and one unmethylated allele as expected (Figure 16C).

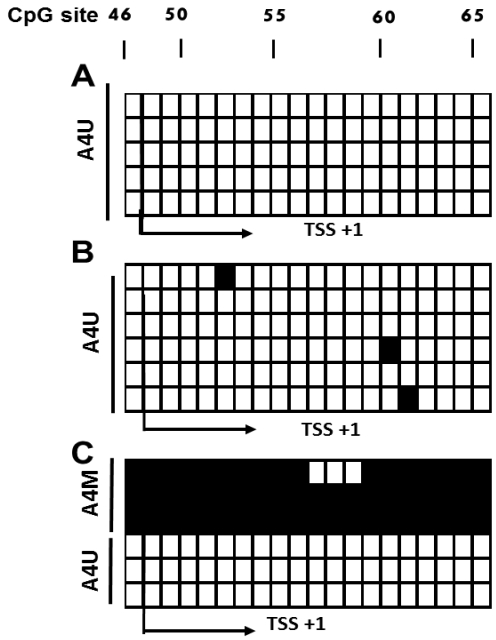

Figure 16: CpG site methylation analysis of *FMR1*-UMR in gDNA from human primary granulosa cells.
CpG methylation pattern in **(A)** COV434, **(B)** NOR primary granulosa cells and **(C)** in NOR leukocytes is presented. (**A)** and (**B)**: amplification products were only got with A4U amplicon confirming absence of the CpG site methylation in this genomic region.■ methylated CpG site, □ unmethylated CpG site.

2.2.3. Human granulosa cells express low levels of *XIST*

Presence of two alleles with an unmethylated *FMR1* core promoter region suggests that in granulosa cells both X chromosomes might generally escape X inactivation. To clarify whether human granulosa cells have indeed two active X chromosome, the expression of the X-inactive specific transcript (*XIST*) levels have been analyzed. *XIST* is a long non coding RNA which is responsible of X-chromosome inactivation in female mammals[151]. *XIST* expression level was first measured in COV434 and compared to female leukocytes using TaqMan based real time PCR. Male fibroblasts and leukocytes were included as positive controls. *XIST* expression level was significantly lower in COV434 (p=0.03) compared to female leukocytes (Figure 17A). As expected, the levels of *XIST* transcripts were below detection level in both male fibroblasts and leukocytes (Figure 17A).

I also analyzed *XIST* expression levels in primary granulosa cells from NOR (n=35) and POR (n=16). The expression level of *XIST* varied largely between patients of both groups and did not show a difference between NORs and PORs (Figure 17C). However, a statistically significant lower expression level of XIST were detected as well in primary granulosa cells from both NOR (p=0.01) and POR (p=0.00) compared to women's leukocytes (Figure 17B).

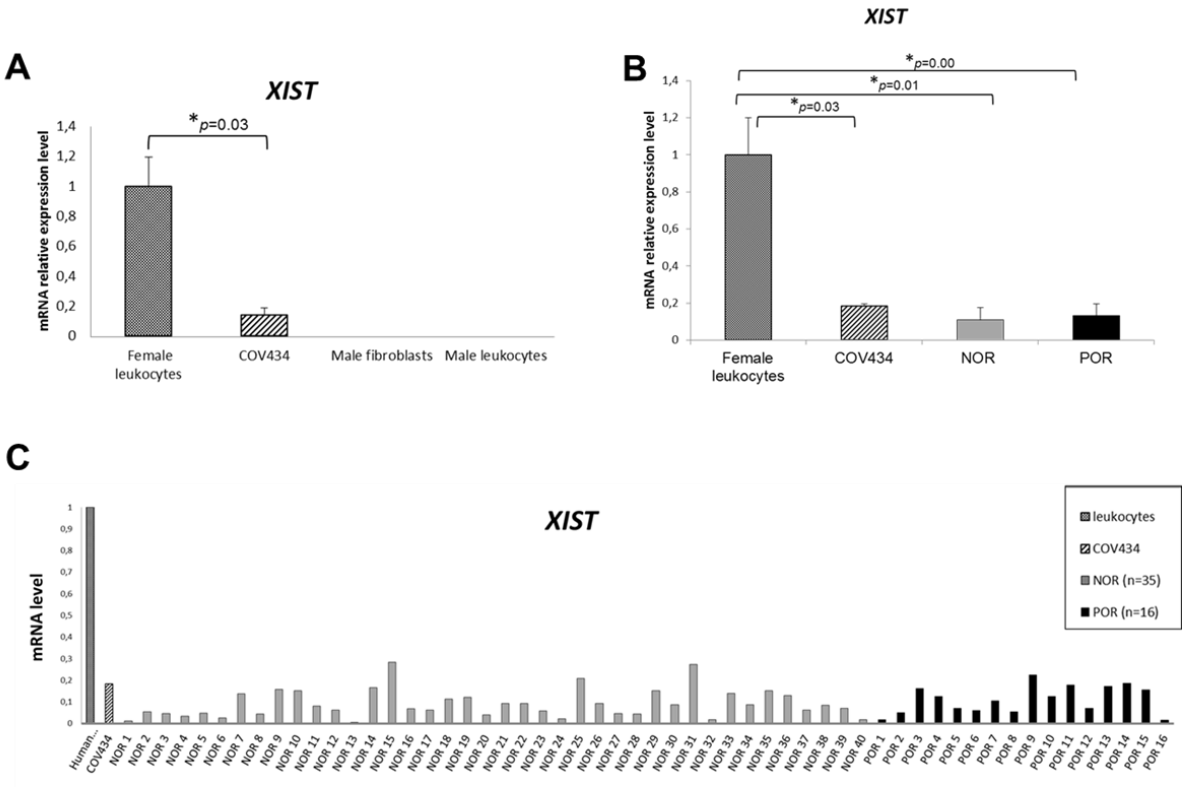

Figure 17: *XIST* expression in human granulosa cells.
XIST mRNA expression levels were analyzed using TaqMan based real time PCR. mRNA levels were normalized to *HPRT* mRNA expression and results are presented as comparative Ct value means ± SD (n = 3). **(A)** *XIST* expression levels were significantly lower expressed in COV434 compared to female's leukocytes and not detectable in male leukocytes and fibroblasts. **(B)** Significant lower expression of *XIST* transcripts was also detected in primary granulosa cells from both NOR and POR. **(C)** Individual variation of *XIST* transcript levels detected in granulosa cells from patients.

2.3.*FMR1*-DMR3 is also present in other human female tissues

Another novel regions identified in my CpG methylation analysis in COV434 cells was *FMR1*-DMR3. Therefore, I investigated whether the differential CpG site methylation pattern of *FMR1*-DMR3 observed in COV434 is also present in other female tissues including ovary, kidney and leukocytes (Figure 18). Although *FMR1*-DMR3 was found in these female tissues, the specific CpG sites methylation pattern displayed some tissue specificities. A statistically significant difference of CpG site methylation rates was reached in CpG sites 94 (p=0.01), 95 (p=1.00x10^{-5}), 96 (p=0.02) and 99 (p=0.02) (Figure 18E).

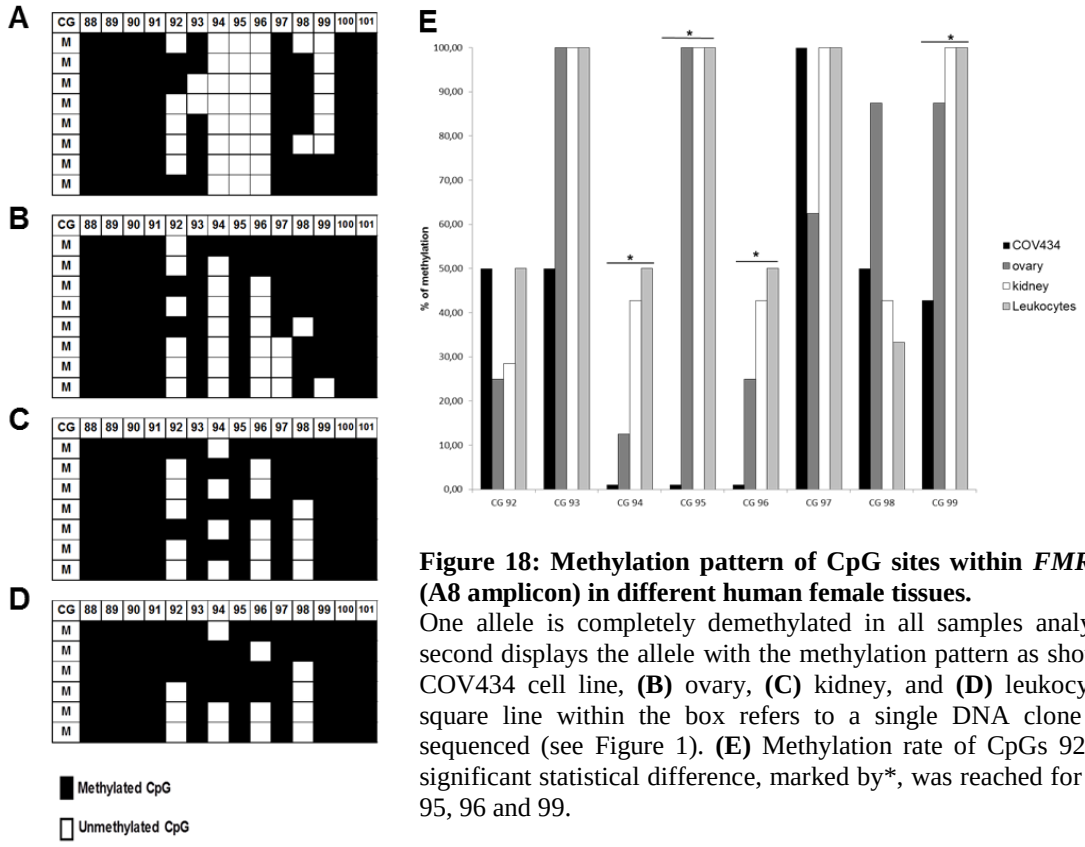

Figure 18: Methylation pattern of CpG sites within *FMR1*-DMR3 (A8 amplicon) in different human female tissues.
One allele is completely demethylated in all samples analyzed. The second displays the allele with the methylation pattern as shown in **(A)** COV434 cell line, **(B)** ovary, **(C)** kidney, and **(D)** leukocytes. Each square line within the box refers to a single DNA clone that was sequenced (see Figure 1). **(E)** Methylation rate of CpGs 92 to 99. A significant statistical difference, marked by*, was reached for CpGs 94, 95, 96 and 99.

2.4.Analysis of FMR1-DMR3 for putatively functional transcription factors binding sites

I examined the proposed *FMR1*-DMR1,-2 and-3 sequence regions for putative Transcription Factors (TFs) binding sites with the TRANSFAC-match tool, using vertebrate matrices and a standard threshold of 0.9. Only TFs whose binding is known to be dependent on CpG site methylation pattern[152-154] are presented in Table 10.

Table 10: Prominent CpG methylation sensitive regulatory motif locations within the *FMR1*-DMR1, 2 and -3

Transcription factor sites/potential regulatory motifs	Sequence	*FMR1*-DMR location
AP2ALPHA	cCACAGGGC	DMR1
GATA3	ccccATCtt	DMR2
AP2ALPHA	gCGGGAGGC	DMR2/DMR3
E2F1_Q6_01	tTTCGGCGcc	DMR3
E2F_Q2	GGCGcc	DMR3
E2F_Q2	ggCGGG	DMR3
GATA1	cggGATgttg	DMR3
E2F_Q2	ccCGCC	DMR3
GATA1_01	gggGATgggc	DMR3
GATA2_01	gggGATgggc	DMR3
AP2ALPHA_01	GCCGGCGGc	DMR3
AP2ALPHA_01	gCCGGCGGC	DMR3

Most interesting was the identification of E2F1 double site present only in *FMR1*-DMR3 (Figure 19). E2F1_Q6 (also known as E2F1) binding is known to depend on CpG methylation, with a preference of binding to unmethylated CpGs[154]. CpG sites 93, 94 and 96 which were higher demethylated in COV434 cells, were found to be part of the E2F1 consensus sequence motif. Presence of two neighbored E2F sites suggests a strong binding just in this DMR domain. Sequence homology analysis showed that *FMR1*-DMR3 is conserved in primate and that E2F1 binding site has evolved probably first during primate evolution 50 million years ago (Table 11).

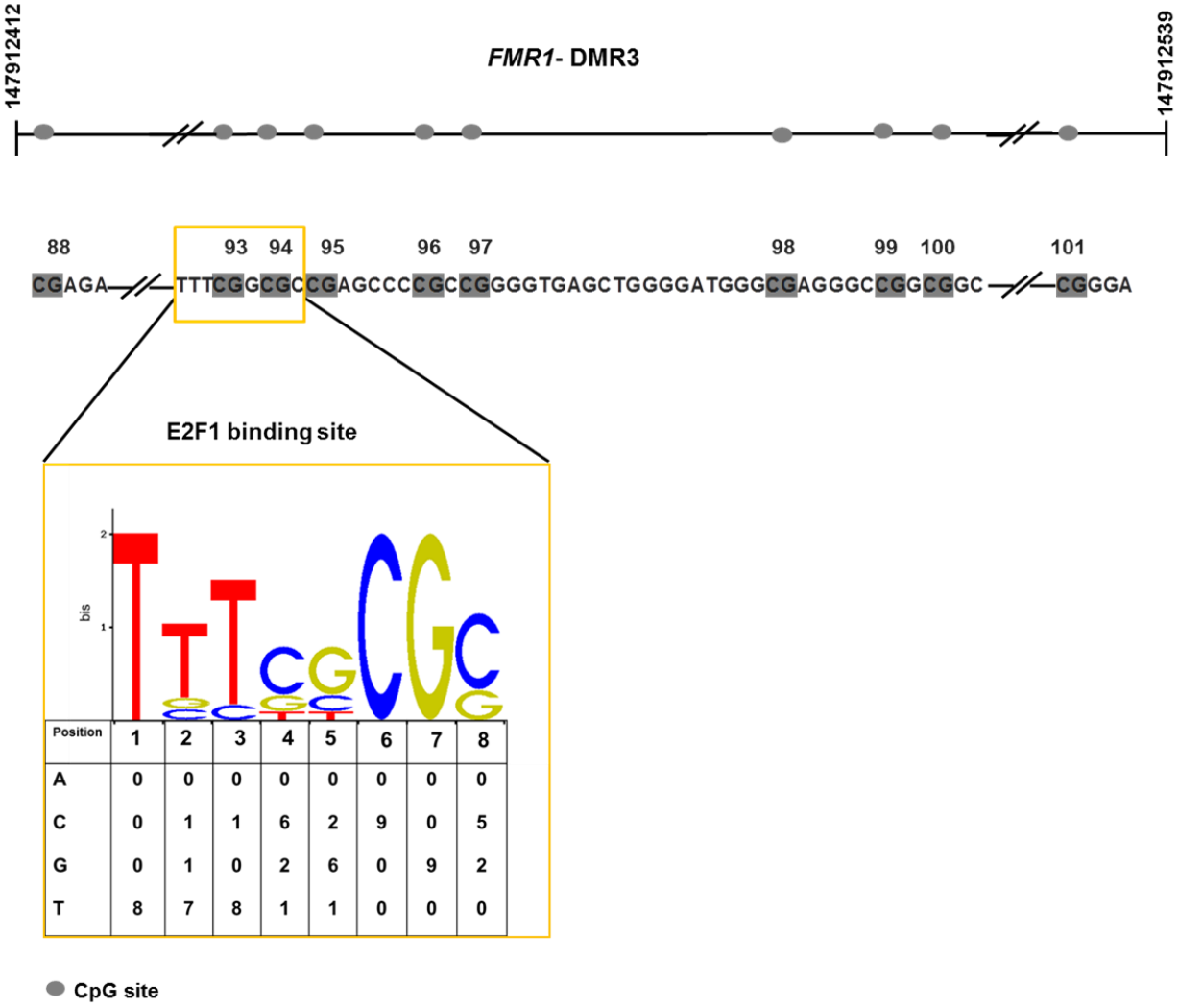

Figure 19: E2F1 binding site motif within *FMR1*-DMR3 sequence.
(A) CpG sites located within *FMR1*-DMR3 are indicated with grey filled circles. **(B)** E2F1 binding site within *FMR1*-DMR3 sequence is highlithed by an orange box. **(C)** Empirical ('True') E2F1 motif logo within *FMR1*-DMR3 predicted by TRANSFAC

Table 11: Sequence homology of the FMR1-DMR1, 2, 3 in different species.

***Homo sapiens* (human hg 19)**	***Pan troglodytes***	***macaca mulatta***	***callithrix jacchus***	***Carlito syrichta***
Divergence time[155] (Mya)	8 Mya	35 Mya		50 Mya
***FMR1*-DMR1**	92.6%	84.4%	34.1%	14%
***FMR1*-DMR2**	99.6%	93.8%	92.2%	27%
***FMR1*-DMR3**	98.4%	97.6%	90.9%	12.8%

2.5.E2F1 binds within *FMR1*-DMR3

I investigated the capacity of nuclear E2F1 to bind within *FMR1*-DMR3 experimentally. A 22bp DNA biotin-labeled probe which contains a non-methylated CpG site 94 within the E2F1 binding site was used as probe to screen for binding from factors in the nuclear extracts from the COV434 cell line. EMSA produced a pattern of retarded bands indicating the binding of nuclear proteins only to the CpG 94 site non-methylated probe (Figure 20, lane 2). This binding was specific for E2F1, since it could be eliminated by an increasing concentration of an unlabeled competitor probe (Figure 20, lanes 3, 4, 5) but not with an unlabeled mutated probe (Figure 20, lane 6).

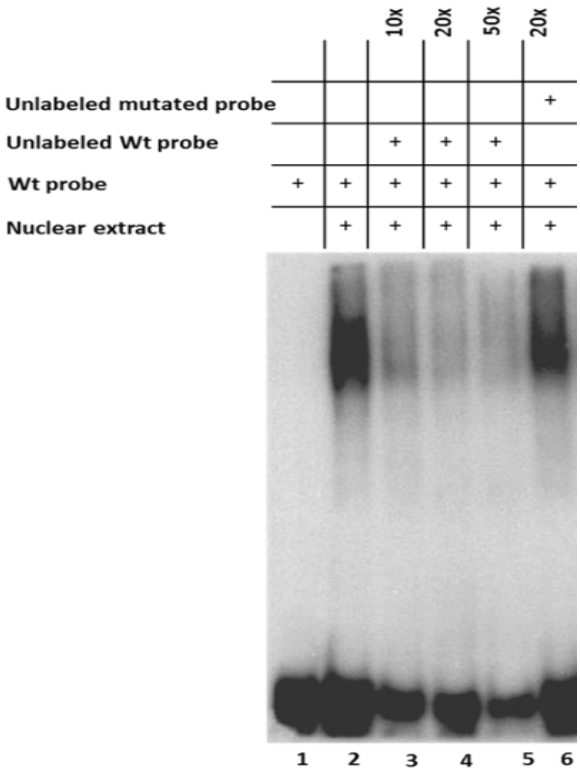

Figure 20: Specific binding of nuclear proteins from COV434 cells within *FMR1*-DMR3.
EMSA was performed with a probe containing the unmethylated CpG site 94 within the E2F1 consensus present in the *FMR1*-DMR3 region. Nuclear extracts from proliferating COV434 cells were incubated with the E2F1 probe alone (lane 2) or in the presence of excess (10X, 20X and 50X) unlabeled probe (lanes 3 and 5) or a probe containing a 20X excess of mutated E2F1 consensus motif (lane 6).

2.6. *FMR1*-DMR3 analysis in primary human granulosa cells

For the CpG sites methylation analysis in human primary granulosa cells I had to concentrate on one of the identified *FMR1*-DMRs due to patient material restrictions. Therefore, I decided to analyze the CpG methylation pattern of *FMR1*-DMR3 due to presence of the unique methylation dependent E2F1 binding sites.

The CpG methylation pattern of *FMR1*-DMR3 sequence was analyzed in human primary granulosa cells, collected from patients that showed a different ovarian response after controlled ovarian stimulation in order to explore whether (1) this domain is also present in primary granulosa cells. (2) Whether the pattern of CpG site methylationis different in NOR and POR samples. Primary granulosa cells from NOR (n=10) and POR (n=9) patients were analyzed in comparison.

The *FMR1*-DMR3 CpG methylation pattern was analyzed in 5 patients of each group. CpG sites 92 to 99 showed a differential methylation pattern (Figure 21A). The degree of methylation of these CpG sites varied between both patient groups as between patients within the same group (Figure 21A). A statistical significant difference was reached with this small number of patients only for CpG site 94 (p=0.01) that was highly demethylated in POR (89.74%) granulosa cells compared to NOR (59.38%) (Figure 21B). In addition, I analyzed the expression of *FMR1* transcripts in primary granulosa cells between the two groups. POR showed a tendency towards higher *FMR1* expression compared to NOR (Figure 21C), although no statistically significant difference was reached.

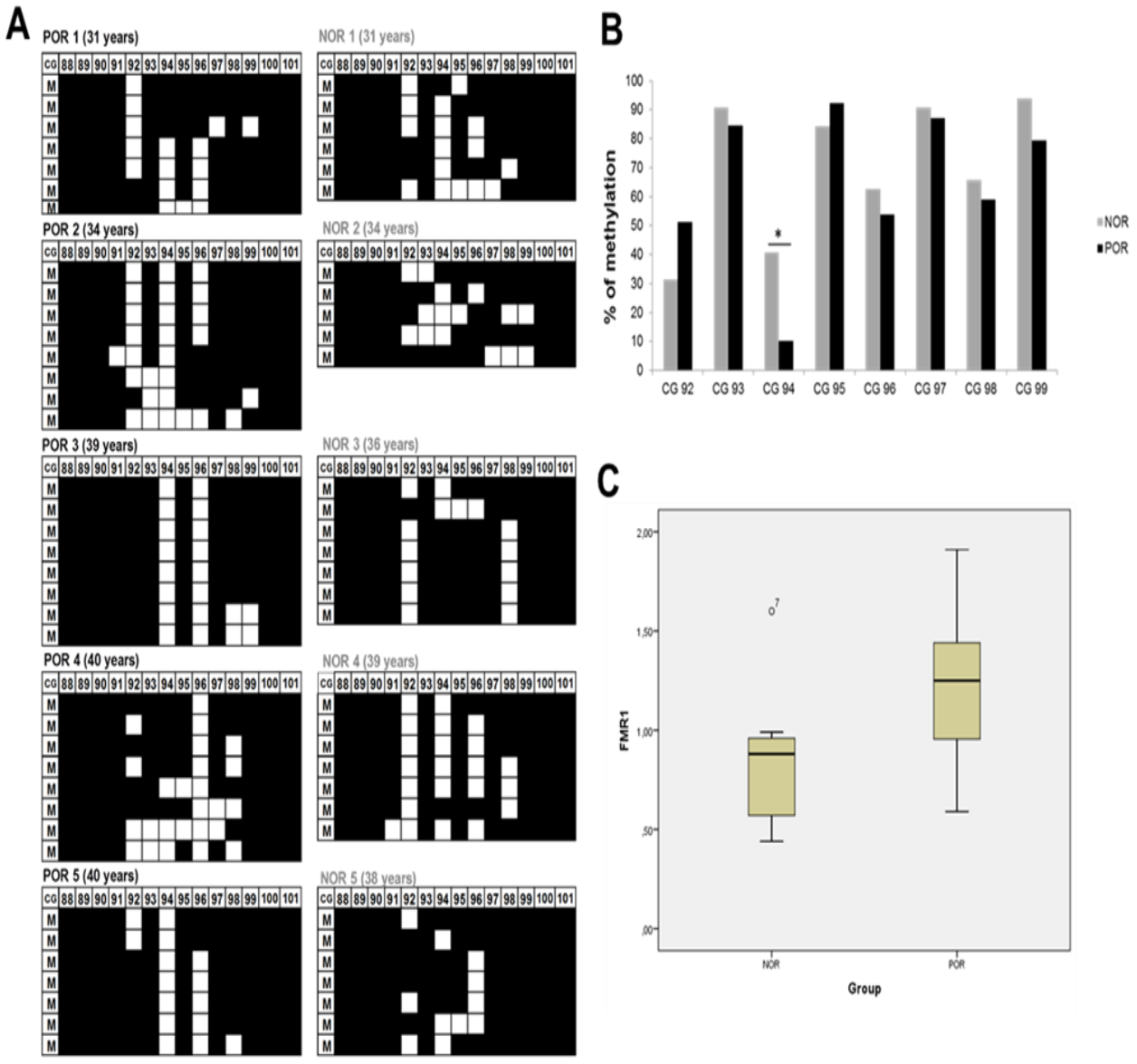

Figure 21: Methylation pattern of CpG sites within *FMR1*-DMR3 in human primary granulosa cells.
In granulosa cells from POR (n=5) and NOR (n=5), MSP analysis of A8 showed the presence of one unmethylated allele and one methylated allele with individual CpGs that remained unmethylated. Only the allele with the methylated pattern is shown here **(A)**. Each box represents one patient and each lane within the box corresponds to a single DNA molecule that was sequenced. **(B)** Quantification of methylation levels of the CpGs 92 to 99. A significant difference (*) was reached in CpG 94 (p=0.01). **(C)** Expression of *FMR1* transcripts in patients'granulosa cells. POR (n=9) showed a tendency towards a higher expression compared to NOR (n=10).

Chapter 3: Characterization of expression pattern of *ASFMR1* long non coding transcripts in human granulosa cells

The aim of this study was to analyze the expression pattern and rate of *ASFMR1* transcripts in the COV434 granulosa cell line and in primary graulosa cells collected from patients with different ovarian response (NOR and POR) in order to compare the results with view to the clinically observed variable ovarian response in NOR and POR samples.

3.1. *ASFMR1* is expressed in the COV434 cell line

Due to known difficulties to amplify transcripts through the CGG repeats, I opted for a nested PCR approach at different transcript positions to analyze the expression of the complex *ASFMR1* transcript splicing pattern (see introduction section 1.3.3). The originality of this approach is that it allowed to characterize complete polyadenylated *ASFMR1* transcripts starting at *FMR1* intron 2 (genomic position +10243 relative to the TSS+1 of the *FMR1* gene) and ending in PAS1 site (genomic position -1815 relative to the TSS+1 of the *FMR1* gene). A first round of PCR was performed to select for polyadenylated transcripts starting at +10243 bp and ending with PAS1 (Figure 22A). Nested PCR results then showed that *ASFMR1* transcripts starting at +10243 are expressed in COV434 cells. Mapping for transcript regions upstream of the CGG repeats revealed presence of an unspliced form and two different spliced isoforms (A and B) in COV434 cells as depicted in Figure 22B. The third isoform (C), reported in lymphoblastoid cell lines[130], was not detected on gel. Mapping of the transcript region containing the CGG repeats, showed the presence of one band with a size corresponding to the *FMR1* transcript allele containing 42 CGG triplet repeats (Figure 22C). Mapping of the region downstream of the CGG triplet repeats also showed the presence of two transcript isoforms. Since the splicing pattern was very complex, it was not possible to associate the isoforms detected upstream and downstream the CGG repeats together, therefore, they were named; ISO1 and 2 (Figure 22D). The first transcript, ISO1, contained a 9.7 kb intron corresponding to the *FMR1* intron1 that uses the complementary splice donor and acceptor sites also used for *FMR1* transcripts, representing a non-consensus CT to AC splice site. The second isoform, ISO2, revealed another alternative splice form of the *ASFMR1* transcript with a small intron from +10155 to +10070 that uses a second non-consensus CT-AC splice site. Surprisingly, this isoform described “PM specific” in former publications[130], was mainly expressed in COV434, which does not carry an *FMR1*-PM allele. A schematic summary of the results is presented in Figure 22E.

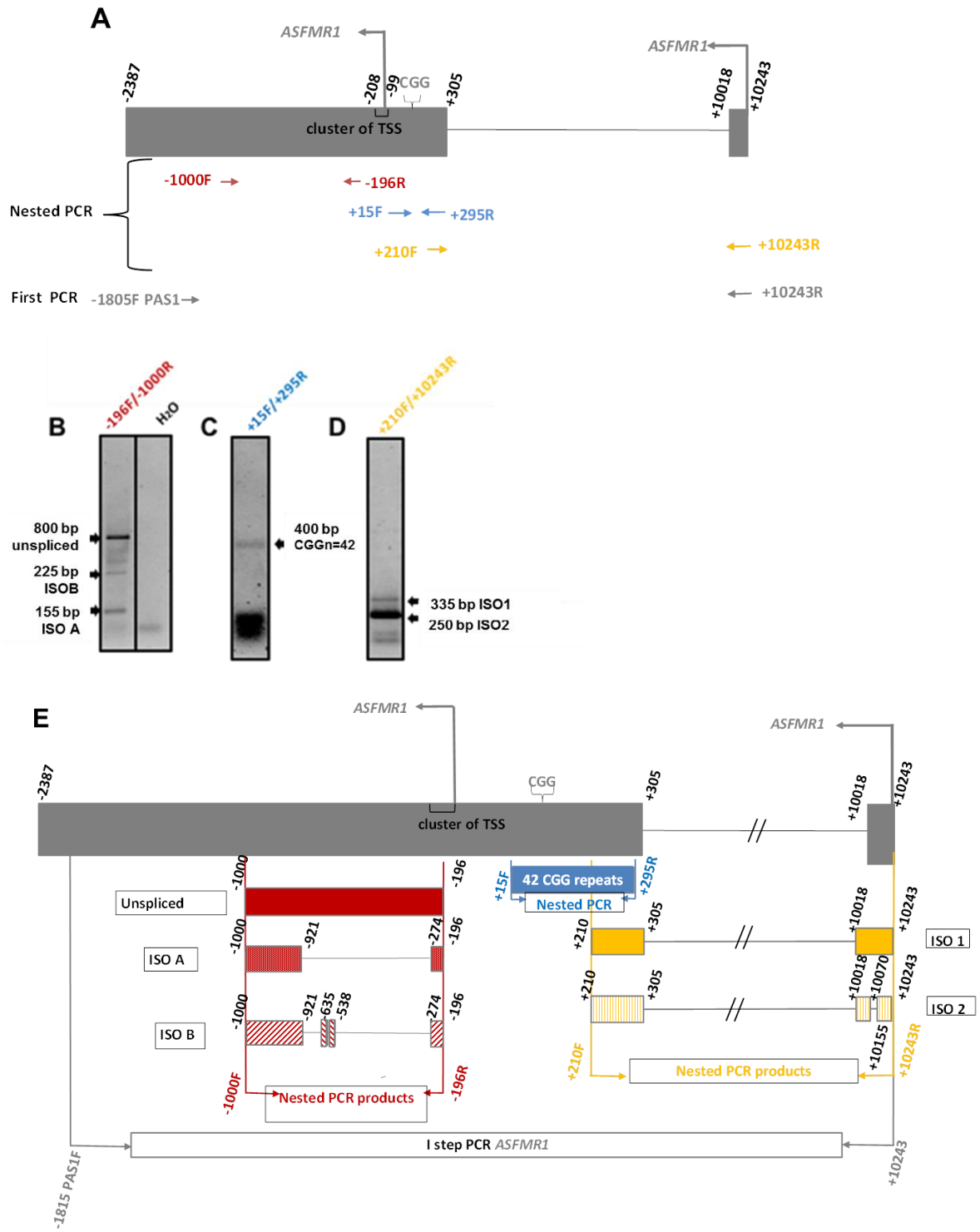

Figure 22: Mapping of *ASFMR1* transcripts in COV434 cells.
(A) Diagram of *ASFMR1* gene according to published results by Ladd et al.[130]. Numeric values indicate the genomic positions relative to the TSS +1 of *FMR1* gene. Exons of *ASFMR1* are indicated by grey rectangles. TSS located at +10243bp and the cluster of TSSs between -99bp and -208bp are indicated with grey arrows. A first round of strand-specific RT–PCR from −1805 bp (PAS1) to +10243 bp (TSS located in intron2 of the *FMR1* gene) was performed and primer positions are indicated by short grey arrows. Position of primers used for nested PCRs are indicated by red, blue and yellow arrows. Nested PCR showed the presence of *ASFMR1* transcripts at the positions **(B)** −196 to −1000, revealing multiple splice forms A, B and the non-processed transcript, and **(D)** +210F to +10243R, revealing transcript splice forms ISO1 and 2. **(C)** Amplification of CGG-

rich sequences identified an antisense transcript spanning the CCG repeat region from +295F to +15R in COV434 containing 42 CGG repeats. **(E)** Schematic summary of *ASFMR1* transcripts and the splice sites detected in COV434 cells.

3.2. Identification of the novel 5′ ends of *ASFMR1* in COV434 cells.

To investigate whether there are different 5'ends of *ASFMR1*transcripts in COV434 cells, 5′-RLM-RACE was performed. Three distinct starts of 5′ends downstream of the CGG triplet repeats were detected on gel (Figure 23B). Sequencing of the detected amplification products showed that in COV434 cells the transcription of the *ASFMR1* transcripts is initiated at positions +305 bp and +10070 bp and +13848 bp. Taken together, these data suggest the presence of three alternative core promoters driving the transcription of *ASFMR1*, with the +305 bp site as major TSS as depicted in Figure 23B. In contrast to TSS located at +305 bp, the +10070 bp and the +13848 bp TSSs were not previously reported in any cell type. Upstream of the CGG triplet block, I did not detect any further TSS.

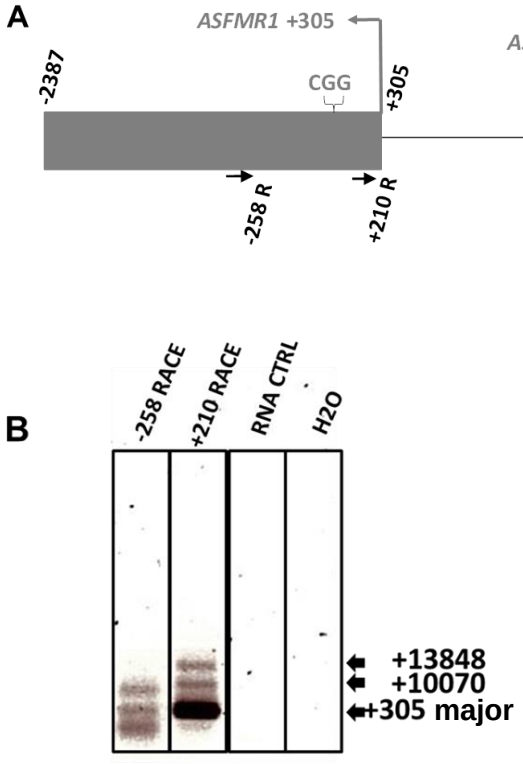

Figure 23: Identification of 5' ends of the *ASFMR1* transcript in COV434 cells.
(A) *ASFMR1* genomic locus is depicted see Figure 19 and the position of primers used for 5′-RLM RACE are indicated with black arrows. Bold grey arrows indicate the three transcription initiation sites identified in COV434 cells at +305bp, +10070bp and +13848bp. **(B)** Detection on gel of *ASFMR1* 5'ends using 5'RLM RACE primers -258 RACE and +210 RACE. The RNA CTRL was used to ensure that the obtained products are specific. The negative control using water indicated the absence of contamination.

3.3. Identification of new *ASFMR1* transcript isoforms in COV434 cells

Next, I aimed to characterize the length of transcripts starting at position +13848bp. Transcripts initiated at TSSs +305 and +10070 were not studied. A similar approach as described above was performed to select for only polyadenylated transcripts (Figure 24A). The presence of different spliced transcript isoforms was detected upstream and downstream of the CGG repeats (Figure 24B, C). Two isoforms (ISO1 and ISO2) were detected between

positions +13848bp and +210bp (Figure 24C). The first isoform, contained two introns corresponding in length and position to *FMR1* intron 1 and part of intron 2 that uses the complementary splice donor and acceptor to *FMR1*, representing a non-consensus CT to AC splice site. The second isoform had an additional small intron between +10070 bp and +10155 bp that uses a non-consensus CT-AC splice site located in *FMR1* intron 2 (Figure 24D). These isoforms are probably the extension of ISO1 and ISO2 depicted in Figure 24D. Upstream of the CGG triplet repeats three spliced transcript isoforms (ISO A, B and C) were expressed; non-spliced *ASFMR1* transcripts were not detected on gel (Figure 24B). Presence of these isoforms suggests that the transcripts initiated at TSS +13848 are continuous and pass through the CGG repeats. Naturally, it was not possible to find out which transcript isoforms upstream of the CGG triplet block (ISO1 and 2) are combined with the three transcript forms downstream of the CGG triplet block (ISO A, B and C). At least, up to 8 transcript variants may be present in the COV434 granulosa cell line. However it can be concluded that there is a high complexity of *ASFMR1* transcript isoforms in COV434 and probably then also in primary human granulosa cells.

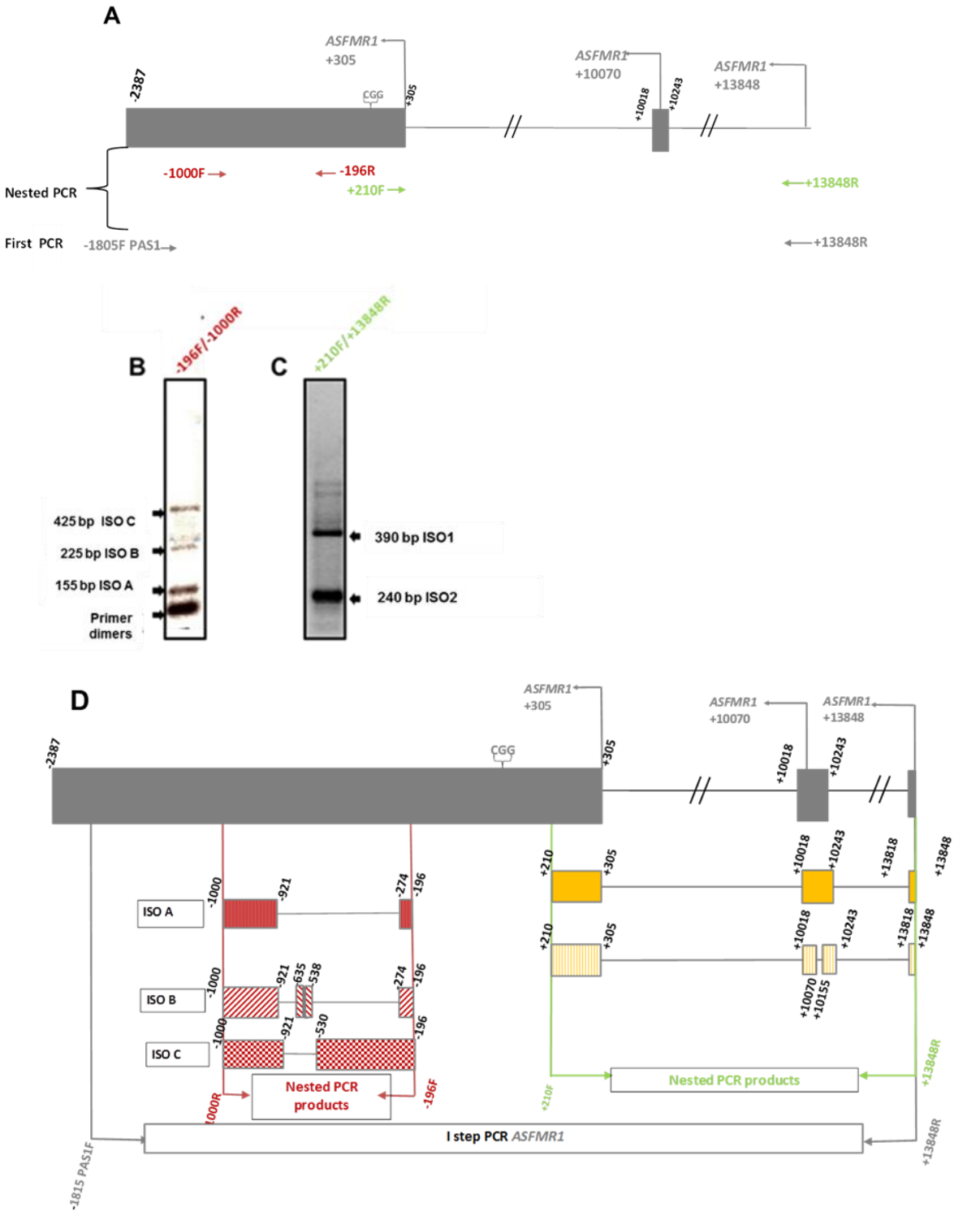

Figure 24: Mapping of the *ASFMR1* transcripts initiated from TSS +13848 in COV434 cells.
(A) Diagram of the *ASFMR1* gene according to results obtained in COV434 cell line. Numeric values indicate the genomic positions relative to the TSS +1 of *FMR1* gene. Exons of *ASFMR1* are indicated by grey rectangles with the CGG repeat region noted. The three newly identified TSSs are indicated with grey arrows. Experimental procedure was performed as noted in Figure 22. A first round of strand-specific RT–PCR from −1805bp (PAS1) to +13848bp was performed and primer positions are indicated by grey arrows. Position of primers used for nested PCRs are indicated by red, and green arrows. Nested PCR showed the presence of *ASFMR1* transcripts at positions **(B)** −196 F to −1000R, revealing multiple transcript splice forms ISO A, B and C, and **(C)** +210F to

+13848R, revealing the extension of splice forms ISO1 and 2. **(D)** Schematic summary of *ASFMR1* transcripts and the splice sites detected in COV434 cells.

3.4. *ASFMR1* is expressed in primary granulosa cells from patients

After having established the complexity of *ASFMR1* expression in COV434, the expression pattern of *ASFMR1* transcript in primary granulosa cells from NOR and PORs patients have been analyzed. My aim was to investigate if the expression pattern of specific isoforms may vary according to womens' ovarian response. Therefore I compared the *ASFMR1* transcript splicing pattern in NORs and PORs. Primary results showed that polyadenylated *ASFMR1* transcripts are expressed in primary granulosa cells of both, NORs and PORs. Mapping of transcripts upstream of the CGG triplet block showed presence of the unspliced transcript and ISO A. Interestingly, the expression pattern of these isoforms varied between patients with the unspliced transcript isoform being majorly expressed (Figure 25).

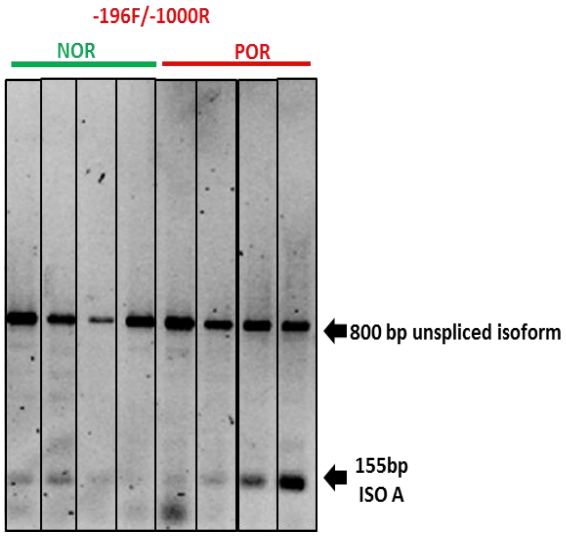

Figure 25: Expression profile of the *ASFMR1* transcript in human primary granulosa cells.
Nested PCR using primer pair -196F/-1000R performed in primary granulosa cells from NOR (n=4) and POR (n=4) revealed mainly the presence of an unspliced isoform and the spliced isoform A.

Chapter 4: *FMR1* gene expression silencing in COV434 cells.

One possibility to examine the influence of *FMR1* gene expression on human granulosa cell function, respectively its association with the expression of potential signal pathways was to inhibit *FMR1* mRNA expression by siRNA-treatment followed by microarray gene expression analysis of the COV434 granulosa cell transcriptome.

4.1. Efficiency of siRNA delivery in COV434 cells

In order to establish an optimal working transfection protocol, COV434 were transfected using FITC siRNA (sc-36869) according to two protocols (see Methods section 4.5). Transfection efficiency varied markedly between reagents (Table 12 and 13). The highest efficiency observed by FITC positive cells was for $4x10^4$ using th reagent, exhibiting 90 % FITC-positive cells when transfected with 50nM (Figure 26) or 100nM siRNA according to protocol 2 (Table 13). Since there was no difference in the transfection efficiency with 50nM or 100nM of siRNA using protocol 2, the 50nM was used as a working concentration in all following transfection experiments.

Table 12: Transfection efficiencies of FITC-labeled siRNA in COV434 cells using transfection protocol 1

Protocol 1	25nM	50nM	100nM
Lipofectamine 2000	20%	36%	39%
Lipofectamine RNAiMax	35%[1]	45%	54%
HiPerFect	23%	32%	30%

[1]% indicates the amount of COV434 cells showing a green signal that corresponds to a positive uptake of the FITC-siRNA: 100 cells were couned per slide.

Table 13: Transfection efficiencies of FITC-labeled siRNA in COV434 cells using transfection protocol 2

Protocol 2	25nM	50nM	100nM
Lipofectamine 2000	25%[1]	45%	48%
Lipofectamine RNAiMax	64%	90%	88%
HiPerFect	20%	39%	38%

[1]% indicates the amount of COV434 cells showing a green signal that corresponds to a positive uptake of the FITC-siRNA: 100 cells were couned per slide

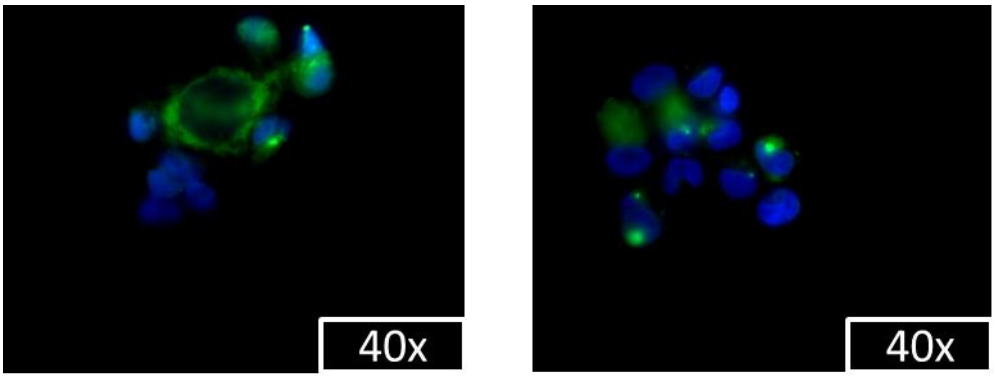

Figure 26: Analysis of transfection efficiencies by fluorescence microscopy.
COV434 cells were transfected with FITC-labeled siRNA at a concentration of 50 nM using Lipofectamine RNAiMax. 6h after transfection, the cells were fixed and analyzed visually. Specific intracellular FITC staining was detected (green). The nuclei were identified by DAPI staining (blue).

4.2. Inhibition of *FMR1* expression in COV434 cells by the siRNA-treatment

After the establishment of a working transfection protocol in COV434 cells, my aim was to examine the effects of *FMR1* in granulosa cells function , therefore the mRNA expression of *FMR1* was inhibited by siRNA treatment. For this, the knock down efficiency of several commercialized siRNA sequences targeting the *FMR1*gene was tested (silencer *FMR1*-siRNA (10919), silencer *FMR1*-siRNA (11010) and siRNA Silencer® Select (4392420). Among these siRNA, The *FMR1* siRNA Silencer® Select showed the highest knock down efficiency and lowest side effects on cell viability and was selected for further analysis.

Using the same protocol as mentioned above, $4*10^4$ COV434 cells were transfected with 50nM Silencer® Select *FMR1*-siRNA or with a Silencer® Select non-silencing control siRNA (ctrl-siRNA). In parallel experiments cells transfected with the transfection reagent without siRNA served as a control to assess whether the transfection impacts cell viability and proliferation. The 96h time point was not used in the following analysis as no knock down effect was detected in all of the analyzed *FMR1*-siRNA (preliminary experiments, data not shown).

Expression of *FMR1* mRNA expression was analyzed using TaqMan based real time PCR. Each experiment was repeated two times and each sample was run in triplicates.

Up to 89% decrease in *FMR1* mRNA expression was detected at 48h post-transfection, as compared to cells transfected with Ctrl-siRNA group (p=0.05) (Figure 27). At 72h, the *FMR1* mRNA levels were comparable to Ctrl-siRNA group and to non-transfected cells group indicating a short half-life for *FMR1* siRNA (Figure 27). There was no difference in *FMR1* mRNA expression between Ctrl-siRNA group and the non-transfected cells group at each time point.

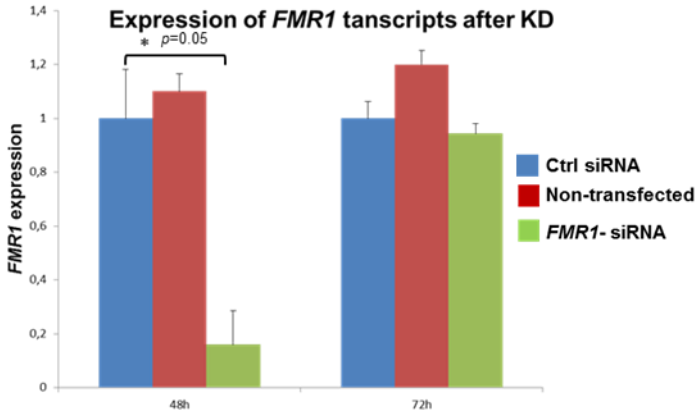

Figure 27: *FMR1* mRNA expression in COV434 transfected cells.
A siRNA Silencer® Select targeting the *FMR1* gene was transfected into COV434 cells at a concentration of 50nM. The silencing activity of *FMR1*-siRNA was monitored by TaqMan based real time PCR. mRNA levels were normalized to *HPRT* mRNA expression and results are presented as comparative Ct value means ± SD (n = 3). *FMR1* mRNA expression was quantified 48h and 72h (C) after transfection.

Specific knock down of *FMR1* mRNA should have a corresponding effect on the protein. To explore this effect, FMRP levels were analyzed 48 and 72h post transfection by western blot using protein extracted from the same samples used for the TaqMan analysis. FMRP has a half-life of 30h[156].

Western blot analysis showed a clear reduction in FMRP levels at 48h in COV434 cells transfected with *FMR1*-siRNA (Figure 28A, lane1) compared to Ctrl-siRNA group (Figure 28A, lane 2) and non-transfected cells (Figure 28A, lane 3). This result is in accordance with the high knockdown efficacy (89%) observed on the mRNA level. As seen in *FMR1* mRNA levels at 72h post-transfection there was no difference anymore in FMRP levels between the groups (Figure 28C).

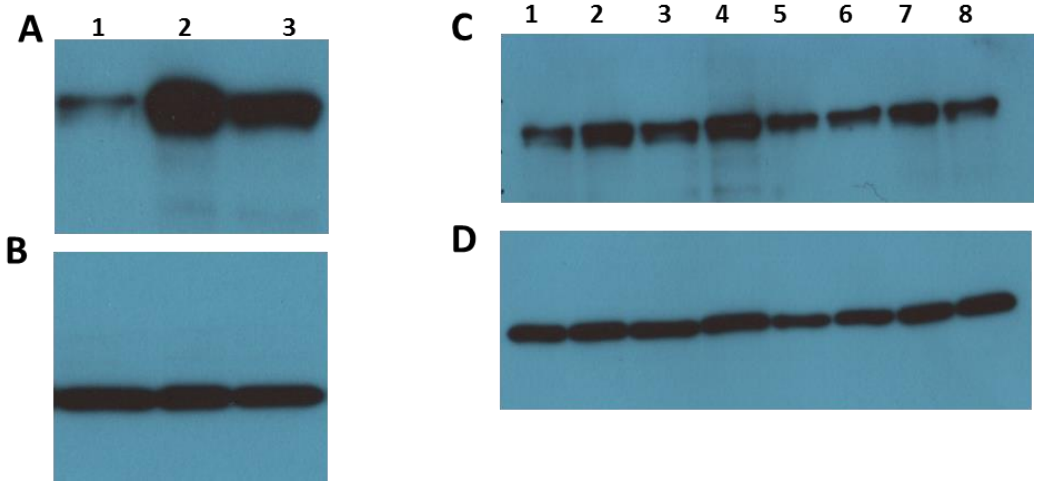

Figure 28: Western blot analysis of FMRP expression after *FMR1* gene knock down.
siRNA was transfected into COV434 cells at a concentration of 50 nM. At 48 and 72 h post-transfection, cells were lysed and protein expression was analyzed by western blot. **(A)** Protein analysis at 48h after transfection in *FMR1*-siRNA (lanes1), Ctrl-siRNA (lane3) and non-transfected cells (lane 4) groups. **(B)** Protein input was normalized using GAPDH. **(C)** Protein analysis at 72 h post-transfection in *FMR1*-siRNA (lanes1, 2 and 3), Control non-silencing siRNA (lanes 4, 5 and 6) and non-transfected cells (lane 7 and 8). **(D)** Protein input was normalized using GAPDH.

4.3. Microarray profiling and signal pathway analysis

After having confirmed the 89% knock down of *FMR1* gene expression on both; mRNA and protein levels at 48h post transfection, these samples were selected for COV434 transcriptome analysis by appropriate microarray assay (Human HT-12 v4 Expression Bead Chip Kits, Illumina). The aim of this experiment was to identify potential biological pathways that are influenced by the decrease in expression of the *FMR1* gene in the COV434 cell line used as a model for human granulosa cells. Total RNA was extracted from cells at 48h post transfection that showed the highest knockdown of the gene expression at both, mRNA and protein levels. Variation in gene expression was compared between cells treated with *FMR1*-siRNA and cells treated with Ctrl-siRNA. The top candidates, which showed a higher differential gene expression compared to the control group are listed in Table 14.

Table 14: List of genes showing the highest variation in gene expression levels in the microarray analysis

Gene symbol	Fold change	*p*-value	Definition
MIR1974	1.84	0.119	Homo sapiens microRNA 1974
PTPMT1	1.81	0.006	Homo sapiens protein tyrosine phosphatase, mitochondrial 1
TPRG1L	0.59	0.001	Homo sapiens tumor protein p63 regulated 1-like
TMX1	0.61	0.005	Homo sapiens thioredoxin-related transmembrane protein 1
PSME3	0.62	0.010	Homo sapiens proteasome (prosome, macropain) activator subunit 3 (PA28 gamma; Ki)
ANKRD46	0.63	0.002	Homo sapiens ankyrin repeat domain 46
TOMM20	1.57	0.0005	Homo sapiens translocase of outer mitochondrial membrane 20 homolog (yeast)
SepT 11	0.65	0.011	Homo sapiens septin 11
FAM44B	1.54	0.0001	Homo sapiens family with sequence similarity 44
SBDSP	0.65	0.0009	Homo sapiens Shwachman-Bodian-Diamond syndrome pseudogene
NUDT21	0.66	0.0013	Homo sapiens nudix (nucleoside diphosphate linked moiety X)-type motif 21
SNCA	1.5	0.120	Homo sapiens synuclein, alpha (non A4 component of amyloid precursor)
MSRB3	1.48	0.001	Homo sapiens methionine sulfoxide reductase B3
RUVBL1	0.68	0.05	Homo sapiens RuvB-like 1

4.3.1. Identification of differential gene pathways potentially involved in *FMR1* expression control in human granulosa cells

Signal pathway analysis of the *FMR1* KD signature was performed at the department of Bioinformatics using the ConsensusPathDB-human (http://cpdb.molgen.mpg.de/) software package. The identified pathways are presented in table 15.

Table 15: Predicted pathways to be altered after *FMR1* knockdown using $p<0.05$

p-value	pathway	members	Size[1]
0.0002	**Methionine salvage pathway**	**ADI1; GOT1; MTAP; APIP**	6
0.0053	Integrin alphaIIb beta3 signaling	CRK; PTPN1; RAP1B; CSK; RAP1A	28
0.0067	Platelet Aggregation (Plug Formation)	CRK; PTPN1; RAP1B; CSK; RAP1A	38
0.0071	RHO GTPases Activate Rhotekin and Rhophilins	RHOB; TAX1BP3; RHPN2	9
0.0083	Deadenylation of mRNA	EIF4A1; CNOT1; CNOT7; CNOT6; EIF4A3	25
0.0092	Deadenylation-dependent mRNA decay	CNOT7; LSM7; EXOSC7; EXOSC3; CNOT1; EIF4A1; CNOT6; EIF4A3	57
0.00966	Cysteine and methionine metabolism - Homo sapiens (human)	DNMT3B; ADI1; APIP; GOT1; MTAP; LDHA	45

[1] Size= number of genes included in the pathway. **The Methionine salvage (MTA) pathway is highlighted in bold.**

4.4. Analysis of expression of genes involved in the *mTOR/AKT* signalling pathway after *FMR1* gene knock down in COV434 cells.

I decided to analyse the expression of key genes involved in the AKT/mTOR signalling pathway (*S6K*, *AKT*, and *mTOR)* and *FOXO3* expression as a possible functional link between the human *FMR1* expression and the expression of key genes involved in the AKT/mTOR signalling pathway was reported recently[80; 88]. Expression of these genes was below the detection limit of the microarray analysis. Therefore, I quantified their expression in COV434 cells, at 48h and 72h in cells treated with *FMR1*-siRNA or with Ctrl-siRNA at the mRNA and protein levels using individual TaqMan probes and ELISAs.

At 48h post-transfection, silencing of the *FMR1* gene resulted in a significant decrease in *FMR1* transcripts levels as noticed earlier (p=0.05). In addition a significant increase in both, *S6K* (p=0.05) and *AKT1* (p=0.05), levels were present in group treated with *FMR1*-siRNA compared to control group. *mTOR* and *FOXO3* expression were also increased although they did not reach a statistically significant difference (Figure 29A). In contrast, at 72h post

transfection, no significant difference in expression level was noticed between the two groups (Figure 29B).

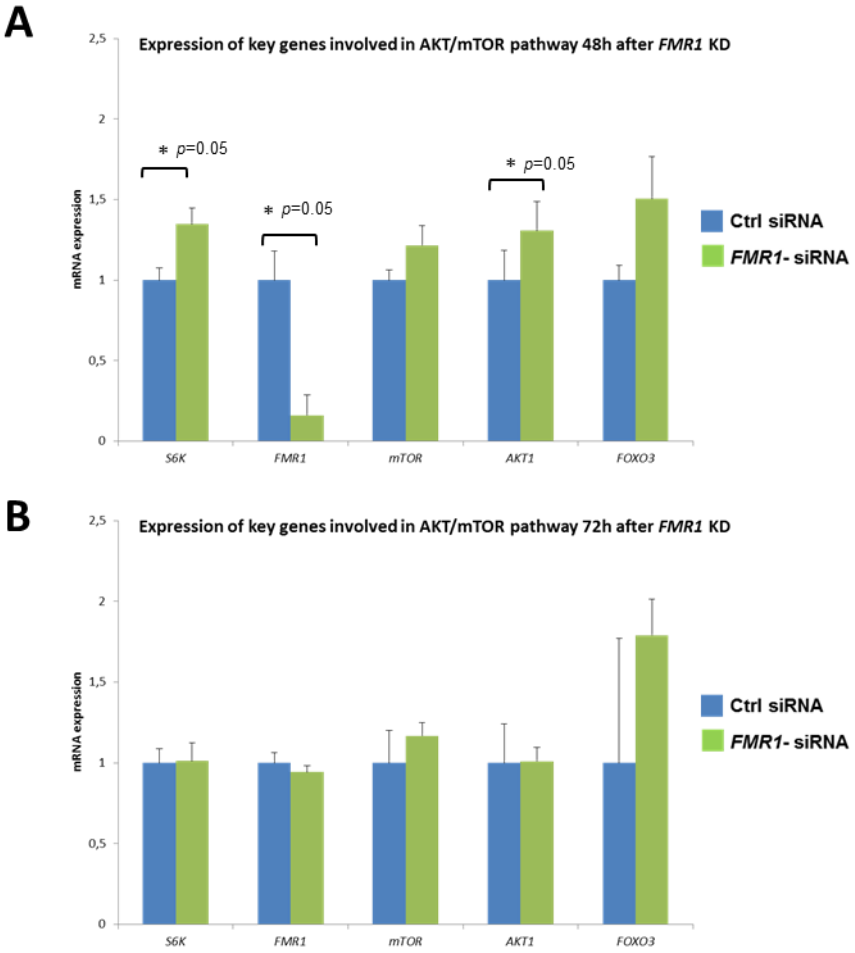

Figure 29: Gene expression changes of key genes involved in the AKT/mTOR signaling pathway in human granulosa cells following treatment with *FMR1*-siRNA.
COV434 cells were transfected with FMR1-siRNA or with a non-silencing control siRNA (ctrl siRNA) at a concentration of 50 nM. Gene expression of *S6K*, *FMR1*, *mTOR*, *AKT1* and *FOXO3* was measured at **(A)** 48h and **(B)** 72h post-transfection. mRNA levels were normalized to *HPRT* mRNA expression and results are presented as comparative Ct value means ± SD (n = 3).

Next, the protein expression levels of FMRP, S6K, mTOR, phospho-mTOR, AKT1 and phosphor AKT/ERK/S6K were analyzed using ELISAs at 48h and 72h post transfection. At 48h post transfection, a significant reduction in the FMRP levels (p= 0.05) was present in cells treated with *FMR1*-siRNA. This result is in accordance with results obtained from western blot analysis (see Figure 28). In addition, a significant increase in S6K protein (p=0.03) was also detected in cells treated with *FMR1*-siRNA (Figure 30A). Surprisingly, at 72h post-transfection the reestablishment of *FMR1* gene expression to control levels (Figure 29B) was accompanied by a significant increase in FMRP levels (p=0.04) (Figure 30B). In addition, there was an increase, although not significant, in the total and in the phosphorylated

protein form of mTOR and in the phosphorylated form of AKT/ERK/S6K in the group treated with *FMR1*-siRNA compared to the control group.

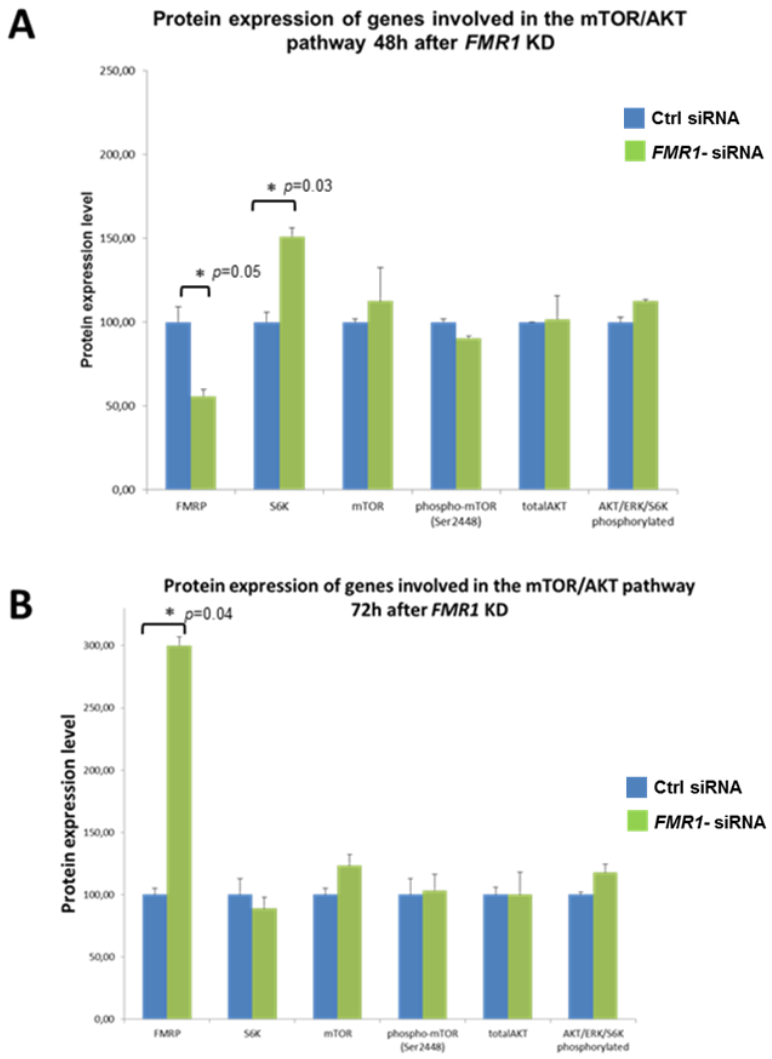

Figure 30: Protein expression changes of key genes involved in the AKT/mTOR signaling pathway in human granulosa cells following treatment with *FMR1*-siRNA.
COV434 cells were transfected with *FMR1*-siRNA or with a non-silencing control siRNA (ctrl-siRNA) at a concentration of 50 nM and protein expression was at 48h (A) and 72h (B) post-transfection. The expression of FMRP, S6K, mTOR, phospho-mTOR (Ser 2448), AKT1 and phospho-AKT/ERK/S6K was monitored using specific ELISAs. Protein expression levels are represented relative to the control group ± SD (n = 3).

In summary analysis of COV434 transcriptome after *FMR1* mRNA expression knock down revealed presence of several potential pathways affected by *FMR1* expression level. Most interesting, with view to the female germ cell development seem to be the MTA and AKT/mTOR signal pathways.

6- Discussion

6.1. Validation of COV434 cell line as a human granulosa cell model to study *FMR1* gene transcriptional control.

In this study, I present strong experimental evidences that the granulosa cell line, COV434 can be used as a viable model system to analyze transcript complexity and epigenetic control of the human *FMR1* gene in human primary granulosa cells.

CpG methylation analysis of the extended *FMR1* promoter in COV434 cells revealed the presence of a completely unmethylated CpG sequence domain around its core promoter (*FMR1*-UMR), i.e, on both gene alleles. *FMR1*-UMR was then found to be also present in human primary granulosa cells but not in female leukocytes nor in fibroblasts (Figure 14 and 16). The differentially CpG methylation pattern within *FMR1*-DMR3 detected in COV434 was also found to be comparable to human primary granulosa cells and different from that in female leukocytes, ovary and kidney tissues (Figure 18 and 21). Furthermore, investigation of *FMR1* and *ASFMR1* transcript splicing patterns in COV434 cells revealed only minor differences with the pattern of *FMR1* transcript splice variants detected in human primary granulosa cells. These results were an essential perquisite to study then also the variation of CpG site methylation in *FMR1*-UMR and -DMR3 in NORs and PORs granulosa cells; dependent on women ovarian reserve and to start functional knock down assays for the *FMR1* gene in COV434 by optimized siRNA tools developed for this gene.

6.2. *FMR1* gene transcriptional control in primary human granulosa cells from patients with different ovarian reserve.

Comparison of CpG site methylation patterns in women with different ovarian reserves (NORs and PORs) revealed that *FMR1*-UMR in primary human granulosa cells was present independent of women ovarian reserve, suggesting that this region is generally important for control of *FMR1* gene expression during human folliculogenesis. In contrast, analysis of the CpG methylation pattern of *FMR1*-DMR3 in the same primary granulosa cells (NORs and PORs) was found to be dependent on women ovarian reserve. Statistically confirmed difference was found for CpG 94 site being higher demethylated in granulosa cells from women with lower ovarian maturation potential (PORs). Since CpG 94 is part of the doubled target site of E2F1, these results suggest that E2F1 binding efficiency to *FMR1*-DMR3

functionally contribute to the rate of *FMR1* expression being variable and depending on women ovarian reserve.

Expression of splice variants of the *FMR1* and *ASFMR1* genes seem not to be depending on women ovarian reserve. Although a complex splicing pattern of both genes was present in the primary granulosa cells like in COV434, no differences in the set of transcript variants expressed in granulosa cells of both NORs and PORs could be identified.

6.3. *FMR1*-UMR part of *FMR1* gene activation in human granulosa cells.

CpG sites located within *FMR1*-UMR were found to be demethylated on both gene alleles only in human granulosa cells. It suggests that the *FMR1* gene was expressed from both gene alleles in granulosa cells thus escapes inactivation on the second X chromosome. It has been repeatedly assumed that at least some of the X genes functional during folliculogenesis and the female reproduction cycle require the expression of both X gene alleles genes that means escape X-inactivation[30; 31]. This view gained support by the observation that most women with Turner syndrome carrying one copy of the X chromosome suffer from an accelerated depletion of their follicular pool and develop POF[27; 33; 157; 158].

Indeed, most of the identified female reproduction related genes are concentrated on the X chromosome[27; 31] and at least 15% of genes located on the X chromosome escape X inactivation[32; 159]. These genes are called escapee genes[32; 102; 160]. However, escapee genes seem to exhibit some tissue-specific differences in their rate of escaping from X inactivation[32]. X chromosomal deletions and translocations found in women with POF strongly indicate that at least some X genes require indeed two gene alleles for female ovarian function[161-163].

In adult tissues, CpG islands located in the promoter region of escapee genes are demethylated and are associated with a histone code which is characteristic for active chromatin[164]. In female leukocytes and fibroblasts, *FMR1* gene was reported to be subjected to X inactivation[159; 165-168]. In granulosa cells however, *FMR1* transcription may be active on both gene alleles because I found only a low expression of *XIST* (Figure17). This fits to the biallelic expression of the *FMR1* core promoter including *FMR1*-UMR. However, the additional presence of *FMR1*-DMR1, -2 and -3 with specific CpG site methylation patterns in granulosa cells suggests some molecular mechanisms probably controlling the efficiency of the proposed biallelic gene expression in these germ line cells. One possibility may be that *FMR1*-DMR1, -2 and -3 include some repressive control elements to attenuate quantitatively

this biallelic gene expression. If this holds true, it suggests that some epigenetic dosage control of a biallelic *FMR1* gene expression is required at least in human granulosa cells.

6.4. E2F1 binding site in *FMR1*-DMR3 is functional for *FMR1* expression in human granulosa cells.

In this study, I present strong experimental evidence that the efficiency of *FMR1* gene transcription in human granulosa cells is controlled by some epigenetic mechanism located in the *FMR1*-DMR3 region identified in intron1 (Figure 13). *FMR1*-DMR3 was also found in different female tissues; however, its CpG methylation pattern showed tissue specificity (Figure 18).

FMR1-DMR3 is part of the extended *FMR1* gene promoter extending to intron 1[111]. Intronic CpG islands were found to be equally essential for gene expression as the genomic regions located close to the core promoter[169; 170]. Indeed, silencing of several genes has been shown to be induced by hypermethylation of the CpG island located in the first intronic region[169-171]. Also the methylation pattern of a single CpG site located in an intronic region has been shown with an impact on gene expression. In prostate cancer cell lines, hypermethylation of a single CpG site located in intron1 of the *peroxisomal membrane protein 24 gene* (*PMP24*) resulted in gene silencing, probably by preventing binding of some methylation sensitive AP-2- or a Sp1 factors[171].

The influence of a single CpG methylation rate within a gene on the development of diseases is well studied in cancer[172]. Recently, it has also been reported to be involved in the development of PCOS syndrome[173] .Therefore, the methylation rate of single CpG sites if part of Transcription Factor (TF) target site; can generally serve as a dynamic switch module to activate or inactivate gene expression.

TFs analysis along the distinct differential CpG methylated sequence regions, *FMR1*-DMR1, -2 and -3 predicted the presence of several E2F binding sites only in *FMR1*-DMR3. E2F1 is known to be a transcriptional activation factor, controlling its DNA binding affinity by methylation of single CpG sites in its target sequence[153; 154]. Using EMSA analysis, I confirmed that E2F1 binds indeed to its predicted consensus sequence within *FMR1*-DMR3 when containing a non-methylated CpG 94 site. Conservation of the doubled E2F1 target site in *FMR1*-DMR3 since 50 Mya supports that this E2F1 binding site is functionally required for *FMR1* expression in granulosa cells. This assumption gained further support by the experimentally observed variation of CpG 94 site methylation dependent on ovarian reserve; being part of the doubled E2F1 target site. In women with lower ovarian reserve (POR), the

CpG 94 site displayed a lower methylation rate increasing E2F1 binding affinity. Since E2F1 is usually a transcriptional activator we can assume that increasing E2F1 binding to *FMR1*-DMR3 should increase the transcription rate of *FMR1* in POR granulosa cells (shown in Figure21C).

E2F1 is expressed in granulosa cells from human[174], mouse[175], rat[174], and bovine[176]. In mouse and bovine ovaries, E2F1 was reported to be involved in granulosa cells proliferation and steroidogenesis[175; 176]. In human, E2F1 expression was reported to affect the transcription of key genes involved in granulosa cells differentiation and proliferation such as the *FSH receptor* and the *forkhead box L2 gene* (*FOXL2*)[174; 177], but not for the *FMR1* gene. Additionally, in human primary granulosa cells, reduced *E2F1* expression level was suggested to be associated with the development of PCOS[175]. Recently, a possible implication of E2F1 in the development of POF syndrome was described in a transgenic mouse model with an ovarian granulosa cell conditional knockout of the retinoblastoma protein (Rb)[178]. Indeed, E2F1 is the most studied target of pRB[179]. pRB binds to E2F1 and leads to its inactivation[179]. In this mouse model, depletion of pRb was associated with increased follicular atresia that may arise from increased *E2f1* levels in preantral follicles[178]. Another studied protein seeming to interact with E2F1 is prohibitin, a tumor suppresser protein. Prohibitin plays an important role in the transcriptional regulation of various genes involved in cell-cycle control and proliferation[180]. In HEK293 and T47D cells, the growth-suppressive property of the prohibitin protein is exhibited by its physical interaction with E2F1 and its subsequent repression of their transcriptional activity[181; 182]. Most interesting, in rat ovary, prohibitins are differentially expressed in granulosa cells in which they may function as a molecular switch that control cell fate and thereby determine the progress of follicular development in the ovary[183-185]. It would be therefore meaningful to investigate whether prohibitin interact with E2F1 then also in human granulosa cells.

In a mouse POF model carrying a *FMR1* human transgene, the increase of *FMR1* RNA was associated with a reduction in the number of growing follicles in ovaries and was sufficient to impair female fertility[80]. The impairment in phosphorylation of key genes involved in the Akt/mTOR pathway expressed in the ovaries of these mice led the authors to hypothesize the presence of a functional link between *FMR1* and the mTOR pathway[80]. A link between *FMR1* expression and the Akt/mTOR pathway was also reported recently in a human granulosa cell line under proliferation conditions[88]. Interestingly, E2F1 is capable to modulate cellular growth and proliferation in osteosarcoma cell lines by regulating mTORC1 activity, and this effect does not depend on Akt[186]. It can therefore be assumed that variation in E2F1

expression levels in granulosa cells may impact ovarian reserve directly via *FMR1* expression control as indirectly by expression in mTORC1 signal pathway.

In summary, my data confirm completely earlier experimental data with regards to the presence of FREE1 and FREE2 in leukocytes[111; 120]. These epigenetic control elements were found to be also present in COV434 cells. Additionally, a novel third DMR was found downstream of *FMR1*-DMR2 in COV434 and in primary granulosa cells, as well as in leukocytes and fibroblasts. *FMR1*-DMR3 contains a double E2F1 target site. However, in the *FMR1* minimal core promoter region binding of α-Pal/Nrf-1 and USF1/USF2 transcription factors were reported to be functionally influenced by methylation of the CpG site[187]. Since this promoter region is completely demethylated on both alleles (*FMR1*-UMR), it is obviously also required for epigenetic control of *FMR1* expression just in granulosa cells. Although more E2F1 binding sites have not been identified along the 2kb long *FMR1* extended promoter, more CpG methylation sensitive TF binding sites have been predicted in *FMR1*-DMR1 and -DMR2 (Table 10). It can therefore be assumed that fine-tuned epigenetic control mechanisms are required for controlling quantitatively the rate of the proposed bi-allelic *FMR1* gene expression in human granulosa cells.

6.5. Transcription at the *FMR1* locus and *ASFMR1* in human granulosa cells

Further aim of this work was to study the initiation of *FMR1* transcripts and to search for possible specific splicing variants expressed in human granulosa cells and their possible influence on human folliculogenesis. In this study, it was possible to characterize, for the first time, also the initiation sites of *FMR1* transcripts in human granulosa cells. In COV434 cells, transcription of *FMR1* seems to be initiated from one TSS (Figure 9); corresponding to the major TSS previously reported in other tissues[68; 145; 188]. Complexity of *FMR1* splice variants in both COV434 cells and in primary human granulosa cells were found to be comparable to that in leukocytes[37] (Figure 10 and 11).

Several lncRNAs were found to be part of the *FMR1* locus[129-131; 189]. In my thesis, I aimed to characterize the expression of *ASFMR1*, a natural antisense transcript (NAT), since it has not yet been investigated in human granulosa cells.

Up to 61-72% of all transcribed human gene regions possess LncRNAs in an antisense orientation[190-193]. NATs contribute to epigenetic silencing of the associated gene loci by recruiting epigenetic complexes as reported for imprinting genes[192; 193]. Additionally, NATs play an important role in regulating mRNA dynamics and splicing pattern of associated sense

genes[194]. Recently, an increased number of studies focused on the implication of NATs expression in human diseases and proposed that NATs expression can be serve as prognostic markers for tumorigenesis and cancer progression[195-197].

In this study, I report for the first time expression of *ASFMR1* transcripts in primary human granulosa cells (Figure 22). As reported in lymphoblastoids cell lines[130], *ASFMR1* transcripts were found to be capped, spliced and polyadenylated also in COV434 cells. However, in COV434, *ASFMR1* transcripts seem to be initiated from three distinct *FMR1* exon sites located in exon1, 2 and 3, respectively (Figure 23). The major TSS was located at exon 1 of the *FMR1* gene (Figure 23). These TSSs were not reported in the literature suggesting some tissue specificity for the initiation of expression of *ASFMR1*. Interestingly, the putative main *ASFMR1* promoter region located in exon1 overlaps with *FMR1*-DMR2 and -DMR3, respectively. This suggests that these epigenetic control elements may be also involved in regulation of *ASFMR1* expression in COV434 cells.

Although I was not able to amplify full *ASFMR1* transcript lengths bridging the CGG repeat block with an amount visible in agarose gels, the complexity of the identified splicing patterns suggests the presence of at least 8 *ASFMR1* possible isoforms originating from TSS at exon 3 (Figure 24). Interestingly, the PM-specific alternative splice form in lymphoblastoid cells reported by Ladd et al.,[130] was found here to be part of an transcript isoform in COV434 cells which do not carry an *FMR1*-PM allele. Whether this transcriptional start site is specific to human granulosa cells is still unclear and an investigation in different cell types will clarify this matter.

Like for *FMR1*, variations in *ASFMR1* expression were also detected in human granulosa cells of NORs and PORs (Figure 25). The aberrant expression of several other lncRNAs was found to be associated with PCOS in human ovarian cumulus cells[126]. Therefore, expression of specific *ASFMR1* isoforms in human primary granulosa cells in regards to patient ovarian reserve may be also important from a clinical perspective.

6.6. Pathways involved in *FMR1* gene regulation and Clinical perspectives

To identify potential signaling pathways involved in *FMR1* gene expression control in COV434 cells, *FMR1* mRNA expression was knocked down to 89% using a specific siRNA followed by analysis of its transcriptome by microarray assays. Microarrays containing more than 48,000 probes were analyzed and approximately 33% of the probes had a detectable signal using RNA isolated from COV434 cells. Only genes showing a statistically significant differential expression (748 genes, $p < 0.05$) compared to controls were selected for pathway

analysis. Differentially expressed genes could be grouped then into 7 main signal pathways (Table 15). The genes included in the identified pathways were found to cover a wide range of regulatory networks, including cell cycle regulation, apoptosis and mRNA decay and vesicle transport.

The most significant pathway which was altered by *FMR1* gene knock down seems to be the methionine salvage pathway (MTA; $p = 2x10^{-4}$). MTA cycle allows regenerating methionine and is also responsible for the production of polyamines which are critical for cell proliferation[198; 199]. The biochemical reactions in the MTA cycle are mainly carried out by six enzymes which are conserved from bacteria to yeast to human[200]. Methionine, an essential amino acid, is required for protein synthesis and normal cell metabolism. Interestingly, in *Drosophila*, Acireductone Dioxygenase 1 (ADI1), an MTA cycle enzyme conserved in human[200] and also a hit in our microarray analysis (1.8 fold change after *FMR1* knock down), was shown to affect fly fecundity probably through the regulation of amino acid signals via mTOR and insulin signal pathways[201]. Indeed, there is evidence of amino acid control by S6K1 expression through a mechanism involving the mTOR signaling pathway[202; 203]. In a chicken muscle cell line, availability of methionine was able to regulate S6K1 phosphorylation, thus its activation, through the mTOR/PI3-kinase pathway in an insulin-independent manner[204]. This may explain why the mTOR pathway and S6K expression at both protein and transcript levels was also affected by *FMR1* knock down in this study. In human cells, ADI1 is involved in several processes including apoptosis and RNA processing[205; 206]. Therefore, exploring the expression of more genes involved in both signal pathways, MTA and mTOR, in primary granulosa cells from POR and NOR may give more insight regarding possible interference of these pathways with human ovarian reserve.

PI3K/AKT/mTOR pathway that plays a critical role in primordial follicle activation and follicular pool maintenance was also altered by *FMR1* knock down. Recently, a functional link between *FMR1* gene expression and the AKT/mTOR pathway was already reported in a POF mouse model and in COV434 cells under proliferation conditions[80; 88] (see Introduction section 1.2.3 b). In this study, inhibition of *FMR1* gene expression using siRNA technology induced an increase of *mTOR, AKT, S6K* at both transcripts and protein levels. Most interesting *S6K* (the endpoint of the signaling pathway) expression reached a statistical significant difference at both mRNA (p=0.05) and protein level (p=0.03). It has been already reported that an increase in S6K phosphorylation lead to follicle depletion and results in POF[84]. However, in my study the total protein levels of S6K were analyzed, therefore future analysis evaluating the phosphorylation status of this protein will further give confidence in

the obtained results. In addition, although there was a tendency towards an increase in total protein levels of mTOR and AKT, the levels of phosphorylated mTOR were comparable to control. These results may be also explained by the still incomplete silencing of *FMR1* expression (only 87%). Using more effective approaches to silence *FMR1* gene expression completely (e.g. CRIPSR-Cas technology) will be therefore helpful to clarify the obtained results.

Additionally, both western blot and ELISA analyses showed a significant decrease in FMRP expression levels at 48h post transfection, however, the results of both analyses were not in accordance at 72h post transfection. Western blot analysis showed that FMRP levels were comparable to control; in contrast using ELISA a threefold increase in FMRP levels was detected. This difference should be clarified in future experiments in order to exclude that the obtained results may be due to a difference in the detection sensitivity of the technique. A negative feedback loop control mechanism for *FMR1*/FMRP was already reported in the COV434 cell line[88]. This may explain the significant increase of FMRP at 72h post transfection.

These results stress the importance of *FMR1* gene expression in follicle pool activation and its probably recruitment via interaction with the AKT/mTOR signal pathway. In order to further validate the obtained results, the analysis of proteins involved in this pathway and their phosphorylation status in primary granulosa cells of patients is required.

In summary, this is the first study investigating candidate pathways altered by *FMR1* gene knock down in a human granulosa cell model system. Several potential candidate pathways were identified. From the clinical perspective, this study provides new starting points for functional research of potential molecular mechanisms involved in the recruitment, development and maturation of follicles in the human ovary. A closer look to the identified pathways may also provide better understanding of ovarian pathologies such as poor ovarian reserve/response and POI/POF leading to female infertility.

7- Future directions

My thesis presents strong experimental evidence that complex epigenetically based mechanisms control the transcriptional activity of *FMR1* from both gene alleles in human granulosa cells. This points to the importance of dosage control of *FMR1*/FMRP function in human granulosa cells. As a perspective, screening for CpG methylation pattern of *FMR1*-DMR3 in a higher number of patients is required to further support the data presented in this study. Besides E2F1, other CpG methylation sensitive binding sites were predicted in *FMR1*-DMR1 and -DMR2 such as GATA factors and AP2α (Table 10). Binding of these TFs within *FMR1*-DMR1and-2 has not been yet investigated. Studying the dynamic of binding efficiency of these factors depending on CpG methylation will improve analysis of the complexity of these DMRs based epigenetic control mechanisms; as potential repressor elements of the transcriptional activity of *FMR1* from both gene alleles in human granulosa cells.

Another aspect is to investigate the molecular function of E2F1 putative expression in human granulosa cells and its association with human ovarian reserve. E2F1 was reported to affect human folliculogenesis by targeting key genes of granulosa cells proliferation and differentiation such as *FOXL2* and *FSH* receptor[174; 177]. However the underlying molecular signal pathways were not yet described. In mouse and rat ovaries, E2F1 seem to control granulosa cells activity through its interaction with RB and prohibitins[178; 181; 182]. Functional study of expression of RB and prohibitins and genes associated in their signaling network in granulosa cells of women with different ovarian reserve will be helpful to better understand the function of E2F1in human granulosa cells.

Another possible mechanism to control E2F1 expression is by miRNA expression as was shown in mouse granulosa cells[175]. MiRNA-320 interfered with granulosa cell proliferation through inhibiting the expression of *E2F1*. If also miRNA-320 impact transcription regulation of E2F1in human granulosa cells and if some variability might have an influence on human ovarian reserve needs to be further investigated.

References

1. Khalili, M.A., Shahedi, A., Ashourzadeh, S., Nottola, S.A., Macchiarelli, G., and Palmerini, M.G. (2017). Vitrification of human immature oocytes before and after in vitro maturation: a review. Journal of assisted reproduction and genetics.
2. Cserepes, R.E., Bugán, A., Korösi, T., Toth, B., Rösner, S., Strowitzki, T., and Wischmann, T. (2014). Infertility Specific Quality of Life and Gender Role Attitudes in German and Hungarian Involuntary Childless Couples. Geburtshilfe und Frauenheilkunde 74, 1009-1015.
3. Herrmann, D., Scherg, H., Verres, R., von Hagens, C., Strowitzki, T., and Wischmann, T. (2011). Resilience in infertile couples acts as a protective factor against infertility-specific distress and impaired quality of life. Journal of assisted reproduction and genetics 28, 1111-1117.
4. Agarwal, A., Aponte-Mellado, A., Premkumar, B.J., Shaman, A., and Gupta, S. (2012). The effects of oxidative stress on female reproduction: a review. Reproductive biology and endocrinology : RB&E 10, 49-49.
5. Myrskyla, M., Kohler, H.P., and Billari, F.C. (2009). Advances in development reverse fertility declines. Nature 460, 741-743.
6. (2012). Health and fertility in World Health Organization group 2 anovulatory women. Human reproduction update 18, 586-599.
7. Matzuk, M.M., and Lamb, D.J. (2008). The biology of infertility: research advances and clinical challenges. Nat Med 14, 1197-1213.
8. Showell, M.G., Mackenzie-Proctor, R., Jordan, V., and Hart, R.J. (2017). Antioxidants for female subfertility. Cochrane Database of Systematic Reviews.
9. Gougeon, A. (1986). Dynamics of follicular growth in the human: a model from preliminary results. Human reproduction (Oxford, England) 1, 81-87.
10. McGee, E.A., and Hsueh, A.J. (2000). Initial and cyclic recruitment of ovarian follicles. Endocrine reviews 21, 200-214.
11. Kobayashi, A., and Behringer, R.R. (2003). Developmental genetics of the female reproductive tract in mammals. Nature reviews Genetics 4, 969-980.
12. Kezele, P.R., Ague, J.M., Nilsson, E., and Skinner, M.K. (2005). Alterations in the ovarian transcriptome during primordial follicle assembly and development. Biology of reproduction 72, 241-255.
13. Matzuk, M.M., Burns, K.H., Viveiros, M.M., and Eppig, J.J. (2002). Intercellular communication in the mammalian ovary: oocytes carry the conversation. Science 296, 2178-2180.
14. Zeleznik, A.J. (2004). The physiology of follicle selection. Reproductive biology and endocrinology : RB&E 2, 31.
15. Rimon-Dahari, N., Yerushalmi-Heinemann, L., Alyagor, L., and Dekel, N. (2016). Ovarian Folliculogenesis. Results and problems in cell differentiation 58, 167-190.
16. Gittens, J.E., Barr, K.J., Vanderhyden, B.C., and Kidder, G.M. (2005). Interplay between paracrine signaling and gap junctional communication in ovarian follicles. Journal of cell science 118, 113-122.
17. Binelli, M., and Murphy, B.D. (2010). Coordinated regulation of follicle development by germ and somatic cells. Reproduction, fertility, and development 22, 1-12.
18. Scott, R.T., Jr., and Hofmann, G.E. (1995). Prognostic assessment of ovarian reserve. Fertility and sterility 63, 1-11.
19. Forabosco, A., Sforza, C., De Pol, A., Vizzotto, L., Marzona, L., and Ferrario, V.F. (1991). Morphometric study of the human neonatal ovary. The Anatomical record 231, 201-208.
20. Gougeon, A. (1996). Regulation of Ovarian Follicular Development in Primates: Facts and Hypotheses. Endocrine reviews 17, 121-155.
21. Broekmans, F.J., Knauff, E.A., te Velde, E.R., Macklon, N.S., and Fauser, B.C. (2007). Female reproductive ageing: current knowledge and future trends. Trends in endocrinology and metabolism: TEM 18, 58-65.
22. Tal, R., and Seifer, D.B. (2017). Ovarian reserve testing: a user's guide. American journal of obstetrics and gynecology 217, 129-140.

23. Lambalk, C.B., van Disseldorp, J., de Koning, C.H., and Broekmans, F.J. (2009). Testing ovarian reserve to predict age at menopause. Maturitas 63, 280-291.
24. Ferraretti, A.P., and Gianaroli, L. (2014). The Bologna criteria for the definition of poor ovarian responders: is there a need for revision? Human reproduction (Oxford, England) 29, 1842-1845.
25. Ferraretti, A.P., La Marca, A., Fauser, B.C., Tarlatzis, B., Nargund, G., and Gianaroli, L. (2011). ESHRE consensus on the definition of 'poor response' to ovarian stimulation for in vitro fertilization: the Bologna criteria. Human reproduction (Oxford, England) 26, 1616-1624.
26. Jirge, P.R. (2016). Poor ovarian reserve. Journal of Human Reproductive Sciences 9, 63-69.
27. Fassnacht, W., Mempel, A., Strowitzki, T., and Vogt, P.H. (2006). Premature ovarian failure (POF) syndrome: towards the molecular clinical analysis of its genetic complexity. Current medicinal chemistry 13, 1397-1410.
28. Webber, L., Davies, M., Anderson, R., Bartlett, J., Braat, D., Cartwright, B., Cifkova, R., de Muinck Keizer-Schrama, S., Hogervorst, E., Janse, F., et al. (2016). ESHRE Guideline: management of women with premature ovarian insufficiency. Human reproduction (Oxford, England) 31, 926-937.
29. Allingham-Hawkins, D.J., Babul-Hirji, R., Chitayat, D., Holden, J.J., Yang, K.T., Lee, C., Hudson, R., Gorwill, H., Nolin, S.L., Glicksman, A., et al. (1999). Fragile X premutation is a significant risk factor for premature ovarian failure: the International Collaborative POF in Fragile X study--preliminary data. American journal of medical genetics 83, 322-325.
30. Vialard, F., Cocquet, J., Christin-Maitre, S., Veitia, R., and Fellous, M. (2002). The X chromosome and ovarian function. Cytogenetic and genome research 99, 218-223.
31. Saifi, G.M., and Chandra, H.S. (1999). An apparent excess of sex- and reproduction-related genes on the human X chromosome. Proceedings Biological sciences 266, 203-209.
32. Berletch, J.B., Yang, F., Xu, J., Carrel, L., and Disteche, C.M. (2011). Genes that escape from X inactivation. Human genetics 130, 237-245.
33. Simpson, J.L., and Rajkovic, A. (1999). Ovarian differentiation and gonadal failure. American journal of medical genetics 89, 186-200.
34. Vogt, P.H. (2017). Genetic disorders of human infertility. ENCYCLOPEDIA OF THE HUMAN GENOME.
35. Verkerk, A.J., Pieretti, M., Sutcliffe, J.S., Fu, Y.H., Kuhl, D.P., Pizzuti, A., Reiner, O., Richards, S., Victoria, M.F., Zhang, F.P., et al. (1991). Identification of a gene (FMR-1) containing a CGG repeat coincident with a breakpoint cluster region exhibiting length variation in fragile X syndrome. Cell 65, 905-914.
36. Eichler, E.E., Richards, S., Gibbs, R.A., and Nelson, D.L. (1994). Fine structure of the human FMR1 gene. Human molecular genetics 3, 684-685.
37. Pretto, D.I., Eid, J.S., Yrigollen, C.M., Tang, H.-T., Loomis, E.W., Raske, C., Durbin-Johnson, B., Hagerman, P.J., and Tassone, F. (2015). Differential increases of specific FMR1 mRNA isoforms in premutation carriers. Journal of medical genetics 52, 42-52.
38. Pretto, D.I., Eid, J.S., Yrigollen, C.M., Tang, H.T., Loomis, E.W., Raske, C., Durbin-Johnson, B., Hagerman, P.J., and Tassone, F. (2015). Differential increases of specific FMR1 mRNA isoforms in premutation carriers. Journal of medical genetics 52, 42-52.
39. Fu, Y.H., Kuhl, D.P., Pizzuti, A., Pieretti, M., Sutcliffe, J.S., Richards, S., Verkerk, A.J., Holden, J.J., Fenwick, R.G., Jr., Warren, S.T., et al. (1991). Variation of the CGG repeat at the fragile X site results in genetic instability: resolution of the Sherman paradox. Cell 67, 1047-1058.
40. Hagerman, R.J., Leavitt, B.R., Farzin, F., Jacquemont, S., Greco, C.M., Brunberg, J.A., Tassone, F., Hessl, D., Harris, S.W., Zhang, L., et al. (2004). Fragile-X–Associated Tremor/Ataxia Syndrome (FXTAS) in Females with the FMR1 Premutation. American journal of human genetics 74, 1051-1056.
41. Hagerman, R.J., and Hagerman, P. (2016). Fragile X-associated tremor/ataxia syndrome - features, mechanisms and management. Nature reviews Neurology 12, 403-412.
42. Sullivan, A.K., Marcus, M., Epstein, M.P., Allen, E.G., Anido, A.E., Paquin, J.J., Yadav-Shah, M., and Sherman, S.L. (2005). Association of FMR1 repeat size with ovarian dysfunction. Human reproduction (Oxford, England) 20, 402-412.
43. Pieretti, M., Zhang, F.P., Fu, Y.H., Warren, S.T., Oostra, B.A., Caskey, C.T., and Nelson, D.L. (1991). Absence of expression of the FMR-1 gene in fragile X syndrome. Cell 66, 817-822.

44. Verheij, C., de Graaff, E., Bakker, C.E., Willemsen, R., Willems, P.J., Meijer, N., Galjaard, H., Reuser, A.J., Oostra, B.A., and Hoogeveen, A.T. (1995). Characterization of FMR1 proteins isolated from different tissues. Human molecular genetics 4, 895-901.
45. Brackett, D.M., Qing, F., Amieux, P.S., Sellers, D.L., Horner, P.J., and Morris, D.R. (2013). FMR1 transcript isoforms: association with polyribosomes; regional and developmental expression in mouse brain. PloS one 8, e58296.
46. Tamanini, F., Meijer, N., Verheij, C., Willems, P.J., Galjaard, H., Oostra, B.A., and Hoogeveen, A.T. (1996). FMRP is associated to the ribosomes via RNA. Human molecular genetics 5, 809-813.
47. Zalfa, F., Adinolfi, S., Napoli, I., Kuhn-Holsken, E., Urlaub, H., Achsel, T., Pastore, A., and Bagni, C. (2005). Fragile X mental retardation protein (FMRP) binds specifically to the brain cytoplasmic RNAs BC1/BC200 via a novel RNA-binding motif. The Journal of biological chemistry 280, 33403-33410.
48. Cheever, A., and Ceman, S. (2009). Translation regulation of mRNAs by the fragile X family of proteins through the microRNA pathway. RNA biology 6, 175-178.
49. Cheever, A., and Ceman, S. (2009). Phosphorylation of FMRP inhibits association with Dicer. RNA (New York, NY) 15, 362-366.
50. Feng, Y., Gutekunst, C.A., Eberhart, D.E., Yi, H., Warren, S.T., and Hersch, S.M. (1997). Fragile X mental retardation protein: nucleocytoplasmic shuttling and association with somatodendritic ribosomes. The Journal of neuroscience : the official journal of the Society for Neuroscience 17, 1539-1547.
51. Siomi, H., Choi, M., Siomi, M.C., Nussbaum, R.L., and Dreyfuss, G. (1994). Essential role for KH domains in RNA binding: impaired RNA binding by a mutation in the KH domain of FMR1 that causes fragile X syndrome. Cell 77, 33-39.
52. Musco, G., Kharrat, A., Stier, G., Fraternali, F., Gibson, T.J., Nilges, M., and Pastore, A. (1997). The solution structure of the first KH domain of FMR1, the protein responsible for the fragile X syndrome. Nature structural biology 4, 712-716.
53. Bardoni, B., Sittler, A., Shen, Y., and Mandel, J.L. (1997). Analysis of domains affecting intracellular localization of the FMRP protein. Neurobiology of disease 4, 329-336.
54. Fernandez, E., Rajan, N., and Bagni, C. (2013). The FMRP regulon: from targets to disease convergence. Frontiers in neuroscience 7, 191.
55. Blice-Baum, A.C., and Mihailescu, M.R. (2014). Biophysical characterization of G-quadruplex forming FMR1 mRNA and of its interactions with different fragile X mental retardation protein isoforms. Rna 20, 103-114.
56. Gareau, C., Houssin, E., Martel, D., Coudert, L., Mellaoui, S., Huot, M.E., Laprise, P., and Mazroui, R. (2013). Characterization of fragile X mental retardation protein recruitment and dynamics in Drosophila stress granules. PloS one 8, e55342.
57. Stetler, A., Winograd, C., Sayegh, J., Cheever, A., Patton, E., Zhang, X., Clarke, S., and Ceman, S. (2006). Identification and characterization of the methyl arginines in the fragile X mental retardation protein Fmrp. Human molecular genetics 15, 87-96.
58. Tassone, F., Beilina, A., Carosi, C., Albertosi, S., Bagni, C., Li, L., Glover, K., Bentley, D., and Hagerman, P.J. (2007). Elevated FMR1 mRNA in premutation carriers is due to increased transcription. RNA (New York, NY) 13, 555-562.
59. Tassone, F., Hagerman, R.J., Taylor, A.K., Gane, L.W., Godfrey, T.E., and Hagerman, P.J. (2000). Elevated levels of FMR1 mRNA in carrier males: a new mechanism of involvement in the fragile-X syndrome. American journal of human genetics 66, 6-15.
60. Elizur, S.E., Lebovitz, O., Derech-Haim, S., Dratviman-Storobinsky, O., Feldman, B., Dor, J., Orvieto, R., and Cohen, Y. (2014). Elevated levels of FMR1 mRNA in granulosa cells are associated with low ovarian reserve in FMR1 premutation carriers. PloS one 9, e105121.
61. Sherman, S.L., Curnow, E.C., Easley, C.A., Jin, P., Hukema, R.K., Tejada, M.I., Willemsen, R., and Usdin, K. (2014). Use of model systems to understand the etiology of fragile X-associated primary ovarian insufficiency (FXPOI). Journal of neurodevelopmental disorders 6, 26-26.
62. Tassone, F., Beilina, A., Carosi, C., Albertosi, S., Bagni, C., Li, L., Glover, K., Bentley, D., and Hagerman, P.J. (2007). Elevated FMR1 mRNA in premutation carriers is due to increased transcription. RNA (New York, NY) 13, 555-562.

63. García-Alegría, E., Ibáñez, B., Mínguez, M., Poch, M., Valiente, A., Sanz-Parra, A., Martinez-Bouzas, C., Beristain, E., and Tejada, M.-I. (2007). Analysis of FMR1 gene expression in female premutation carriers using robust segmented linear regression models. RNA (New York, NY) 13, 756-762.
64. Allen, E.G., He, W., Yadav-Shah, M., and Sherman, S.L. (2004). A study of the distributional characteristics of FMR1 transcript levels in 238 individuals. Human genetics 114, 439-447.
65. Tassone, F., Hagerman, R.J., Chamberlain, W.D., and Hagerman, P.J. (2000). Transcription of the FMR1 gene in individuals with fragile X syndrome. American journal of medical genetics 97, 195-203.
66. Greco, C.M., Berman, R.F., Martin, R.M., Tassone, F., Schwartz, P.H., Chang, A., Trapp, B.D., Iwahashi, C., Brunberg, J., Grigsby, J., et al. (2006). Neuropathology of fragile X-associated tremor/ataxia syndrome (FXTAS). Brain : a journal of neurology 129, 243-255.
67. Greco, C.M., Hagerman, R.J., Tassone, F., Chudley, A.E., Del Bigio, M.R., Jacquemont, S., Leehey, M., and Hagerman, P.J. (2002). Neuronal intranuclear inclusions in a new cerebellar tremor/ataxia syndrome among fragile X carriers. Brain : a journal of neurology 125, 1760-1771.
68. Beilina, A., Tassone, F., Schwartz, P.H., Sahota, P., and Hagerman, P.J. (2004). Redistribution of transcription start sites within the FMR1 promoter region with expansion of the downstream CGG-repeat element. Human molecular genetics 13, 543-549.
69. Chen, L.S., Tassone, F., Sahota, P., and Hagerman, P.J. (2003). The (CGG)n repeat element within the 5' untranslated region of the FMR1 message provides both positive and negative cis effects on in vivo translation of a downstream reporter. Human molecular genetics 12, 3067-3074.
70. Khateb, S., Weisman-Shomer, P., Hershco-Shani, I., Ludwig, A.L., and Fry, M. (2007). The tetraplex (CGG)n destabilizing proteins hnRNP A2 and CBF-A enhance the in vivo translation of fragile X premutation mRNA. Nucleic acids research 35, 5775-5788.
71. Schuettler, J., Peng, Z., Zimmer, J., Sinn, P., von Hagens, C., Strowitzki, T., and Vogt, P.H. (2011). Variable expression of the Fragile X Mental Retardation 1 (FMR1) gene in patients with premature ovarian failure syndrome is not dependent on number of (CGG)n triplets in exon 1. Human reproduction (Oxford, England) 26, 1241-1251.
72. Gleicher, N., Weghofer, A., Oktay, K., and Barad, D. (2009). Relevance of triple CGG repeats in the FMR1 gene to ovarian reserve. Reproductive biomedicine online 19, 385-390.
73. Gleicher, N., Weghofer, A., Oktay, K., and Barad, D.H. (2009). Correlation of triple repeats on the FMR1 (fragile X) gene to ovarian reserve: a new infertility test? Acta obstetricia et gynecologica Scandinavica 88, 1024-1030.
74. Gleicher, N., Yu, Y., Himaya, E., Barad, D.H., Weghofer, A., Wu, Y.G., Albertini, D.F., Wang, V.Q., and Kushnir, V.A. (2015). Early decline in functional ovarian reserve in young women with low (CGGn < 26) FMR1 gene alleles. Translational research : the journal of laboratory and clinical medicine 166, 502-507.e501-502.
75. Gustin, S.L., Ding, V.Y., Desai, M., Leader, B., and Baker, V.L. (2015). Evidence of an age-related correlation of ovarian reserve and FMR1 repeat number among women with "normal" CGG repeat status. Journal of assisted reproduction and genetics 32, 1669-1676.
76. Voorhuis, M., Onland-Moret, N.C., Fauser, B.C., Ploos van Amstel, H.K., van der Schouw, Y.T., and Broekmans, F.J. (2013). The association of CGG repeats in the FMR1 gene and timing of natural menopause. Human reproduction (Oxford, England) 28, 496-501.
77. Ruth, K.S., Bennett, C.E., Schoemaker, M.J., Weedon, M.N., Swerdlow, A.J., and Murray, A. (2016). Length of FMR1 repeat alleles within the normal range does not substantially affect the risk of early menopause. Human reproduction (Oxford, England) 31, 2396-2403.
78. Hoffman, G.E., Le, W.W., Entezam, A., Otsuka, N., Tong, Z.-B., Nelson, L., Flaws, J.A., McDonald, J.H., Jafar, S., and Usdin, K. (2012). Ovarian Abnormalities in a Mouse Model of Fragile X Primary Ovarian Insufficiency. Journal of Histochemistry and Cytochemistry 60, 439-456.
79. Bontekoe, C.J., Bakker, C.E., Nieuwenhuizen, I.M., van der Linde, H., Lans, H., de Lange, D., Hirst, M.C., and Oostra, B.A. (2001). Instability of a (CGG)98 repeat in the Fmr1 promoter. Human molecular genetics 10, 1693-1699.

80. Lu, C., Lin, L., Tan, H., Wu, H., Sherman, S.L., Gao, F., Jin, P., and Chen, D. (2012). Fragile X premutation RNA is sufficient to cause primary ovarian insufficiency in mice. Human molecular genetics 21, 5039-5047.
81. Zhang, P., Chao, H., Sun, X., Li, L., Shi, Q., and Shen, W. (2010). Murine folliculogenesis in vitro is stage-specifically regulated by insulin via the Akt signaling pathway. Histochemistry and cell biology 134, 75-82.
82. Sobinoff, A.P., Mahony, M., Nixon, B., Roman, S.D., and McLaughlin, E.A. (2011). Understanding the Villain: DMBA-induced preantral ovotoxicity involves selective follicular destruction and primordial follicle activation through PI3K/Akt and mTOR signaling. Toxicological sciences : an official journal of the Society of Toxicology 123, 563-575.
83. Sobinoff, A.P., Sutherland, J.M., and McLaughlin, E.A. (2013). Intracellular signalling during female gametogenesis. Molecular human reproduction 19, 265-278.
84. Wang, Z.P., Mu, X.Y., Guo, M., Wang, Y.J., Teng, Z., Mao, G.P., Niu, W.B., Feng, L.Z., Zhao, L.H., and Xia, G.L. (2014). Transforming growth factor-beta signaling participates in the maintenance of the primordial follicle pool in the mouse ovary. The Journal of biological chemistry 289, 8299-8311.
85. Castrillon, D.H., Miao, L., Kollipara, R., Horner, J.W., and DePinho, R.A. (2003). Suppression of Ovarian Follicle Activation in Mice by the Transcription Factor Foxo3a. Science 301, 215-218.
86. Moniruzzaman, M., Lee, J., Zengyo, M., and Miyano, T. (2010). Knockdown of FOXO3 induces primordial oocyte activation in pigs. Reproduction (Cambridge, England) 139, 337-348.
87. Bao, R.M., Hayakawa, K., Moniruzzaman, M., Taketsuru, H., and Miyano, T. (2011). FOXO3 knockdown accelerates development of bovine primordial follicles. The Journal of reproduction and development 57, 475-480.
88. Rehnitz, J., Alcoba, D.D., Brum, I.S., Hinderhofer, K., Youness, B., Strowitzki, T., and Vogt, P.H. (2017). FMR1 and AKT/mTOR signalling pathways: potential functional interactions controlling folliculogenesis in human granulosa cells. Reproductive biomedicine online.
89. Allis, C.D., and Jenuwein, T. (2016). The molecular hallmarks of epigenetic control. Nature reviews Genetics 17, 487-500.
90. Berger, S.L., Kouzarides, T., Shiekhattar, R., and Shilatifard, A. (2009). An operational definition of epigenetics. Genes Dev 23, 781-783.
91. Egger, G., Liang, G., Aparicio, A., and Jones, P.A. (2004). Epigenetics in human disease and prospects for epigenetic therapy. Nature 429, 457-463.
92. Boyes, J., and Bird, A. (1992). Repression of genes by DNA methylation depends on CpG density and promoter strength: evidence for involvement of a methyl-CpG binding protein. Embo j 11, 327-333.
93. Jones, P.A. (2012). Functions of DNA methylation: islands, start sites, gene bodies and beyond. Nature reviews Genetics 13, 484-492.
94. Bestor, T.H. (2000). The DNA methyltransferases of mammals. Human molecular genetics 9, 2395-2402.
95. Newell-Price, J., Clark, A.J., and King, P. (2000). DNA methylation and silencing of gene expression. Trends in endocrinology and metabolism: TEM 11, 142-148.
96. Brenet, F., Moh, M., Funk, P., Feierstein, E., Viale, A.J., Socci, N.D., and Scandura, J.M. (2011). DNA methylation of the first exon is tightly linked to transcriptional silencing. PloS one 6, e14524.
97. Bird, A., Taggart, M., Frommer, M., Miller, O.J., and Macleod, D. (1985). A fraction of the mouse genome that is derived from islands of nonmethylated, CpG-rich DNA. Cell 40, 91-99.
98. Hellman, A., and Chess, A. (2007). Gene body-specific methylation on the active X chromosome. Science 315, 1141-1143.
99. Gardiner-Garden, M., and Frommer, M. (1987). CpG islands in vertebrate genomes. Journal of molecular biology 196, 261-282.
100. Saxonov, S., Berg, P., and Brutlag, D.L. (2006). A genome-wide analysis of CpG dinucleotides in the human genome distinguishes two distinct classes of promoters. Proceedings of the National Academy of Sciences of the United States of America 103, 1412-1417.

101. Illingworth, R.S., Gruenewald-Schneider, U., Webb, S., Kerr, A.R.W., James, K.D., Turner, D.J., Smith, C., Harrison, D.J., Andrews, R., and Bird, A.P. (2010). Orphan CpG Islands Identify Numerous Conserved Promoters in the Mammalian Genome. PLoS Genetics 6, e1001134.
102. Deng, X., Berletch, J.B., Nguyen, D.K., and Disteche, C.M. (2014). X chromosome regulation: diverse patterns in development, tissues and disease. Nature reviews Genetics 15, 367-378.
103. Choy, M.-K., Movassagh, M., Goh, H.-G., Bennett, M.R., Down, T.A., and Foo, R.S. (2010). Genome-wide conserved consensus transcription factor binding motifs are hyper-methylated. BMC Genomics 11, 519.
104. Kass, S.U., Pruss, D., and Wolffe, A.P. How does DNA methylation repress transcription? Trends in Genetics 13, 444-449.
105. Sarraf, S.A., and Stancheva, I. (2004). Methyl-CpG Binding Protein MBD1 Couples Histone H3 Methylation at Lysine 9 by SETDB1 to DNA Replication and Chromatin Assembly. Molecular Cell 15, 595-605.
106. Drouin, R., Angers, M., Dallaire, N., Rose, T.M., Khandjian, E.W., and Rousseau, F. (1997). Structural and functional characterization of the human FMR1 promoter reveals similarities with the hnRNP-A2 promoter region. Human molecular genetics 6, 2051-2060.
107. Kumari, D., and Usdin, K. (2001). Interaction of the transcription factors USF1, USF2, and alpha -Pal/Nrf-1 with the FMR1 promoter. Implications for Fragile X mental retardation syndrome. The Journal of biological chemistry 276, 4357-4364.
108. Schwemmle, S., de Graaff, E., Deissler, H., Glaser, D., Wohrle, D., Kennerknecht, I., Just, W., Oostra, B.A., Doerfler, W., Vogel, W., et al. (1997). Characterization of FMR1 promoter elements by in vivo-footprinting analysis. American journal of human genetics 60, 1354-1362.
109. Naumann, A., Hochstein, N., Weber, S., Fanning, E., and Doerfler, W. (2009). A distinct DNA-methylation boundary in the 5'- upstream sequence of the FMR1 promoter binds nuclear proteins and is lost in fragile X syndrome. American journal of human genetics 85, 606-616.
110. Naumann, A., Kraus, C., Hoogeveen, A., Ramirez, C.M., and Doerfler, W. (2014). Stable DNA methylation boundaries and expanded trinucleotide repeats: role of DNA insertions. Journal of molecular biology 426, 2554-2566.
111. Godler, D.E., Tassone, F., Loesch, D.Z., Taylor, A.K., Gehling, F., Hagerman, R.J., Burgess, T., Ganesamoorthy, D., Hennerich, D., Gordon, L., et al. (2010). Methylation of novel markers of fragile X alleles is inversely correlated with FMRP expression and FMR1 activation ratio. Human molecular genetics 19, 1618-1632.
112. Chiurazzi, P., and Neri, G. (2003). Reactivation of silenced genes and transcriptional therapy. Cytogenetic and genome research 100, 56-64.
113. Eiges, R., Urbach, A., Malcov, M., Frumkin, T., Schwartz, T., Amit, A., Yaron, Y., Eden, A., Yanuka, O., Benvenisty, N., et al. (2007). Developmental study of fragile X syndrome using human embryonic stem cells derived from preimplantation genetically diagnosed embryos. Cell stem cell 1, 568-577.
114. Genc, B., Muller-Hartmann, H., Zeschnigk, M., Deissler, H., Schmitz, B., Majewski, F., von Gontard, A., and Doerfler, W. (2000). Methylation mosaicism of 5'-(CGG)(n)-3' repeats in fragile X, premutation and normal individuals. Nucleic acids research 28, 2141-2152.
115. Hall, D.A., Robertson-Dick, E.E., O'Keefe, J.A., Hadd, A.G., Zhou, L., and Berry-Kravis, E. (2016). X-inactivation in the clinical phenotype of fragile X premutation carrier sisters. Neurology: Genetics 2, e45.
116. Leehey, M.A., Berry-Kravis, E., Goetz, C.G., Zhang, L., Hall, D.A., Li, L., Rice, C.D., Lara, R., Cogswell, J., Reynolds, A., et al. (2008). FMR1 CGG repeat length predicts motor dysfunction in premutation carriers. Neurology 70, 1397-1402.
117. Bodega, B., Bione, S., Dalprà, L., Toniolo, D., Ornaghi, F., Vegetti, W., Ginelli, E., and Marozzi, A. (2006). Influence of intermediate and uninterrupted FMR1 CGG expansions in premature ovarian failure manifestation. Human Reproduction 21, 952-957.
118. Godler, D.E., Slater, H.R., Amor, D., and Loesch, D.Z. (2010). Methylation analysis of fragile X-related epigenetic elements may provide a suitable newborn screening test for fragile X syndrome. Genetics in medicine : official journal of the American College of Medical Genetics 12, 595-595.
119. Godler, D.E., Slater, H.R., Bui, Q.M., Ono, M., Gehling, F., Francis, D., Amor, D.J., Hopper, J.L., Hagerman, R., and Loesch, D.Z. (2011). FMR1 intron 1 methylation predicts FMRP

expression in blood of female carriers of expanded FMR1 alleles. The Journal of molecular diagnostics : JMD 13, 528-536.
120. Godler, D.E., Slater, H.R., Bui, Q.M., Storey, E., Ono, M.Y., Gehling, F., Inaba, Y., Francis, D., Hopper, J.L., Kinsella, G., et al. (2012). Fragile X mental retardation 1 (FMR1) intron 1 methylation in blood predicts verbal cognitive impairment in female carriers of expanded FMR1 alleles: evidence from a pilot study. Clinical chemistry 58, 590-598.
121. Ma, L., Bajic, V.B., and Zhang, Z. (2013). On the classification of long non-coding RNAs. RNA biology 10, 925-933.
122. Mercer, T.R., Dinger, M.E., and Mattick, J.S. (2009). Long non-coding RNAs: insights into functions. Nature reviews Genetics 10, 155-159.
123. Battaglia, R., Vento, M.E., Borzì, P., Ragusa, M., Barbagallo, D., Arena, D., Purrello, M., and Di Pietro, C. (2017). Non-coding RNAs in the Ovarian Follicle. Frontiers in genetics 8, 57.
124. Burnik Papler, T., Vrtacnik Bokal, E., Maver, A., Kopitar, A.N., and Lovrečić, L. (2015). Transcriptomic Analysis and Meta-Analysis of Human Granulosa and Cumulus Cells. PloS one 10, e0136473.
125. Yerushalmi, G.M., Salmon-Divon, M., Yung, Y., Maman, E., Kedem, A., Ophir, L., Elemento, O., Coticchio, G., Dal Canto, M., Mignini Renzinu, M., et al. (2014). Characterization of the human cumulus cell transcriptome during final follicular maturation and ovulation. Molecular human reproduction 20, 719-735.
126. Huang, X., Hao, C., Bao, H., Wang, M., and Dai, H. (2016). Aberrant expression of long noncoding RNAs in cumulus cells isolated from PCOS patients. Journal of assisted reproduction and genetics 33, 111-121.
127. Li, J., Cao, Y., Xu, X., Xiang, H., Zhang, Z., Chen, B., Hao, Y., Wei, Z., Zhou, P., and Chen, D. (2015). Increased New lncRNA-mRNA Gene Pair Levels in Human Cumulus Cells Correlate With Oocyte Maturation and Embryo Development. Reproductive sciences (Thousand Oaks, Calif) 22, 1008-1014.
128. Xiong, Y., Liu, T., Wang, S., Chi, H., Chen, C., and Zheng, J. (2017). Cyclophosphamide promotes the proliferation inhibition of mouse ovarian granulosa cells and premature ovarian failure by activating the lncRNA-Meg3-p53-p66Shc pathway. Gene 596, 1-8.
129. Khalil, A.M., Faghihi, M.A., Modarresi, F., Brothers, S.P., and Wahlestedt, C. (2008). A novel RNA transcript with antiapoptotic function is silenced in fragile X syndrome. PloS one 3, e1486.
130. Ladd, P.D., Smith, L.E., Rabaia, N.A., Moore, J.M., Georges, S.A., Hansen, R.S., Hagerman, R.J., Tassone, F., Tapscott, S.J., and Filippova, G.N. (2007). An antisense transcript spanning the CGG repeat region of FMR1 is upregulated in premutation carriers but silenced in full mutation individuals. Human molecular genetics 16, 3174-3187.
131. Pastori, C., Peschansky, V.J., Barbouth, D., Mehta, A., Silva, J.P., and Wahlestedt, C. (2014). Comprehensive analysis of the transcriptional landscape of the human FMR1 gene reveals two new long noncoding RNAs differentially expressed in Fragile X syndrome and Fragile X-associated tremor/ataxia syndrome. Human genetics 133, 59-67.
132. Peschansky, V.J., Pastori, C., Zeier, Z., Wentzel, K., Velmeshev, D., Magistri, M., Silva, J.P., and Wahlestedt, C. (2016). The long non-coding RNA FMR4 promotes proliferation of human neural precursor cells and epigenetic regulation of gene expression in trans. Molecular and Cellular Neuroscience 74, 49-57.
133. Elizur, S.E., Dratviman-Storobinsky, O., Derech-Haim, S., Lebovitz, O., Dor, J., Orvieto, R., and Cohen, Y. (2016). FMR6 may play a role in the pathogenesis of fragile X-associated premature ovarian insufficiency. Gynecological endocrinology : the official journal of the International Society of Gynecological Endocrinology 32, 334-337.
134. Zhang, H., Vollmer, M., De Geyter, M., Litzistorf, Y., Ladewig, A., Durrenberger, M., Guggenheim, R., Miny, P., Holzgreve, W., and De Geyter, C. (2000). Characterization of an immortalized human granulosa cell line (COV434). Molecular human reproduction 6, 146-153.
135. Pfaffl, M.W. (2006). Relative Quantification. Real-time PCR 63, 63-82.
136. Schramm, G., Bruchhaus, I., and Roeder, T. (2000). A simple and reliable 5′-RACE approach. Nucleic acids research 28, e96-e96.

137. Tassone, F., De Rubeis, S., Carosi, C., La Fata, G., Serpa, G., Raske, C., Willemsen, R., J Hagerman, P., and Bagni, C. (2011). Differential usage of transcriptional start sites and polyadenylation sites in FMR1 premutation alleles†.
138. Frommer, M., McDonald, L.E., Millar, D.S., Collis, C.M., Watt, F., Grigg, G.W., Molloy, P.L., and Paul, C.L. (1992). A genomic sequencing protocol that yields a positive display of 5-methylcytosine residues in individual DNA strands. Proc Natl Acad Sci U S A 89, 1827-1831.
139. Herman, J.G., Graff, J.R., Myöhänen, S., Nelkin, B.D., and Baylin, S.B. (1996). Methylation-specific PCR: a novel PCR assay for methylation status of CpG islands. Proceedings of the National Academy of Sciences of the United States of America 93, 9821-9826.
140. Sasaki, M., Anast, J., Bassett, W., Kawakami, T., Sakuragi, N., and Dahiya, R. (2003). Bisulfite conversion-specific and methylation-specific PCR: a sensitive technique for accurate evaluation of CpG methylation. Biochemical and biophysical research communications 309, 305-309.
141. Sanger, F., Nicklen, S., and Coulson, A.R. (1977). DNA sequencing with chain-terminating inhibitors. Proceedings of the National Academy of Sciences of the United States of America 74, 5463-5467.
142. Ludwig, L.B., Hughes, B.J., and Schwartz, S.A. (1995). Biotinylated probes in the electrophoretic mobility shift assay to examine specific dsDNA, ssDNA or RNA-protein interactions. Nucleic acids research 23, 3792-3793.
143. Zhang, M., Guller, S., and Huang, Y. (2007). Method to enhance transfection efficiency of cell lines and placental fibroblasts. Placenta 28, 779-782.
144. van den Berg-Bakker, C.A., Hagemeijer, A., Franken-Postma, E.M., Smit, V.T., Kuppen, P.J., van Ravenswaay Claasen, H.H., Cornelisse, C.J., and Schrier, P.I. (1993). Establishment and characterization of 7 ovarian carcinoma cell lines and one granulosa tumor cell line: growth features and cytogenetics. International journal of cancer 53, 613-620.
145. Tassone, F., De Rubeis, S., Carosi, C., La Fata, G., Serpa, G., Raske, C., Willemsen, R., Hagerman, P.J., and Bagni, C. (2011). Differential usage of transcriptional start sites and polyadenylation sites in FMR1 premutation alleles. Nucleic Acids Research 39, 6172-6185.
146. Verkerk, A.J., de Graaff, E., De Boulle, K., Eichler, E.E., Konecki, D.S., Reyniers, E., Manca, A., Poustka, A., Willems, P.J., Nelson, D.L., et al. (1993). Alternative splicing in the fragile X gene FMR1. Human molecular genetics 2, 1348.
147. Kawakami, T., Okamoto, K., Sugihara, H., Hattori, T., Reeve, A.E., Ogawa, O., and Okada, Y. (2003). The roles of supernumerical X chromosomes and XIST expression in testicular germ cell tumors. The Journal of urology 169, 1546-1552.
148. Busque, L., and Gilliland, D.G. (1998). X-inactivation analysis in the 1990s: promise and potential problems. Leukemia 12, 128-135.
149. Kassim, S., Zoheiry, N.M., Hamed, W.M., Going, J.J., and Craft, J.A. (2004). Androgen receptor gene methylation and exon one CAG repeat length in ovarian cancer: differences from breast cancer. IUBMB life 56, 417-426.
150. Crona, D.J., and Whang, Y.E. (2017). Androgen Receptor-Dependent and -Independent Mechanisms Involved in Prostate Cancer Therapy Resistance. Cancers 9.
151. Brockdorff, N. (1998). The role of Xist in X-inactivation. Current Opinion in Genetics & Development 8, 328-333.
152. Zhu, H., Wang, G., and Qian, J. (2016). Transcription factors as readers and effectors of DNA methylation. Nature reviews Genetics 17, 551-565.
153. Álvaro-Blanco, J., Martínez-Gac, L., Calonge, E., Rodríguez-Martínez, M., Molina-Privado, I., Redondo, J.M., Alcamí, J., Flemington, E.K., and Campanero, M.R. (2009). A novel factor distinct from E2F mediates C-MYC promoter activation through its E2F element during exit from quiescence. Carcinogenesis 30, 440-448.
154. Campanero, M.R., Armstrong, M.I., and Flemington, E.K. (2000). CpG methylation as a mechanism for the regulation of E2F activity. Proceedings of the National Academy of Sciences of the United States of America 97, 6481-6486.
155. Gonder, P.S.C.M.K. (2012). Macroevolution: Examples from the Primate World. Nature Education Knowledge

156. Ceman, S., O'Donnell, W.T., Reed, M., Patton, S., Pohl, J., and Warren, S.T. (2003). Phosphorylation influences the translation state of FMRP-associated polyribosomes. Human molecular genetics 12, 3295-3305.
157. Qin, Y., Jiao, X., Simpson, J.L., and Chen, Z.-J. (2015). Genetics of primary ovarian insufficiency: new developments and opportunities. Human reproduction update 21, 787-808.
158. Persani, L., Rossetti, R., and Cacciatore, C. (2010). Genes involved in human premature ovarian failure. Journal of molecular endocrinology 45, 257-279.
159. Carrel, L., and Willard, H.F. (2005). X-inactivation profile reveals extensive variability in X-linked gene expression in females. Nature 434, 400-404.
160. Heard, E., and Disteche, C.M. (2006). Dosage compensation in mammals: fine-tuning the expression of the X chromosome. Genes Dev 20, 1848-1867.
161. Ferreira, S.I., Matoso, E., Pinto, M., Almeida, J., Liehr, T., Melo, J.B., and Carreira, I.M. (2010). X-chromosome terminal deletion in a female with premature ovarian failure: Haploinsufficiency of X-linked genes as a possible explanation. Molecular cytogenetics 3, 14.
162. Davison, R.M., Quilter, C.R., Webb, J., Murray, A., Fisher, A.M., Valentine, A., Serhal, P., and Conway, G.S. (1998). A familial case of X chromosome deletion ascertained by cytogenetic screening of women with premature ovarian failure. Human reproduction (Oxford, England) 13, 3039-3041.
163. Rossetti, F., Rizzolio, F., Pramparo, T., Sala, C., Bione, S., Bernardi, F., Goegan, M., Zuffardi, O., and Toniolo, D. (2004). A susceptibility gene for premature ovarian failure (POF) maps to proximal Xq28. Eur J Hum Genet 12, 829-834.
164. Filippova, G.N., Cheng, M.K., Moore, J.M., Truong, J.P., Hu, Y.J., Nguyen, D.K., Tsuchiya, K.D., and Disteche, C.M. (2005). Boundaries between chromosomal domains of X inactivation and escape bind CTCF and lack CpG methylation during early development. Developmental cell 8, 31-42.
165. Wolff, D.J., Gustashaw, K.M., Zurcher, V., Ko, L., White, W., Weiss, L., Van Dyke, D.L., Schwartz, S., and Willard, H.F. (1997). Deletions in Xq26.3-q27.3 including FMR1 result in a severe phenotype in a male and variable phenotypes in females depending upon the X inactivation pattern. Human genetics 100, 256-261.
166. Probst, F.J., Roeder, E.R., Enciso, V.B., Ou, Z., Cooper, M.L., Eng, P., Li, J., Gu, Y., Stratton, R.F., Chinault, A.C., et al. (2007). Chromosomal microarray analysis (CMA) detects a large X chromosome deletion including FMR1, FMR2, and IDS in a female patient with mental retardation. American journal of medical genetics Part A 143a, 1358-1365.
167. Hall, D.A., Robertson-Dick, E.E., O'Keefe, J.A., Hadd, A.G., Zhou, L., and Berry-Kravis, E. (2016). X-inactivation in the clinical phenotype of fragile X premutation carrier sisters. Neurology Genetics 2, e45.
168. Alvarez-Mora, M.I., Rodriguez-Revenga, L., Feliu, A., Badenas, C., Madrigal, I., and Mila, M. (2016). Skewed X Inactivation in Women Carrying the FMR1 Premutation and Its Relation with Fragile-X-Associated Tremor/Ataxia Syndrome. Neuro-degenerative diseases 16, 290-292.
169. Unoki, M., and Nakamura, Y. (2003). Methylation at CpG islands in intron 1 of EGR2 confers enhancer-like activity. FEBS Letters 554, 67-72.
170. Strathdee, G., Davies, B.R., Vass, J.K., Siddiqui, N., and Brown, R. (2004). Cell type-specific methylation of an intronic CpG island controls expression of the MCJ gene. Carcinogenesis 25, 693-701.
171. Zhang, X., Wu, M., Xiao, H., Lee, M.-T., Levin, L., Leung, Y.-K., and Ho, S.-M. (2010). Methylation of a Single Intronic CpG Mediates Expression Silencing of the PMP24 Gene in Prostate Cancer. The Prostate 70, 765-776.
172. Baylin, S.B., and Ohm, J.E. (2006). Epigenetic gene silencing in cancer - a mechanism for early oncogenic pathway addiction? Nature reviews Cancer 6, 107-116.
173. Sagvekar, P., Mangoli, V., Desai, S., Patil, A., and Mukherjee, S. (2017). LINE1 CpG-DNA Hypomethylation in Granulosa Cells and Blood Leukocytes Is Associated With PCOS and Related Traits. The Journal of Clinical Endocrinology & Metabolism 102, 1396-1405.
174. Putowski, L., Gasior, W., Gogacz, M., Gagala, J., and Jakowicki, J.A. (2001). [Differences in human and rat FSH receptors promote activity as a result of the transcriptional factors: E2F1, E2F4 and E2F5 overexpression]. Ginekologia polska 72, 1560-1566.

175. Yin, M., Wang, X., Yao, G., Lu, M., Liang, M., Sun, Y., and Sun, F. (2014). Transactivation of microrn A-320 by microRNA-383 regulates granulosa cell functions by targeting E2F1 and SF-1 proteins. The Journal of biological chemistry 289, 18239-18257.
176. Douville, G., and Sirard, M.A. (2014). Changes in granulosa cells gene expression associated with growth, plateau and atretic phases in medium bovine follicles. J Ovarian Res 7, 50.
177. Georges, A., Auguste, A., Bessiere, L., Vanet, A., Todeschini, A.L., and Veitia, R.A. (2014). FOXL2: a central transcription factor of the ovary. Journal of molecular endocrinology 52, R17-33.
178. Andreu-Vieyra, C., Chen, R., and Matzuk, M.M. (2008). Conditional deletion of the retinoblastoma (Rb) gene in ovarian granulosa cells leads to premature ovarian failure. Molecular endocrinology (Baltimore, Md) 22, 2141-2161.
179. Helin, K., Harlow, E., and Fattaey, A. (1993). Inhibition of E2F-1 transactivation by direct binding of the retinoblastoma protein. Mol Cell Biol 13, 6501-6508.
180. Mishra, S., Murphy, L.C., and Murphy, L.J. (2006). The Prohibitins: emerging roles in diverse functions. Journal of cellular and molecular medicine 10, 353-363.
181. Wang, S., Nath, N., Fusaro, G., and Chellappan, S. (1999). Rb and prohibitin target distinct regions of E2F1 for repression and respond to different upstream signals. Mol Cell Biol 19, 7447-7460.
182. Choi, D., Lee, S.J., Hong, S., Kim, I.H., and Kang, S. (2008). Prohibitin interacts with RNF2 and regulates E2F1 function via dual pathways. Oncogene 27, 1716-1725.
183. Wang, Q., Leader, A., and Tsang, B.K. (2013). Follicular stage-dependent regulation of apoptosis and steroidogenesis by prohibitin in rat granulosa cells. Journal of Ovarian Research 6, 23.
184. Thompson, W.E., Powell, J.M., Whittaker, J.A., Sridaran, R., and Thomas, K.H. (1999). Immunolocalization and expression of prohibitin, a mitochondrial associated protein within the rat ovaries. The Anatomical record 256, 40-48.
185. Chowdhury, I., Thomas, K., and Thompson, W.E. (2016). Prohibitin (PHB) roles in granulosa cell physiology. Cell and tissue research 363, 19-29.
186. Real, S., Meo-Evoli, N., Espada, L., and Tauler, A. (2011). E2F1 regulates cellular growth by mTORC1 signaling. PloS one 6, e16163.
187. Kumari, D., and Usdin, K. (2001). Interaction of the transcription factors USF1, USF2, alpha - Pal/Nrf-1 with the FMR1 promoter. Implications for Fragile X mental retardation syndrome. The Journal of biological chemistry 276.
188. Beilina, A., Tassone, F., Schwartz, P.H., Sahota, P., and Hagerman, P.J. (2004). Redistribution of transcription start sites within the FMR1 promoter region with expansion of the downstream CGG-repeat element. Human Molecular Genetics 13, 543-549.
189. Pastori, C., and Wahlestedt, C. (2012). Involvement of long noncoding RNAs in diseases affecting the central nervous system. RNA biology 9, 860-870.
190. Morris, K.V. (2009). Long antisense non-coding RNAs function to direct epigenetic complexes that regulate transcription in human cells. Epigenetics 4, 296-301.
191. Kiyosawa, H., Yamanaka, I., Osato, N., Kondo, S., and Hayashizaki, Y. (2003). Antisense transcripts with FANTOM2 clone set and their implications for gene regulation. Genome Res 13, 1324-1334.
192. Wahlestedt, C. (2006). Natural antisense and noncoding RNA transcripts as potential drug targets. Drug discovery today 11, 503-508.
193. Galante, P.A., Vidal, D.O., de Souza, J.E., Camargo, A.A., and de Souza, S.J. (2007). Sense-antisense pairs in mammals: functional and evolutionary considerations. Genome Biol 8, R40.
194. Beltran, M., Puig, I., Pena, C., Garcia, J.M., Alvarez, A.B., Pena, R., Bonilla, F., and de Herreros, A.G. (2008). A natural antisense transcript regulates Zeb2/Sip1 gene expression during Snail1-induced epithelial-mesenchymal transition. Genes Dev 22, 756-769.
195. Maruyama, R., Shipitsin, M., Choudhury, S., Wu, Z., Protopopov, A., Yao, J., Lo, P.K., Bessarabova, M., Ishkin, A., Nikolsky, Y., et al. (2012). Altered antisense-to-sense transcript ratios in breast cancer. Proc Natl Acad Sci U S A 109, 2820-2824.
196. Nagai, K., Kohno, K., Chiba, M., Pak, S., Murata, S., Fukunaga, K., Kobayashi, A., Yasue, H., and Ohkohchi, N. (2012). Differential expression profiles of sense and antisense transcripts between HCV-associated hepatocellular carcinoma and corresponding non-cancerous liver tissue. International journal of oncology 40, 1813-1820.

197. Monti, L., Cinquetti, R., Guffanti, A., Nicassio, F., Cremona, M., Lavorgna, G., Bianchi, F., Vignati, F., Cittaro, D., Taramelli, R., et al. (2009). In silico prediction and experimental validation of natural antisense transcripts in two cancer-associated regions of human chromosome 6. International journal of oncology 34, 1099-1108.
198. Albers, E. (2009). Metabolic characteristics and importance of the universal methionine salvage pathway recycling methionine from 5'-methylthioadenosine. IUBMB life 61, 1132-1142.
199. Kusano, T., Berberich, T., Tateda, C., and Takahashi, Y. (2008). Polyamines: essential factors for growth and survival. Planta 228, 367-381.
200. Pirkov, I., Norbeck, J., Gustafsson, L., and Albers, E. (2008). A complete inventory of all enzymes in the eukaryotic methionine salvage pathway. FEBS Journal 275, 4111-4120.
201. Chou, H.Y., Lin, Y.H., Shiu, G.L., Tang, H.Y., Cheng, M.L., Shiao, M.S., and Pai, L.M. (2014). ADI1, a methionine salvage pathway enzyme, is required for Drosophila fecundity. J Biomed Sci 21, 64.
202. Kimball, S.R., and Jefferson, L.S. (2002). Control of protein synthesis by amino acid availability. Current opinion in clinical nutrition and metabolic care 5, 63-67.
203. Proud, C.G. (2002). Regulation of mammalian translation factors by nutrients. European Journal of Biochemistry 269, 5338-5349.
204. Tesseraud, S., Bigot, K., and Taouis, M. (2003). Amino acid availability regulates S6K1 and protein synthesis in avian insulin-insensitive QM7 myoblasts. FEBS Lett 540, 176-180.
205. Oram, S.W., Ai, J., Pagani, G.M., Hitchens, M.R., Stern, J.A., Eggener, S., Pins, M., Xiao, W., Cai, X., Haleem, R., et al. (2007). Expression and function of the human androgen-responsive gene ADI1 in prostate cancer. Neoplasia 9, 643-651.
206. Gotoh, I., Uekita, T., and Seiki, M. (2007). Regulated nucleo-cytoplasmic shuttling of human aci-reductone dioxygenase (hADI1) and its potential role in mRNA processing. Genes to Cells 12, 105-117.

Publications

Original articles (from the thesis)

Youness B, Dietrich J, Strowitzki T, Rehnitz J, Vogt PH "E2F1 binding site in *FMR1* intron1 dependent on CpG methylation is functional for *FMR1* expression in human granulosa cells" (manuscript submitted).

Other publications

Rehnitz J, Alcoba DD, Brum IS, Hinderhofer K, **Youness B**, Strowitzki T, Vogt PH (2017). "*FMR1* and AKT/mTOR signalling pathways: potential functional interactions controlling folliculogenesis in human granulosa cells." Reprod Biomed Online S1472-6483(17)30373-5.

Léger P*, Tetrad M*, **Youness B**, Cordes N, Rouxel R, Flamand M, Lozach PY (2016) „Differential Use of the C-Type Lectins L-SIGN and DC-SIGN for Phlebovirus Endocytosis" Traffic 17(6):639-56.

Younes BG, Hazzouri KM, Chaaban MJ, Karam WG, Abou Jaoude IF, Attieh JH, Hazzouri MM (2011) „High frequency of sex chromosomal disomy in spermatozoa of Lebanese infertile men" J Androl 32(5): 518-52.

Conference oral presentations and posters

27. May. - 30 May 2017: ESHG (European Society of Human Genetics) 50th congress, Copenhagen, Denmark. "*FMR1* epigenetic control can explain variable response of women ovarian reserve to clinical stimulation protocol" (Poster).

03. May - 06. May 2017: EMBL (European Molecular Biology laboratory) Epigenetics and Chromatin congress, Heidelberg, Germany. "*FMR1* epigenetic control can explain variable response of women ovarian reserve to clinical stimulation protocol" (Poster).

02. July - 06. July 2016: ESHRE (European Society for Human Reproduction and Endocrinology) 32th annual meeting, Helsinki, Finland. "Methylation of a novel *FMR1* epigenetic element depends on women ovarian reserve" (Oral presentation).

22. October. - 24. October 2015: EMBL, 17th EMBL PhD Symposium, Heidelberg, Germany. "Complex epigenetic *FMR1* expression control during human folliculogenesis" (Poster).

Acknowledgments

Develop an 'Attitude of Gratitude'. Say thank you to everyone you meet for everything they do for you."- Brian Tracy

Foremost I would like to express my special appreciation and thanks to my mentor and supervisor Prof. Dr. rer. nat. Peter. H. Vogt for the opportunity to work in his group and for his guidance throughout my PhD work. His support and the freedom he gave me allowed me to grow both, scientifically and personally. Thank you for showing me the way out of my own cage and for always challenging me to go out of my comfort zone. **"The teacher who is indeed wise does not bid you to enter the house of his wisdom but rather leads you to the threshold of your mind."- Gibran Khalil Gibran.**

This work would not have been possible without the clinical and financial support offered by Dr. med. Julia Rehnitz and the Deutsche Forschungsgemeinschaft (grant number RE 3647/1-1 to JR). Thank you Julia for your kindness, advices and support throughout the good and hard times and for generously providing funding that allowed me to go to several conferences.

I would also like to acknowledge Prof. Dr. med. Thomas Strowitzki, all medical doctors and the members of the IVF laboratory for recruiting and offering patient material. I also thank all patients who contributed to this project by donating blood and/or tissue samples.

I also would like to sincerely thank my Thesis Advisory Committee members, Prof. Dr. Jochen Hess and PD. Dr. rer. nat. Beate Niesler, for their valuable input in this study and for their support whenever requested. I gratefully acknowledge the statistical support provided by Prof. Dr. Justo Lorenzo Bermejo.

I want to express my appreciation for Prof. Dr. rer. nat. Gudrun Rappold for being my co-referee. I also acknowledge Prof. Dr. rer. nat. Stefan Wiemann and Prof. Dr. rer. nat. Jochen Hess for accepting to act as examiners for my defense.

Special thanks go to our technical assistants Ulrike Bender, Jutta Zimmer and Birgitta Messmer for their excellent technical assistance and for making working in the laboratory a pleasant experience. I really learned a lot from you: Uli and Jutta, thank you from the bottom of my heart.

Special thanks for our lovely secretaries Petra Blim and Christine Mahrla for their pleasant presence and for always being there to help with all administrative papers.

Furthermore, I want to thank my past and present colleagues who made my working hours personally enjoyable besides good scientific exchange and who went with me through all the ups and downs in our office especially Melanie and Amanda.

I also appreciate the stimulating atmosphere with plenty of advanced training courses and lectures outside my specific PhD topic provided by the HBIGS graduate school. Thank you as well for the travel grant that allowed me to travel to Copenhagen.

I am deeply indebted to my family for their faith in me and their support over all the years and for giving me the opportunity to start and pursue a career in science. Thank you Mum and Dad for all sacrifices you made for me. I know it was hard for you letting me travel far away from our beloved Lebanese home, but you were sure that it will build my character. I still remember the first time I stepped out of the plane in France. I took my luggage and cried because I was afraid. Now, 8 years later, I lived in many countries and I enjoy the way you look up to me. I also thank my brothers, Samer

and Elias and my sweet sister Aline for always believing in my potential. Samer you always managed to come to visit me wherever I was and managed to take my mind off the lab, even if things did not work out as planned before.

I thank my friends all over the world for all the great hours we spent together especially my best friends Julie and Sayde and my German Opa Siggi. I would also thank every person that made my integration in Germany during the last four years enjoyable and very special for me.

Finally, I want to say a very special thanks to my husband Roland. Only with your confidence and motivation I could achieve this PhD study. You moved to Germany and accepted to start a new life because you believed in me. Thanks for helping me in whatever way you could during this challenging period and for always pushing me forward.